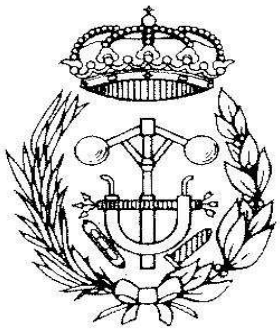

ESCUELA TÉCNICA SUPERIOR DE INGENIEROS INDUSTRIALES Y DE TELECOMUNICACIÓN

Titulación :

INGENIERO TÉCNICO INDUSTRIAL MECÁNICO

Título del proyecto:

ANALYSIS OF THE LOW AROUND A SAVONIUS ROTOR

Alumno: José María Jaurrieta Zarranz

Tutores: Marco Torresi y Luis Marroyo Palomo

Pamplona, septiembre de 2011

Index

1. Summary

In this project, we experimentally analyze the flow field through a Savonius rotor, which operates inside a wind-tunnel.

For this we have made 3 sets of experiments:

In the first one, we compare the information taken by a one directional probe, and the information taken by a two directional probe, so we give information about the way, or the different ways of measuring the speed of the wind.

In the second one we compare the computation of the flow rate by mean of two meshes: one with 81 points of measuring, the other with 25 points of measuring, moreover we measure the speed of the wind ahead the rotor with different values of frequency for the fan and different values of rotational speed for the turbine.

In the third one we analyze the flow field behind the Savonius rotor by means of an in-fase average technique.

This project is useful for the researchers who are trying to find the best way of combining different kind of rotors, also for the researchers who are trying to improve the wind farms of vertical axis, therefore it is not an isolated project, it is into the development of alternative energy sources and, especially in the development in the field of domestic use.

The present thesis begins describing the situation and the importance of the wind energy in the world and in Italy, and how important the rotor of vertical axis are, we´ll describe this kind of rotors and specifically the Savonius rotor.

Secondly, we describe the tools and the instruments that we have used to carry out these experiments, and the scientific theory about the wind energy.

Eventually, we describe the details of any experiment, and we show the information that we got, through all this information we´ll give conclusions.

2. The wind energy in Italy, Spain and the world

THE IMPORTANCE OF RENEWABLE ENERGIES

Nowadays, the production of the energy in the world is 138.900 TWh, most of this energy is produced by fossil fuels (oil, coal, gas).

As the next list shows:

Oil 37 %

Coal 25 %

Gas 23 %

Nuclear 6 %

Renewable energies 9 %

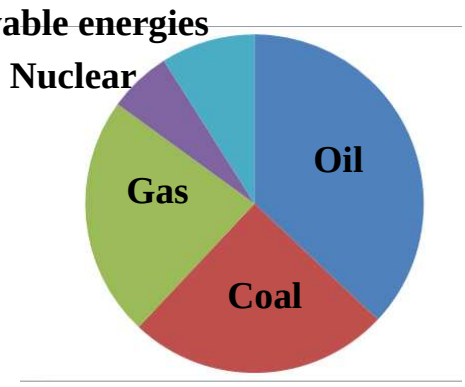

Fig. 1. Energy production

In the group of the Renewable Energies there are many types of production, and there are big differences among them, they only have one thing in common, are unlimited.

BIOMASS: This kind of energy uses plants and plant residual as a fuel. It is a renewable energy because obviously it can take so much fuel as the crops can produce. In terms of CO_2 emissions, this source is neutral since biomass emits as much CO_2 as the quantity absorbed during the growth. It is not a importance source of energy, and according with the Autorità per l'Energia Elettrica ed il Gas (AEEG) it is marginally use in Italy to produce electrical energy, and in the rest of the countries the percentage is so small that we can consider as zero.

HYDROELECTRIC: This source produces energy through the conversion of the gravitational potential energy of water, therefore it needs a huge construction and extraordinary natural conditions. It does not contaminate but it is necessary to destroy the environment in an area, and building this kind of plant involves destroying the natural riverbank, for this reason, countries like France prefer not to use this kind of energy. The main advantage is the fact that it is possible to control the amount of energy to be obtained. Obviously it can't be an alternative because it is not possible to build this kind of plants everywhere. It is one of the most important sources of renewable energy, and it represents, for example in Spain the 40% of the energy produced by the renewable energies and in Italy is about the 60%, but nowadays the energy produced by this source is not increasing so it is losing importance.

SOLAR: In this group we have two types of energies, the energy is directly converted in electricity by means of photovoltaic panels and the energy produce in the form of heat.

The former technology is mainly used either in small facilities or directly on site because it produces small amount of energy, however there are photovoltaic plants, which currently work because the governments are subsidizing them.

Fig. 2. Photovoltaic panels

The latter technology is mainly applied in domestic application even if there are many examples of solar plants or integrated solar plants.

There is a huge hope in solar energy, which is said to be able to become the alternatives to the traditional energies, since the heat and the light of the sun are around all over the world so it should be possible to set up one plant in any place. The percentage of this energy is about the 20 % in countries like Italy and Spain, and even if it could be a bit amazing. The country with more power already installed is Germany.

GEOTHERMAL ENERGY: This kind of production takes the heat from the earth to produces electrical energy, it is absolutely clean and easy to set up but the efficiency is very low, and only in some areas like Iceland is useful this kind of production of energy. This energy would be the best but actually it is possible to exploit it only in some areas. It is only important in areas with a temperature gradient bigger than 32 ºC/km. To install a plant of geothermal energy it is necessary to produce explosions. That is the reason why it is not possible to install one around the Vesuvio, because those explosions can activate the volcano.

WIND ENERGY: Nowadays this type of production of energy is the one with more future together with the solar energy. It is possible to install wind turbines almost in any geographic area, being only necessary strong winds, that is possible to get them in the peak of the hills and mountains. It is experiencing a great develop in Europe and United States. In countries with many mountain areas is an important source of energy, such as Spain, but in countries with many kilometers of coast like Denmark it is also an important source of energy. Wind energy with solar energy is the most important renewable energy. Currently the production is mainly obtained by means of horizontal axis wind turbines in big wind farms, but there is an intense research process in the field of vertical axis wind turbine in small installations.

Fig. 3. Wind turbines in the sea

All this energies are not the main energy sources in any country in the world, just small regions like Greek islands or mountain areas use this renewable energies as the single source of energy, whereas the big cities are still taking the energy from thermal power plants that works with petrol gas or coal, or from nuclear plants, that is changing but very slowly, besides every day is necessary more and more energy. However there are two points that are changing the fact that renewable are not actually important.

This first one is that the developed countries in Europe, United States and Japan don´t have enough petrol or any source of fuel in their territories, in order to avoid being Oil-dependent countries, are trying to reduce the importations.

The second one, according to the Kyoto protocol, is that the developed countries have to reduce the amount of CO_2 emissions, and they can only satisfy this if they start to use energies like wind energy of solar energy, though many countries are increasing the number of nuclear plants as well.

To sum up, the renewable energies are only the 9 % of all energy that we use so they are still a marginal source of energy but they are getting more importance. In fact in 2000 the renewable energies were only the 5 % in the world and now are the 9 %.

The importance of wind energy

The importance of wind energy depends on the country taken into consideration.

In Italy the wind energy is 5660 MW and represents 6% of all the energy produced.

In Spain this is 20676 MW, about the 28%.

In all the European Union is 84708 MW, 5.8 %.

In the world is just 1.2%.

With this data we can say that the European Union is a particularly active in this field but this is a logical consequence of the fact that the European Union lacks in petroleum and gas.

In any case the MW already installed are growing more than it was expected in the previous year. This is a table that shows the evolution in many countries of the world.

EUROPEAN UNION

TOTAL INSTALLED CAPACITY

Year	2001	2002	2003	2004	2005	2006	2007	2008	2009	2010
MW	17315	23159	28598	34371	40511	48029	56531	64719	74767	84074

GERMANY

TOTAL INSTALLED CAPACITY

Year	2001	2002	2003	2004	2005	2006	2007	2008	2009	2010
MW	8754	11994	14609	16629	18415	20622	22247	23903	25777	27214

SPAIN

TOTAL INSTALLED CAPACITY

Year	2000	2001	2002	2003	2004	2005	2006	2007	2008	2009	2010
MW	2235	3337	4825	6203	8263	10027	11623	15145	16689	19160	20676

ITALY

TOTAL INSTALLED CAPACITY

Year	2000	2001	2002	2003	2004	2005	2006	2007	2008	2009	2010
MW	427	690	797	913	1255	1718	2123	2726	3736	4849	5660

UNITED STATES

TOTAL INSTALLED CAPACITY

Year	2000	2001	2002	2003	2004	2005	2006	2007	2008	2009	2010
MW	2578	4275	4685	6372	6725	9149	11575	16824	25237	35159	40180

PR CHINA

TOTAL INSTALLED CAPACITY

Year	2000	2001	2002	2003	2004	2005	2006	2007	2008	2009	2010
MW	346	402	469	567	764	1260	2599	5910	12020	25805	42287

JAPAN

TOTAL INSTALLED CAPACITY

Year	2000	2001	2002	2003	2004	2005	2006	2007	2008	2009	2010
MW	136	302	338	580	809	1049	1309	1538	1880	2085	2304

BRAZIL

TOTAL INSTALLED CAPACITY

Year	2002	2003	2004	2005	2006	2007	2008	2009	2010
MW	22	29	29	29	237	247	341	606	931

IRAN

TOTAL INSTALLED CAPACITY

Year	2002	2003	2004	2005	2006	2007	2008	2009	2010
MW	12	12	15	20.5	48	74	84	92	92

As we can see, countries like Iran or Brazil, which have a source of petroleum, haven´t developed the wind energy as much as other countries. Two very similar countries like Brazil and China, countries not traditionally developed but which recently becoming the most important in the world, have solved their energy need in two different manners: the first one, Brazil, had covered its necessities through the increase of the production of petroleum, whereas China decided to develop wind energy because of that lack of fuel.

If we compare the production of solar energy and the production of wind energy, we see that nowadays wind energy is much more developed with respect to solar energy: in Italy in 2009 the power installed for solar energy was only 723 MW, whereas it was 19160 MW for wind energy. Moreover we have to say for solar energy that, nowadays there isn´t any project of thermo-solar energy in Europe but a plan of the European Union exists to install in the south of Europe many plants of this kind of energy.

Comparative information between solar and wind energy in the year 2009. Energy produced.

	SOLAR	**WIND**
Italy	723	4849
Spain	60	19160
Germany	3845	25777
United States	4731	35159
Japan	482.98	2085

With this information we can say that wind energy is on the peak of the renewable energies.

The wind energy in Italy

The wind energy in Italy has an important development in the south and especially in the Puglia. The next map shows the energy of the wind in the different regions of Italy, and it explains why Puglia and the islands are the most important areas to install wind farms.

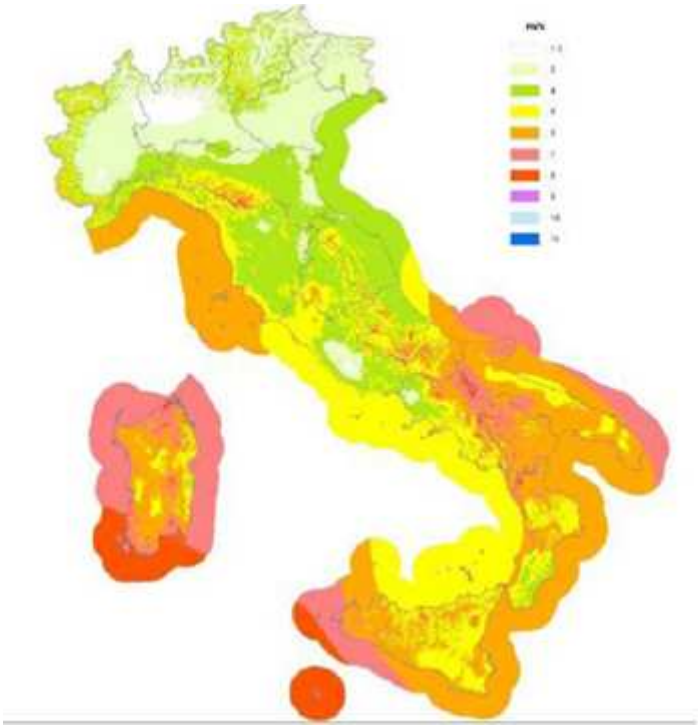

Fig. 4. Wind Energy distribution

This map shows the distribution of the wind energy, the south has more power installed because the wind is strong in these regions, besides the north can get energy imported from France and from the thermal power plants, that´s the reason because of the governments of these regions doesn´t have the necessity of installing wind farms, besides the huge amounts of money that the central government is investing in the south giving a chance for the companies to start new projects of wind energy.

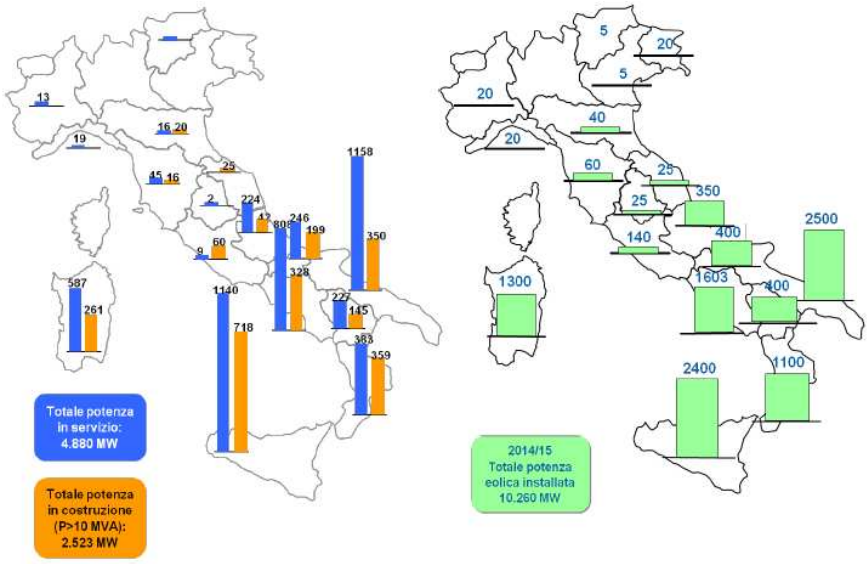

Fig. 5. Wind Energy distribution

Energy in Puglia

Electrical production in Puglia in 2008

Source: Rete Elettrica Nazionale

Elaboration by The European House-Ambrosetti

Fig. 6. Energy in Puglia

In Puglia, as we see in the graph, energy is produced in thermoelectric stations like the one situated in Via Buozzi in Bari. This station has 3 turbines and was bilt in 1958. One of these turbines works now with gas from 2007.

Fig. 7. Enel Bari Thermoelectrical station in Via Buozzi

(Photo by Wasca)

At the end of 2009 Puglia was the greatest producer of wind power of all Italian regions. As we have seen before, Puglia is one of the most windy region in all Italy.

Besides, the Government of Puglia made a law (Regional Law 23/07) in order to improve the renewable energy in the region. The most important ideas of this law are:

1. Promote the development of relations between firms with specific expertise in the production of plant components in different sectors (solar, wind, biomass, etc.);
2. Activate relationship between the creators and the subjects of energy distributors in order to find solutions for the development of new infrastructures and the decongestion of the existing power distribution network;
3. Support regional institutions in the decision-making and legislation;
4. Promote information and support future planning of government in the development of renewables and energy efficiency;
5. Support the training of new professionals specialized in the design, implementation and certification of technologies applied to energy efficiency and renewable energies;
6. Stimulate scientific research and technological innovation;
7. Increase the degree of international openness of the sector;
8. Create a platform of supply and demand in the field of renewable energy sources;
9. Promote efforts to simplify procedures for accessing credit, in agreement with the major banks and financial institutions.

Here is the list of all wind power stations at the end of 2009.

Town-Name (Province)	*Power (MW)*	*Aerogenerators*
Lecce (Lecce)	34	17
Lecce 2 (Lecce)	2	1
Ordona (Foggia)	34	17
Brindisi (Brindisi)	0’08	1
Faeto (Foggia)	14	7
Castelnuovo della Daunia - Casone Romano (Foggia)	2’6	10
Faeto (Foggia)	26’4	44
Orsara la Montagna (Foggia)	18	30
Rocchetta S. Antonio (Foggia)	5’25	15
Volturara Appula e Motta Montecorvino (Foggia)	11’4	19
Volturino (Foggia)	13’08	20
Minervino Murge (Barletta-Andria-Trani)	18’75	22
Pietramontecorvino 2 (Foggia)	4’25	5
Carpignano Salentino (Lecce)	14	7
Faeto (Foggia)	24	
San Cireo (Foggia)	30	
San Vincenzo (Foggia)	42	
Alberona (Foggia)	26	13
Biccari (Foggia)	12	6
Roseto Valfortore (Foggia)	12	6
Pietramontecorvino (Foggia)	48	24
Minervino Murge (Barletta-Andria-Trani)	40	
S. Agata – Olivola (Foggia)	16	8
S. Agata – Palino (Foggia)	20	10
S. Agata – Pezza del Tesoro (Foggia)	16	8
S. Agata - Piano della Capria (Foggia)	8	4
Ordona (Foggia)	26	13
Surbo (Foggia)	36	18
Motta M. (Foggia)	11’88	18
Panni (Foggia)	19’8	30
Poggio Imperiale (Foggia)	30	15
Alberona (Foggia)	39	65
Alberona I (Foggia)	28’8	48
Alberona II (Foggia)	7’2	12
Anzano di Puglia (Foggia)	7’2	12
Monteleone (Foggia)	16’8	28
S.Agata (Foggia)	12’6	21

Accadia (Foggia)	15’9	24
S. Agata di Puglia (Foggia)	66’35	51
Minervino Murge (Barletta-Andria-Trani)	18	9
Montaguto (Foggia)	34’5	15
Serracapriola (Foggia)	42	21
Troia (Foggia)	7’5	5
Casone Romano (Foggia)	52’66	94
Celle San Vito (Foggia)	90’54	156

Source: www.impiantieolici.it

Map of all wind power locations in Puglia:

Fig. 8. Puglia wind power

Source: www.impiantieolici.it

Own elaboration

The development of wind power production in Puglia from 2004 to 2008 has been very fast. We can see it in the next graph.

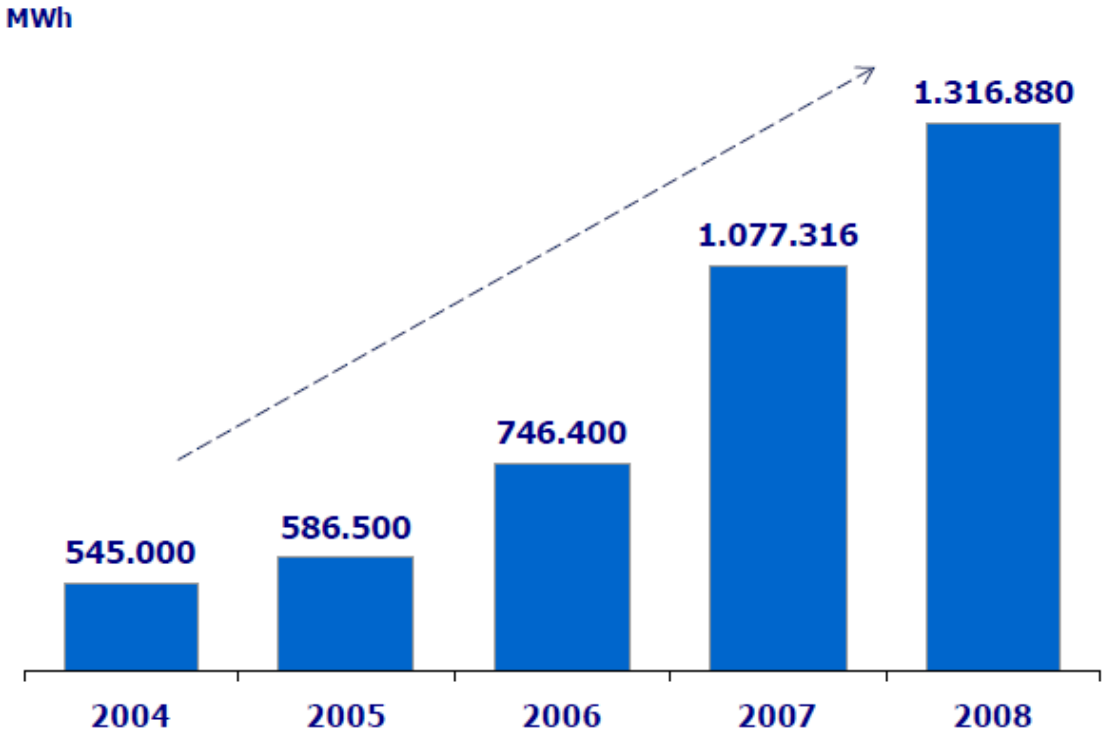

Fig. 9. Variation of wind power production from 2004 to 2008.

Source: "L'eolico. Dati statistici al 31 dicembre 2008. GSE.

Elaboration by The European House-Ambrosetti

Example of a wind power station. The power station of Orsara – La Montagna

The site is located in the town of Orsara di Puglia (FG) at an altitude ranging from about 860 m to 956 m and consists in 30 three-bladed ENERCON E40 wind turbines, of which 11 are in Crepacore and the other 19 in Montagna. Each turbine has a capacity of 0.6 MW for a total of 18 MW installed.

The area examined is not included in any of the protected areas established under the Act 394/91. The project does not affect Sites of Community Importance or Special Areas of Conservation. Wind power plant is associated with the electrical substation of Orsara for the elevation of tension and delivery energy.

The electricity produced by wind turbines is collected in a single half tension (30 kV) underground cable. A system of underground cable lines connecting the type of the half/low voltage continues to Orsara Station where electric energy is transformed and delivered to the public network of high voltage of 150 kV.

Environmental has significance because it is noisy and produces waste, but it does not matter for the visual impact, contamination of soil, flora, fauna and vibration.

Fig. 10. Location map of all wind turbines in the wind energy station of Orsara – La Montagna.

Source and elaboration: Edison Energie Speciale Spa

Wind energy station characteristics:

- Number of wind turbines installed: 30
- Type of wind turbines installed: Wind three-bladed turbines ENERCON E40
- Nominal power of each wind turbine: 0.6 MW
- Total power of the station: 18 MW
- Annual energy production: 46546 MW
- Loss of electricity transmission: 2.5%
- Connection between rotor and alternator: Gearbox
- Electrical systems in central: The electricity produced in the low voltage from each machine is transferred to the control panels and the transformer for the conversion of electrical energy from low voltage (380-600 V) to medium voltage.
  (30000 V) inside the tower.
- Connection between the machines: System of underground cable lines connects them in medium voltage.
- Connection between the station and the National Transmission Grid: The underground cable lines connect the machines with the electrical substation of Orsara where electricity is delivered to the National Transmission Grid at high voltage.

Wind energy in Spain[7,8]

Spain is one of the countries in the world with more power already installed, and besides there are many companies with a developed technology, which currently are exporting their technology to other countries of the European Union.

There are some conditions, which make Spain a country with a high development in wind energy.

1. The orography of Spain is very mountainous, so the wind has areas with high speed where it is possible to install wind farms with a high efficiency.

2. The population in Spain is against the nuclear plants, that's why government don´t want to install this kind of energy again.

3. Spain doesn´t have any oil reservoir and it is getting expensive to get coal in the Spanish coal mines.

Power installed

The wind energy in Spain started late; the first wind farms were installed in 1996, since then the power installed has been increasing very fast.

In fact the different governments have made new laws to make easy the installation of new projects, and they have paid many researches as to develop an accurate map of wind

Fig. 11. Evolution of the wind power installed in Spain

In the year 2005 the government of Spain approved a law to increase the wind power installed until 20000 MW.

The goal for this government according to the investments is to reach the 36000 MW in 2020.

The regions of Spain

1 **GALICIA** 2.852.480

2 **CASTILLA LA MANCHA** 3.108.880

3 **CASTILLA LEÓN** 5.690.310

4 **C. ARAGÓN** 1.446.460

5 **NAVARRA** 1.166.530

6 **ANDALUCÍA** 1.545.000

7 **LA RIOJA** 408.620

8 **ASTURIAS** 762.350

9 **CANARIAS** 746.620

10 **PAÍS VASCO** 1.144.870

11 **CATALUÑA** 944.140

12 **MURCIA** 54.970

13 **C. VALENCIANA** 20.490

14 **BALEARES** 33.200

15 **CANTABRIA** 5.400

16 **EXTREMADURA** 20.340

17 **MADRID** 18.560

TOTAL 19.968.820

There is no region with a special power installed. It draws the attention the fact that Madrid is one of the regions with less wind energy, this is because the regions around Madrid as Castilla y León and Castilla la Mancha have many wind farms.

The fact that some regions have more wind energy than others, it is because some of these regions have different laws, for example the government of Castilla y León subsidize the wind energy.

Companies

In Spain there are many companies that install wind rotors, these companies are currently exporting the technology to South America and the rest of Europe.

The two main companies, which are builders of new rotors and wind farms are:

Gamesa Energía S.A.: It is an international company, that change from the area of the iron and the steal to the area of the wind energy in the year 1993, since this year to the year 2000 its market it was just in Spain, it is the company in the area of wind energy with more market in Asia, and it is getting very important in South America as well. It is the main constructor of wind rotors in Spain.

Elecnor: It is a group of companies, that has a recent history in the world of the wind energy, but its investments in the international market has make the group one of the most important exporters of technology in Spain.

The most important group of managing wind farms is Iberdrola Renovables, this company is a subsidiary of Iberdrola, and manage the 30% of the renewable wind farms in Spain. Iberdrola Renovables has more wind farms in the northern regions.

3. Advantages and disadvantages of the wind energy

Advantages:

- Wind energy, as a clean energy, doesn´t create any kind of pollution.
- As a renewable energy the source of this energy, the wind, is unlimited.
- It is installed in lands that can´t be used for agriculture like the peak of the hills.
- The installation takes only between 4 and 9 months, it depends on the land.
- It is possible to install wind farms on the sea, where the wind is more constant.

Disadvantages:

The mills can only work in a range of speeds of the wind, for a slow speed, the wind doesn´t have enough power to be able of moving the mill, for a too fast speed, the wind is too strong and the axis of the structure can´t stand that movement, so it´s necessary to stop the device.

How to solve these problems:

In order to solve the first the problem the solution is obvious, building structures more resistant, though this will make the problem of a huge cost.

To solve the second problem the solution is more complicated. Predictability is a key in managing wind power's variability, and significant advances have been made in improving forecasting methods. Today, wind power prediction is quite accurate for aggregated wind farms and large areas. Using increasingly sophisticated weather forecasts, wind power generation models and statistical analysis, it is possible to predict generation from five minute to hourly intervals over timescales up to 72 hours in advance, and for seasonal and annual periods. Using current tools, the forecast error for a single wind farm is between 10 and 20% of the power output for a forecast horizon of 36 hours. For regionally aggregated wind farms the forecast error is in the order of 10% for a day ahead and less than 5% for 1-4 hours in advance.

The research in forecasting the wind are improving, but it is not accurate enough to know exactly the amount of energy that we´ll have in a day.

One of the solutions is trying to store the energy produced when that energy is not being consumed, but this is something almost impossible at least storing the 100% of the energy produced.

There is increasing interest in both large scale storage implemented at transmission level, and in smaller scale dedicated storage embedded in distribution networks. The range of storage technologies is potentially wide.

For large-scale storage, pumped hydro accumulation storage (PAC) is the most common and best known technology, which can also be done underground. Another technology option available for large scale is compressed air energy storage (CAES).

On a decentralized scale storage options include flywheels, batteries, possibly in combination with electric vehicles, fuel cells, electrolysis and super-capacitors. Furthermore, an attractive solution consists of the installation of heat boilers at selected combined heat and power locations (CHP) in order to increase the operational flexibility of these units.

However, it has to be pointed out that storage leads to energy losses, and is not necessarily an efficient option for managing wind farm output. If a country does not have favorable geographical conditions for hydro reservoirs, storage is not an attractive solution because of the poor economics at moderate wind power penetration levels (up to 20%). In any case, the use of storage to balance variations at wind plant level is neither necessary nor economic.

Design and operation of power systems

One of the most frequent misunderstandings occurring in the public discussion about integrating wind energy into the electricity network is that it is treated in isolation. An electricity system is in practice much like a massive bath tub, with hundreds of taps (power stations) providing the input and millions of plug holes (consumers) draining the output. The taps and plugs are opening and closing all the time. For the grid operators, the task is to make sure there is enough water in the bath to maintain system security. It is therefore the combined effects of all technologies, as well as the demand patterns, that matter.

Power systems have always had to deal with these sudden output variations from large power plants, and the procedures put in place can be applied to deal with variations in wind power production as well. The issue is therefore not one of variability in itself, but how to predict, manage this variability, and what tools can be used to improve efficiency.

Wind power as a generation source has specific characteristics, which include variability and geographical distribution. These raise challenges for the integration of large amounts of wind power into electricity grids.

In order to integrate large amounts of wind power successfully, a number of issues need to be addressed, including design and operation of the power system, grid infrastructure issues and grid connection of wind power.

Experience has shown that the established control methods and system reserves available for dealing with variable demand and supply are more than adequate for coping with the additional variability from wind energy up to penetration levels of around 20%, depending of the nature of the system in question. This 20% figure is merely indicative, and the reality will vary widely from system to system. The more flexible a power system in terms of responding to variations both on the demand and the

supply side, the easier the integration of variable generation sources such as wind energy. In practice, such flexible systems, which tend to have higher levels of hydro power and gas generation in their power mix, will find that significantly higher levels of wind power can be integrated without major system changes.

Within Europe, Denmark already gets 21% of its gross electricity demand from the wind, Spain almost 12%, Portugal 9%, Ireland 8% and Germany 7%. Some regions achieve much higher penetrations. In the western half of Denmark, for example, more than 100% of demand is sometimes met by wind power.

Grid operators in a number of European countries, including Spain and Portugal, have now introduced central control centers which can monitor and manage efficiently the entire national fleet of wind turbines.

The present levels of wind power connected to electricity systems already show that it is feasible to integrate the technology to a significant extent. Experience with almost 60 GW installed in Europe, for example, has shown where areas of high, medium and low penetration levels take place in different conditions, and which bottlenecks and challenges occur.

Another frequent misunderstanding concerning wind power relates to the amount of 'back up' generation capacity required, as the inherent variability of wind power needs to be balanced in a system.

Wind power does indeed have an impact on the other generation plants in a given power system, the magnitude of which will depend on the power system size, generation mix, load variations, demand size management and degree of grid interconnection. However, large power systems can take advantage of the natural diversity of variable sources. They have flexible mechanisms to follow the varying load and plant outages that cannot always be accurately predicted.

Studies and practice demonstrate that the need for additional reserve capacity with growing wind penetration varies modestly. Up to around 20% of wind power penetration, unpredicted imbalances can be countered with reserves existing in the system. Several national and regional studies indicate additional balancing costs in the order of 0 to 3 €/MWh for levels of wind power up to 20%. In Spain, with 12% of wind penetration, the cost of balancing power was assessed in 2007 at 1.4 €/MWh.

The additional balancing costs associated with large-scale wind integration tend to amount to less than 10% of wind power generation costs, depending on the power system flexibility, the accuracy of short-term forecasting and gate-closure times in the individual power market. The effect of this to the consumer power price is close to zero.

4. Different types of turbines

Nowadays there are two main classes of turbines.

Horizontal axis wind turbine

Horizontal-axis wind turbines (HAWT) have the main rotor shaft and the electrical generator at the top of the tower. They spin around their horizontal axis. The modern turbines are evolved version of the ancient wind mills, that were used in the century XII and XIII in the small factories.

Vertical axis wind turbine

Vertical-axis wind turbines (VAWT) have the main rotor shaft and electrical generator in the down part of the axis; they spin in their vertical axis. There are two types, Savonius and Darrieus. Historically this kind of mills was used by the barbarian peoples who conquered the Roman Empire. They used to build in the rivers, so they were not proper wind mills, they were water mills. The modern designs started to appear in the beginning of the century XX.

Comparison HAWT vs VAWT

The HAWT are used in big farms, and the VAWT are used to provide electricity directly to the buildings. Model more used among the HAWT, is the three blade, because it´s the model with the best ratio “efficiency - minimum speed necessary”, and the model more used among the VAWT is a combination of a three blade Savonius and three blade Darrieus.

The main advantage and the reason because of it the HAWT are used in big wind farms, is the efficiency (percent of energy taken from the wind) of this kind of turbines is 40% bigger, and the higher the tower is the stronger the wind is. 10 meters higher involve an increase of 20% in the speed of the wind.

The reasons because the VAWT are better for small productions is because it is necessary a slower speed to start the turbine.

They take advantage from any kind of wind, and from any direction of the wind.

The turbine of our project is a Savonius, that is a kind of VAWT, so we are going to focus in VAWT and in a different point we describe all the details of the Savonius turbine.

Different types of VAWT

There are two types of VAWT, Savonius and Darrieus, these types can have a different number of blades. For example, in our experiment the Savonius turbine has two blades but the most common and efficient is a turbine with 3 blades. However we explain this in the point where we describe the Savonius turbine.

Darrieus turbine

Its name is due to the French engineering George Darrieus, who made the design in 1931. The turbine is a vertical axis with a number of branches (usually three) that support the blades. The shape of these blades is similar to the shape of the wings of a plane.

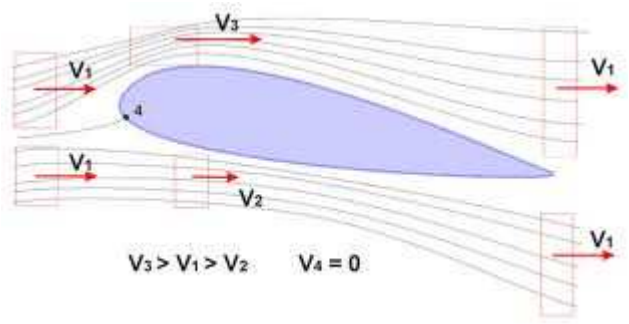

Fig. 12. Aerofoil

The Darrieus turbine needs speed about 4 m/s to start but the efficiency is better than Savonius. The design is more complicated than the Savonius therefore it is more difficult to make.

There are two kinds of design; the first one joins the blades with the axis in the upper and down part of the axis. The second makes the blades straight.

Fig. 13. Darrieus rotors

5. Physical theories about the wind energy[2,3]

Theory of Betz

Wind particles from the air, being in movement, have a certain kinetic energy, which can be transferred to a medium which is in the way of the wind. To know the amount of the power given from the wind to the rotor, we should explain the theory of Betz.

These are the assumptions of the theory of Betz:

1. The rotor does not possess a hub; this is an ideal rotor, with an infinite number of blades which have no drag. Any resulting drag would only lower this idealized value.
2. The flow into and out of the rotor is axial. This is a control volume analysis, and to construct a solution the control volume must contain all flow going in and out, failure to account for that flow would violate the conservation equations.
3. This is incompressible flow. The density remains constant, and there is no heat transfer from the rotor to the flow or vice versa.
4. The rotor is also massless. No account is taken of angular momentum imparted to either the rotor or the air flow behind the rotor, i.e., no account is taken of any wake effect.

The power available in a flow of wind with speed V_∞ is:

$$E = \tfrac{1}{2}\dot{m}V_\infty^2$$

In the case of the wind, the flow is $\dot{m} = \rho A_1 V_\infty$ in this equation A_1 is the area of passing, and ρ the density of the air, so we have the expression:

$$E = \tfrac{1}{2}\rho A_1 V_\infty^3$$

This power can´t be fully exploited theorically either, because the air needs some speed, therefore some energy, to go away from the rotor.

According with the picture, V_1 (V_∞) is the speed of the wind before arriving to the rotor, V_2 is the speed in the plane of the rotor and V_3 is the speed of the wind after the rotor, it means, after giving energy to the rotor.

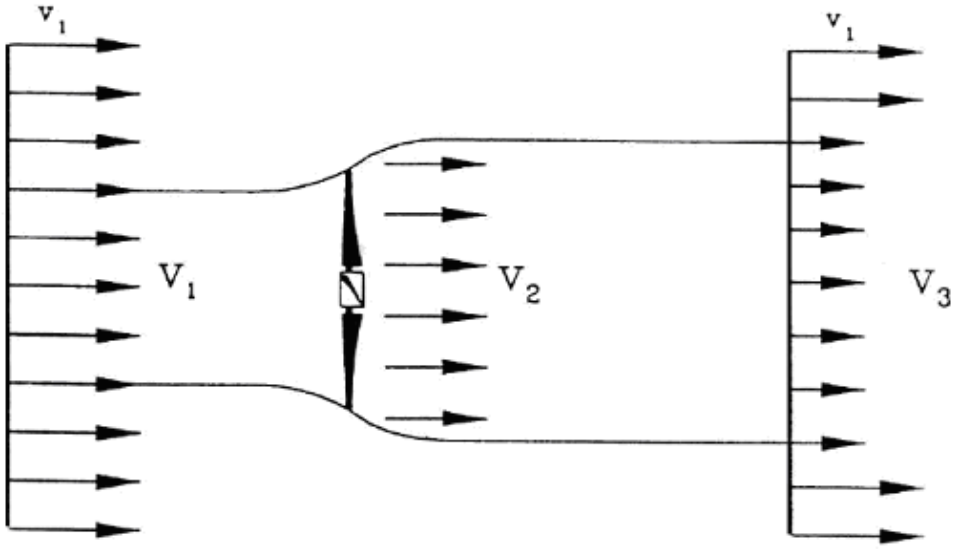

Fig. 14. Velocity profile

For continuity of flow must be:

$$\rho A_1 V_1 = \rho A_2 V_2 = \rho A_3 V_3$$

where it is possible to keep the density constant.

The difference of energy between the point 1 and the point 3 is:

$$Eex = \tfrac{1}{2} m(V_1^2 - V_3^2)$$

Therefore the energy taken from the wind is:

$$Eex = \tfrac{1}{2} \dot{m}(V_1^2 - V_3^2)$$

This is the energy that the rotor can take from the air.

The speed V_2 can be calculated as the average between V_1 and V_3:

$$\dot{m} = \rho A_2 V_2 = \rho A_2 (V_1 + V_3)/2$$

The equation of the energy taken from the wind can be expressed adding a new concept, the Cp (coefficient of power):

$$Eex = \tfrac{1}{2} \rho A V_\infty^3 Cp$$

It means the power taken from the wind is the power that the wind has, multiplied by the coefficient Cp.

This coefficient depends on the V_3/V_1,

$Cp = P/Pmax = ½(1-(V_3/V_1)^2)(1+(V_3/V_1))$
$(P)P_{obtained} = ¼(\rho\ Ar(V_1^2 - V_2^2)\ (V_1+V_2)/2)$
$(P_{max})P_{max} = ½\rho Ar V_1^3$
so we can find the maximum value, making the first derived with this coefficient,

we get the maximum with $V_1 = ⅓\ V_3$
this maximum is Cp = 16/27 = 0.593

This means that with an ideal rotor is just possible to take the 59.3% of the energy of the wind, so this is the limit for the research, and it is the goal of the scientist that are working to improve the wind machines.

The rotor is inside the flow of the wind, the force that is generated has a projection in the direction of the wind whose name is resistance, and there is another projection in the perpendicular direction whose name is lift. A rotor moves because of these forces.

Wind rotor parameters

The parameter $\lambda = U / V_\infty$ gives a measure of the relation between the coefficient of power and the coefficient of torque. U is the peripheral speed and V_∞ the speed of the wind. $Cp = Cm\ \lambda$.
The parameters that we need in a turbine is the power and the torque that they have a relation $P = \omega\ M$ where ω is the angular velocity.
These coefficients Cp and Cm are dimensionless and show the percentage of power and the percentage of torque taken from the wind.

$Cp = P / (½\rho V_\infty^3 Sref)$ $Cm = M / (½\rho V_\infty^2 Sref\ Rm)$

Sref is a reference surface.
P is the density of the air.
Rm is the radius of the machine.

The graphics $Cp(\lambda)$ and $Cm(\lambda)$ represent the way of running of any turbine.
Obviously if we have the relation $Cp(\lambda)$, we have the relation $Cm(\lambda)$.

Devices that work by resistance

The reference is a profile that works under resistance, which is in the middle of the wind with speed V_∞.
Over the device there is a force per distance, in the same direction of the wind.
The profile has a peripheral speed U.

The profile sees the wind in movement, it means, there is a relative speed between the profile and the wind. This speed is $W = V_\infty - U$
The power that the wind gives to the device is $P = D*l*U$

The force D*l is a force of resistance and it is proportional to the kinetic energy, to the density and to a coefficient of resistance Cd:

$$Dl = Cd\tfrac{1}{2}\rho W^2 A$$

The power P will be:

$$P = \tfrac{1}{2}\rho W^2 AcdU$$

The power that we have as a reference can be expressed in the same way:

$$Pd = \tfrac{1}{2}\rho V_\infty^3 A.$$

The coefficient of power of a profile that works under resistance is:

$$Cp,d = P/Pd = Cd\,(W^2U / V_\infty^3) = Cd\,(1 - \lambda^2)\,\lambda$$

The coefficient Cp,d is the same that we said in the previous point, but just for profile of resistance.
Obviously, the parameter λ have values just between 0 and 1, because the wind cannot push faster an object than its own speed.
If we derive the equation of Cp,d respect λ, to find the maximum value, we find the value in $\lambda = \tfrac{1}{3}$.

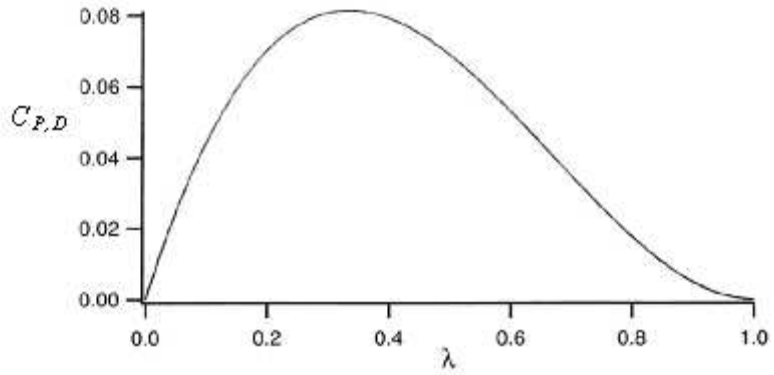

Fig. 15. Relation between λ – $C_{P,D}$

Lift devices

We consider now a wind turbine that works with a force that try to lift the turbine. It means that the profile is like a wing. The profile rotates in a perpendicular surface with a speed U. The wind runs over the profile with a speed V_∞ so the profile has a speed respect the wind W.

$$W = V_\infty - U$$

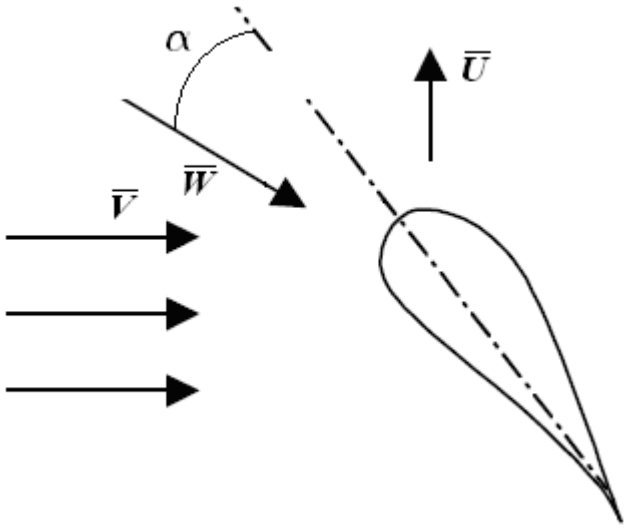

Fig. 16. Velocity vectors in the profile

In this picture α is the angle between the axis of the profile and the direction of the relative speed. If the speed U is constant, this angle gets bigger if the speed of the wind is bigger.

When the airfoil is invested by the flow, velocity distribution around the profile is not symmetric. The speed is less IN the bottom of the profile (pressure side) than that of the top (suction side).
In this way it is determined that the pressure distribution is not symmetrical, with higher values on the pressure side compared to those on the suction side.
In relation to this pressure distribution, we get a force F along the length. This force can be separated in two components: one in the direction of the speed W and another in the perpendicular direction of W.

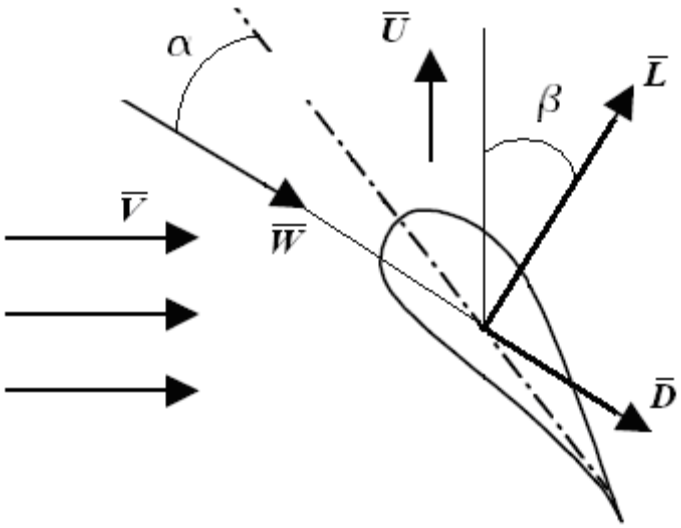

Fig. 17. Velocities and forces in the profile

The component D is named resistance and the component L is named lift. The power P given from the wind to the profile is produced by both forces.

$$P = (L \cos\beta\, l - D \sin\beta\, l)U$$

β is the angle between the speed U and the lift L.

$$L\, l = Cl\, (½\rho W^2)A$$

Cl is a coefficient of power, but the power produced by the force L.

It is the same with the force D

$$Dl = Cd(½\rho W^2)A$$

Cl and Cd depend on the angle α. The lift gets higher with the angle of attach, until this angle is so big that it is necessary to stop the turbine.
In this condition the lift is zero and the resistance keeps the turbine still.
The point of application of this force is placed on the chord of the profile to about a quarter from the leading edge. If the angle of attack is less than 15º, the force that produces power is only the lift power.
The devices of lift are more efficient because of the speed W is higher, it means that the rotor is faster than the proper wind, for this reason the lift devices are better than the resistance devices.
The lift devices has a parameter λ always higher than 1.

Therefore, we have:

$Pd = \frac{1}{2}\rho V_\infty^3 A$

$Cp,p = P / Pd = (Cl\ W^2 \cos\beta - Cd\ W^2 \sin\beta) / V_\infty^3 = W^2U\ (Cl \cos\beta - Cd \sin\beta) / V_\infty^3$

According to the triangle of speeds.

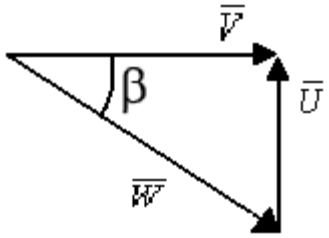

Fig 18. Triangle of velocities

$\lambda = U / V_\infty = \tan\beta \quad ; \quad W^2 = V_\infty^2 + U^2 \quad ; \quad V_\infty = W \cos\beta$

To sum up:

$$W / V_\infty = \sqrt{1 + \left(\frac{U}{V}\right)^2} = \sqrt{1 + \lambda^2}$$

$\cos\beta = V_\infty / W$

If we simplify the equation of Cp.

$Cp,p = (1+\lambda^2)\ (Cl - Cd\ \lambda)\ \lambda$ in this expression $\lambda > 1$

There are two coefficients, because there are two forces that produce power.

This is the graph that shows the relation between Cp,p and λ.

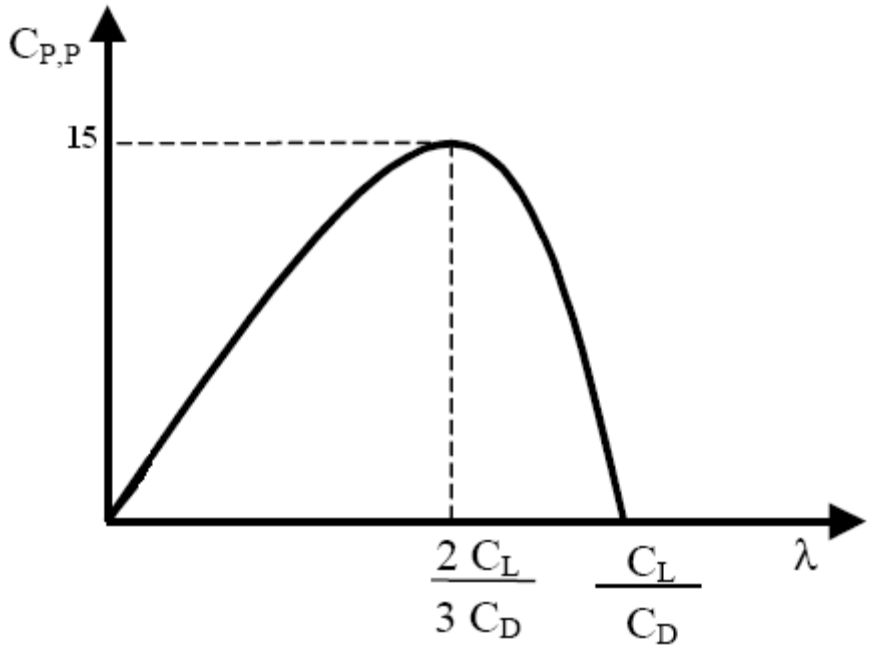

Fig. 19. Relation between $C_{P,P}$ - λ

The maximum value is λ = ⅔ (Cl / Cd)

The maximum value for lift devices is about 15, and the maximum value for resistance devices is 0.3, so the lift devices has a power 45 times higher than the resistance devices.

6. Description of the Savonius rotor

Savonius wind turbines are a type of vertical-axis wind turbine, Savonius rotor is simple in structure, has good starting characteristics, relatively low operating speeds, and an ability to accept wind from any direction. Its aerodynamic efficiency is lower than that of other types of wind turbines, such as Darrieus and propeller rotors of horizontal axis.

Physical description

The Savonius turbine has a vertical axis, where it is connected the electrical generator without any necessity of gearbox, only if we want to reduce or increase the speed.

The axis is a cylinder of a small diameter. From the cylinder are connected the buckets, the buckets can be two or three. On the upper part and on the lower part there are cylinders that delimit the buckets. These cylinders have big diameters, as big as the diameter of both buckets and a low thickness.

The materials used to make this kind of turbine are usually steal for the structure and aluminum for the buckets, sometimes to make some experiments the material used is any kind of polymer.

Fig. 20. Savonius rotor

Working description

The necessary torque for the Savonius turbine is very small; in fact we can consider that any torque can produce any movement in the Savonius turbine. The only thing that the starting torque needs to beat is the friction between the different devices of the turbine such as the axis with electrical generator.

The Cp (power coefficient) of a Savonius rotor has many values according with many experiments, but it is normally very low; about 0.2. That is because of the high friction between the air and the buckets which are against the wind. One bucket is working for the wind and the others are working against the wind.

If we compare these data with the rotors usually used in the big farms, we realize that a Savonius rotor should not be used for big farms, because the common HAWT has a Cp of 0.4 and now new research are getting Cp of 0.48. (Limit is 0.593).

If we compare Savonius rotor with Darrieus rotor we find out that Savonius is the worst about efficiency; in fact some research has got a Cp of 0.35 for the Darrieus rotor. If we compare with Savonius rotor the efficiency is almost the double. It is important to improve the Cp, make a gap in the design between the buckets, as the picture shows. With this gap we get that air makes an effect of pull from the bucket which is doing the friction, but we have to think that that gap reduce the amount of air that push the main bucket, so this gap is one of the parameters of the design.

Other thing that involves a change in the Cp is the material and how it is made this material, because the friction depends also of the friction between the air and the bucket.

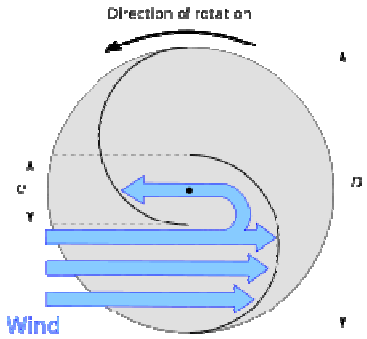

Fig. 21. Savonius working

Advantages and uses

We have said the disadvantages of the Savonius rotor, but it is just one, the Cp is very reduced. It is the most important but Savonius has many advantages that can make this kind of turbine a good method to get energy.

The design and the production of the Savonius rotor is very easy. That is an advantage in the developed countries because the cost is reduced, but this is more important in the underdeveloped countries because many areas of these countries do not have the necessary technology to produce another kind of turbines. In fact, there are many research that test turbines made of exotic materials like bamboo[3].

Another advantage is the high torque that this engine is able to give, that makes this kind of turbine useful for other different uses than the production of energy, for example the Savonius turbine is used in pumping systems.

7. DiMeG's Wind Gallery.

DiMeG's wind gallery is a closed circuit that is 30 meters long and it has the following parts:

- 1 m^2 section's test chamber.
- 4 mm thick steel walls.
- Rectangular floor with 4 curves at 90°.
- Test chamber with transparent Plexiglas's walls with an inspection's window.
- Test section's top speed: 40 m/s approximately.
- Fan driven by an electric motor rated in 55 kW.
- Honeycomb's mesh upstream to control the turbulence in the test chamber and to straighten the flow.
- Guide vanes to better guide the flow and reduce the pressure drop.

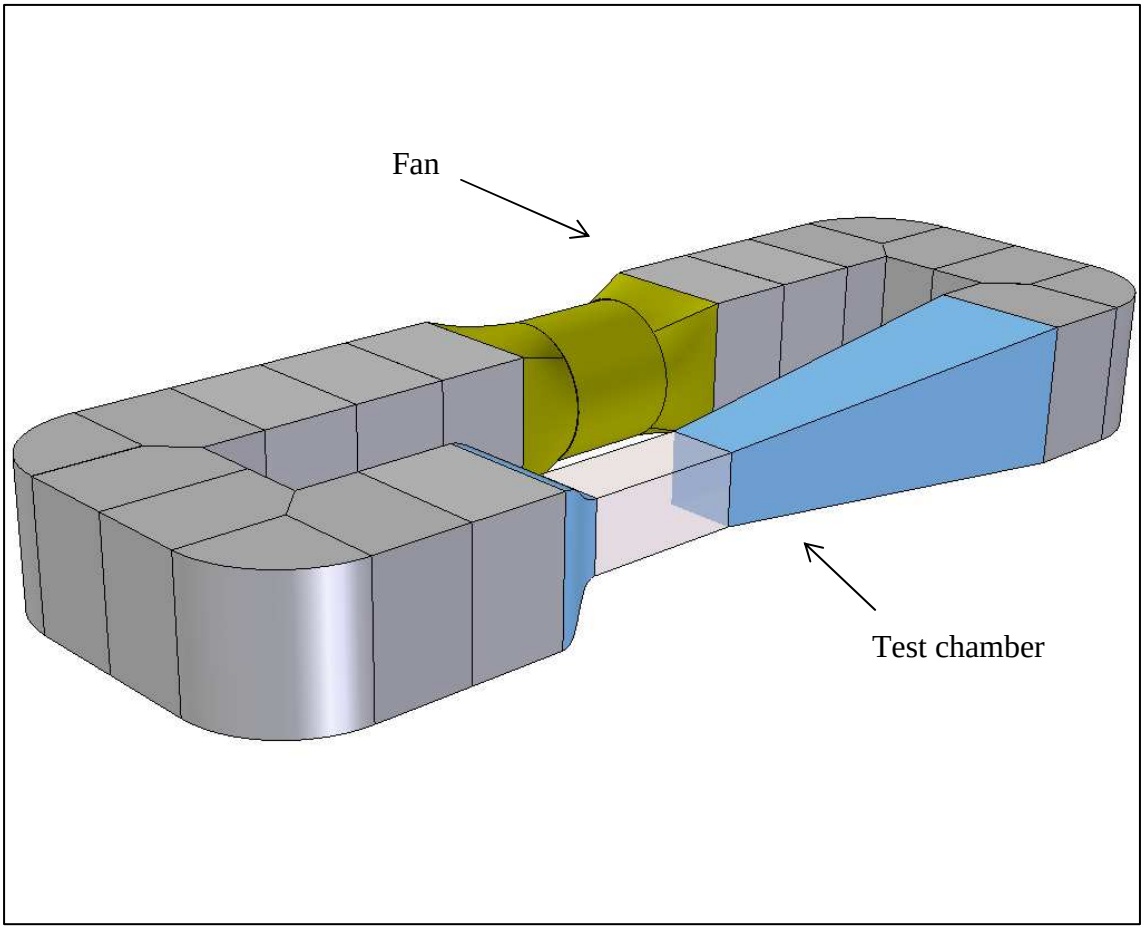

Fig. 22. Wind Gallery's Rendering 3D

In the picture we can see test chamber and fan's relative position, the next picture we can see wind gallery's position inside DiMeG's laboratory.

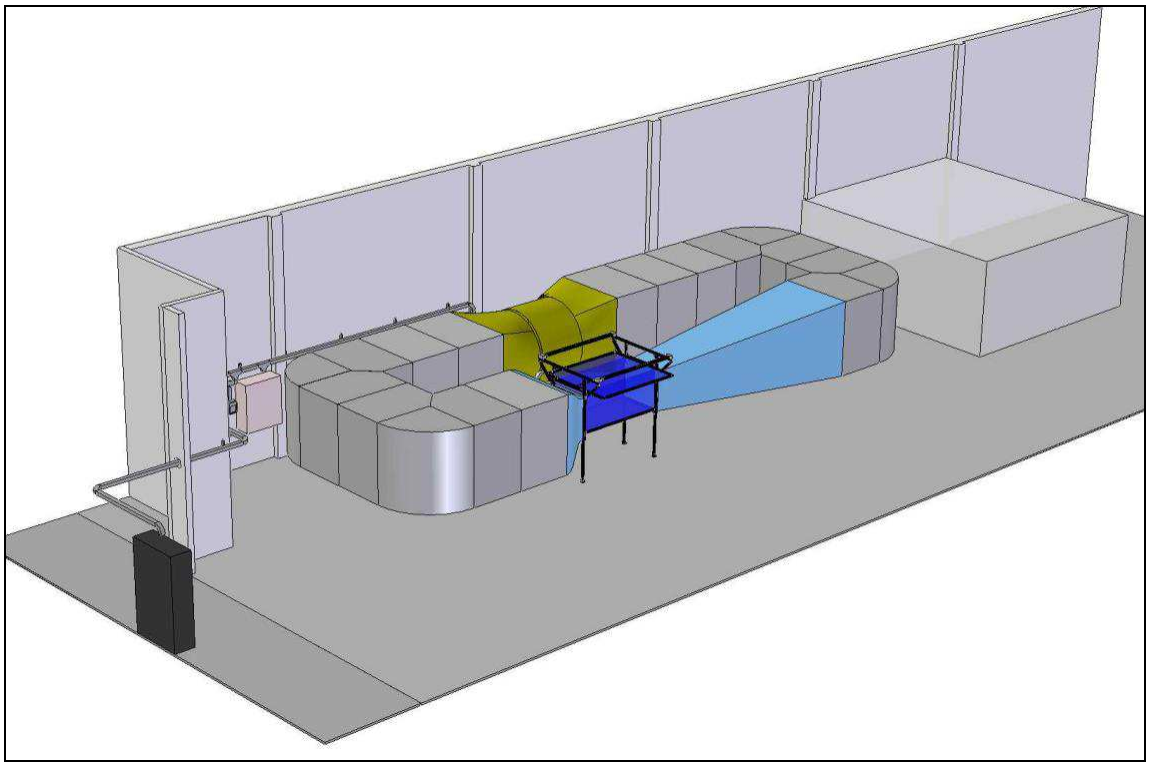

Fig. 23. Wind Gallery in DiMeG's laboratory

DiMeG's wind gallery is a multi-purpose gallery which allows the study of aerodynamic profiles or the study of structures and profile of vehicle's aero elasticity.

In particular, it's equipped for "performance experimental analysis" of wind turbines' prototypes, study profiles, optimizing wind turbines' layout in a power plant.

A key parameter in a wind tunnel is "the energy ratio (E_R)" which is defined as:

$$E_R = \frac{P_t}{P_c}$$

P_t: Power flow in test chamber.

P_c: Power lost in the circuit because of location and distribution.

E_R value for a closed gallery is very high and this allows a significant energy saving in the test compared to an open circuit tunnel.

The tunnel is on a rectangular perimeter shape with a total length of 30 meters, this length is the necessary to ensure a uniform flow in the section between the fan and measurement section.

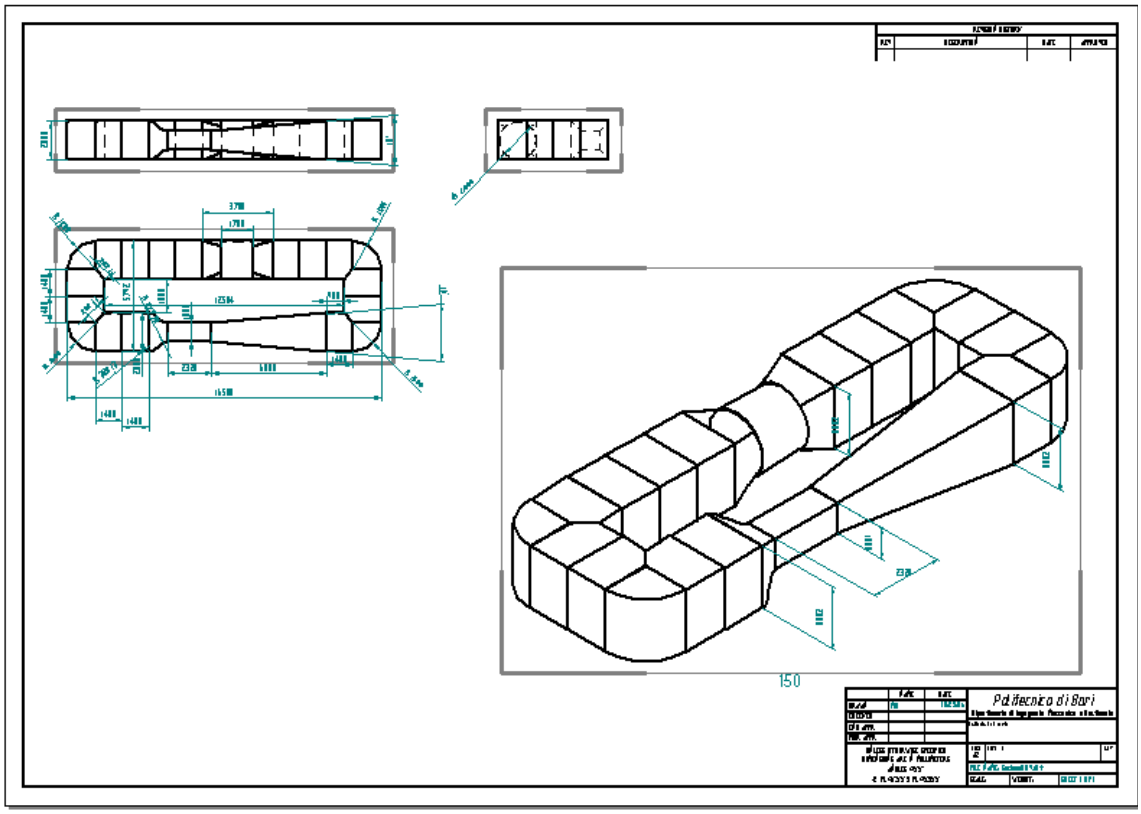

Fig. 24. Wind gallery's design project

The tunnel is divided in 4 zones:

1. The first one, downstream of the test chamber, includes a rectangular section increasing whose task is to recover kinetic energy's part, followed by two bends 90º, which mission is to transport the flow to the fan.

   Upstream of the fan there are provided the holes that prevent tunnel's pressurization that could be generate (in steady state) because of the air circulating's heating.

2. The second one is represented by an axial type fan, powered by a three-phase 3-pole pairs mounted on a special seat inside a cylinder duct that encloses the rotor.

   The fan control is through the variation of the revolution's number of a driving machine. The motor's speed is varied by adjusting the feeding's frequency of three-phase voltage. The fan control allows obtaining variable flow rates in the test section so it can recreate the desired operating conditions in the test chamber.

3. The third zone, located downstream from the fan, comprised two curved sections with curvilinear profiles' arrays that allow the flow's curvature without introducing distortion or significant secondary flows.

   In the convergent duct, which has a contraction ratio of 4:1, the flow accelerates to the rated speed on the test area's input section.

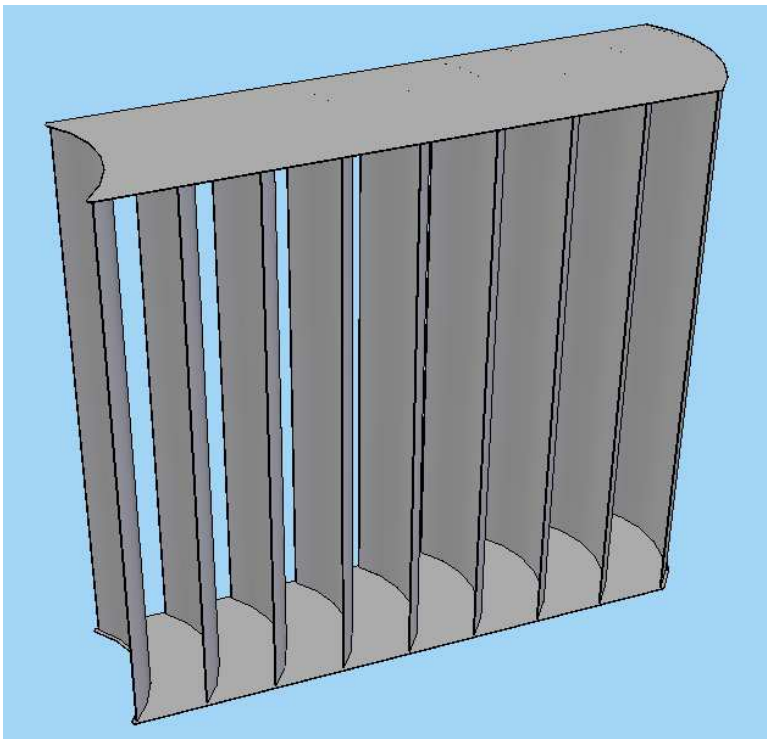

Fig. 25. Corner aerodynamic deflectors that direct the flow curve in

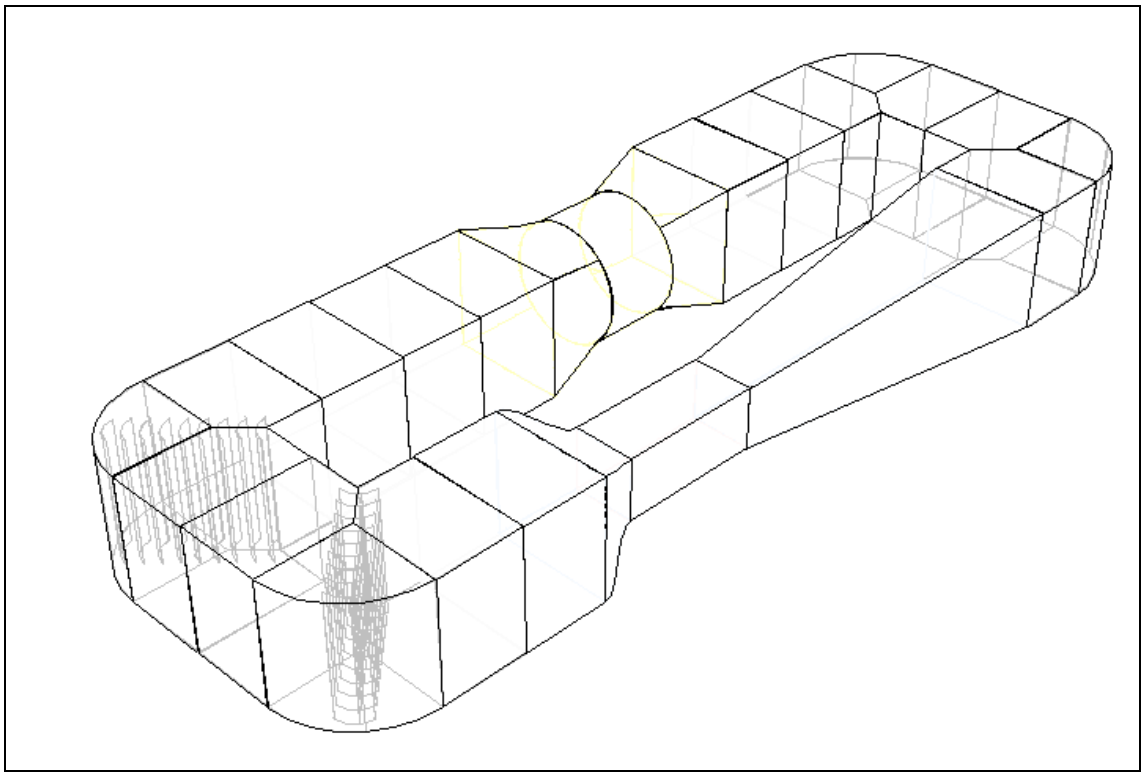

Fig. 26. Blades' position angle in the wind tunnel.

Before converging duct there is a honeycomb panel (shown in Fig. 6) to obtain a uniform flow, without any macro turbulence.

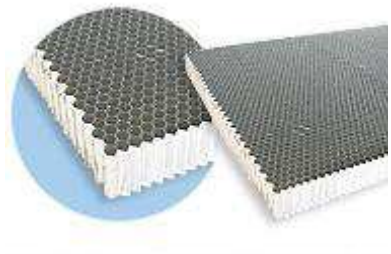

Fig. 27.Honeycomb

4. The fourth zone is the test section, which is composed of a 2.32 meters length duct with a square section (1x1 m^2). The side walls are made of plolymethylmathacrylate (commercially known as Plexiglas) transparent.

   This material makes the test chamber compatible with the measuring instruments' use such as non-intrusive laser, the PIV, acoustic Doppler instruments, etc.

The next pictures show the test chamber's detail, the transparent walls, the frame and the inspection's door.

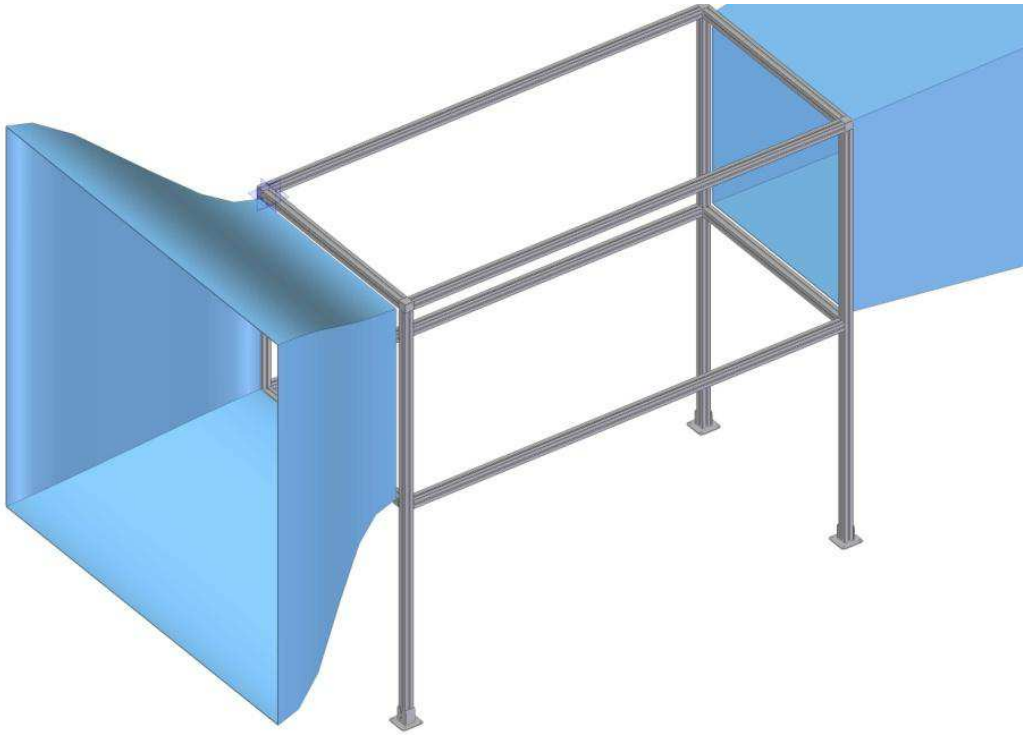

Fig. 29. Test chamber's frame.

Fig. 30. Test chamber

The structure consists of an aluminum frame formed by Rexroth's sections:

Fig. 31. Test chamber and frame structure.

Inside the test chamber is placed the vertical wind turbine's axis, the subject of this project is the Savonius turbine.

DiMeG's wind tunnel has been designed according the highest standard and using modern analytical methods for profiles' development. Particular attention was also dedicated to the ducts' design, the surface finish and the assemble of the different components.

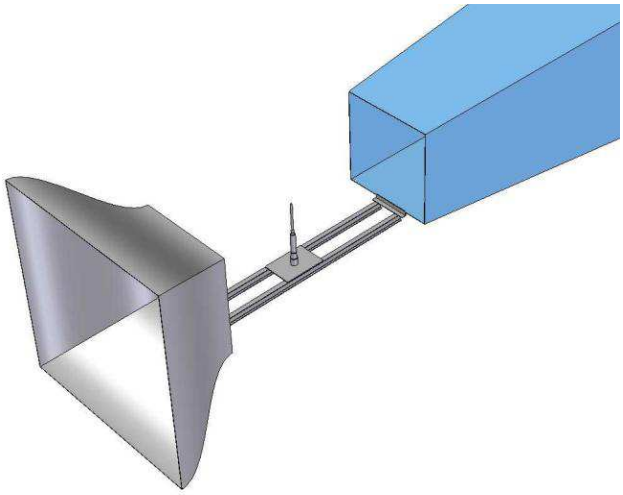

Fig. 32. Test section's detail: wind turbine's rotating axis.

Electric Fan

The fan is an axial fan and its characteristics are listed in the table below:

Table 1: DiMeG Axial fan's characteristics

Model	*Q [m^3/s]*	*P_{ass} [kW]*	*Electric Motor V400/50Hz*	*Blades' number*
AD2000-280M-06	*60*	*47*	*280M-55 kW-6p*	*4*

The impeller has the following characteristics:

- Impeller directly coupled (model AF35-2000-06), with aluminum blades, stationary and a variable pitch hub with keyway for connection to the engine. (Fig. 11)
- Hot-dip galvanized steel body. (Fig. 12)
- Rubber expansion joint bellows (150 mm length).
- Fitting framework for the gallery link in galvanized steel (1165 mm length).
- Resistant vertical supports.
- Phase induction motor, V400/55 Hz 55 kW, with servo ventilation fan.

Fig. 33. Axial electrical fan

Fig. 34. Electrical fan's external body

Fan Control

The fan's steering system (Fig. 13) consists of a complete control panel with speed controller for variable torque induction motors (inverter vector).

The framework's features are shown in the table below:

Table 2: Electric panel control's features

Dimensions	*1050x570x406, weight 110 kg*
Power	*3Ph 55Kw 380V-10% to 460V+10%*
Current rating	*105 A*
Max current to the motor	*116Ax60sec*
Output frequency	*0....500Hz*
Protection	*IP54 cabinet*

The framework includes an inverter with integrated EMC filter, a choke line, a switch-disconnected control external front, a potentiometer to adjust the frequency phase, keyboard, programming and remote view from the front panel.

The inverter-framework is also full of:

- Multiple connecting RS485 MODBUS RTU serial connection to PC, or remote keypad, or microprocessor card.
- Connection kit for PC serial port for calibration and control inverter.
- Emergency button.
- External breaking resistance (5s, IP30, 5 Ω, 1 kW) for emergency stop.

Fig. 35. Electric control panel's detail

The fan control can be done in three different ways:

- Manually from the control panel.
- Via software using the RS485 serial link for communication with the PC via Rack PowerSuite Software.
- Via software using the RS485 serial link for communication with the PC via Rack of Wind Tunnel in LabView 8.2.

Manual operation is performed acting on the potentiometer that is shown in PowerSuite software supplied with the fan which allows also the basic parameters' variation of operations (stopping time, acceleration in the starting phase, etc.).

Operating under LabView will be showed in other part of the project.

8. Description of the robot

The test chamber is equipped with a three-axis Cartesian robot. It is positioned above the test chamber and used for the probes or sensors' handling introduced inside the test volume to measure. The probes or sensors are properly bound to the robot arm, which moves inside test chamber volume.

In the present work it was used to place the probe CTA in the useful volume of the test chamber.

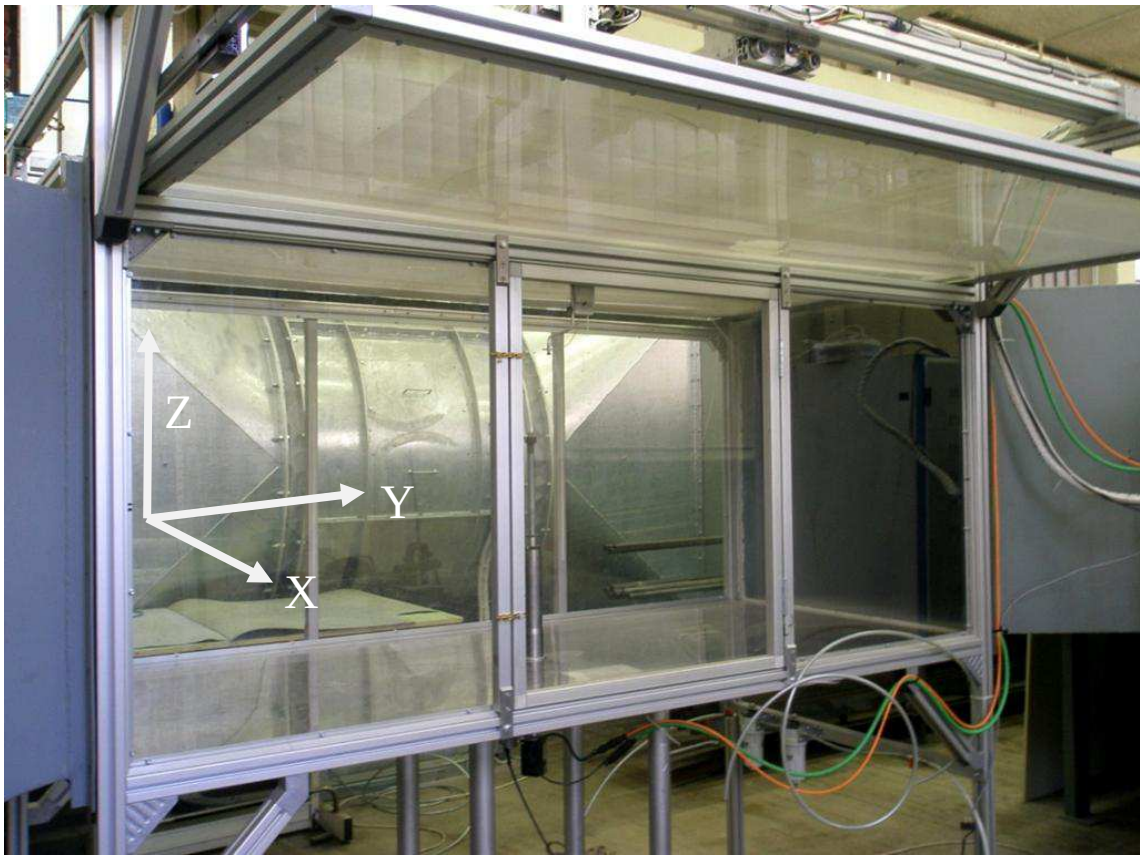

Fig. 36. Robot arm and reference system handling

In the last picture you can see the Cartesian robot arm positioned at the top of the test chamber. The arm can move along the three directions xyz visible in the illustration. The reference's direction and position is the one that was chosen and that is conventionally used in the robot's handling software in LabView environment.

The arm's movement is obtained by a chain drive and motion transmission on the three independent directions, the next picture shows the robot with the chains.

Fig. 37. Robot handling

Test chamber's coverage is a mobile Plexiglas' plate that has a longitudinal opening that allows robot arm's vertical movement in the test chamber. The movement along X is obtained moving the arm and the mobile plate in the test chamber's roof. At the same time the electric motor transmits motion to a toothed belt that drives the vertical arm and the movable plate along the guide section (shown in the next picture).

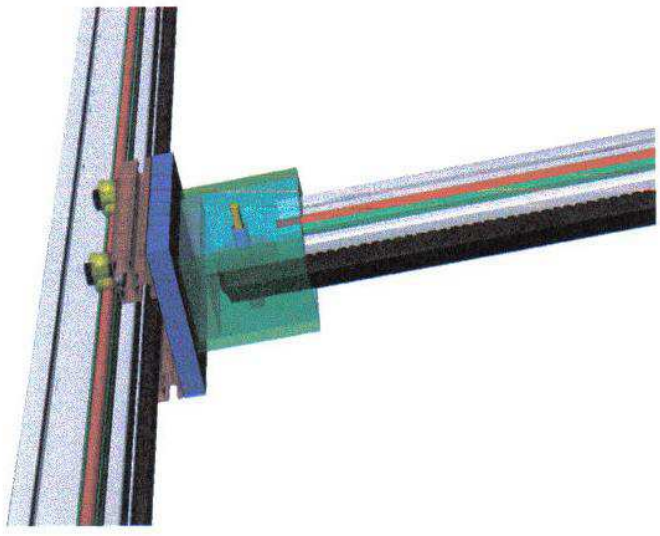

Fig. 38. Special joint to move the X-axis

The Y-axis is moving on to handle the set-arm cross-section along the two guides in y direction. During the cover plate's movement doesn't move and the arm moves along the longitudinal slot. The movement is driven by two electric motors visible in the bottom right and bottom left. The drive, again, is done with timing belts that engage with a gear keyed on the same shaft engine. The two motors' drive is designed in the way that they work perfectly synchronized and applying the same torque so as not to cause locking during group's movement.

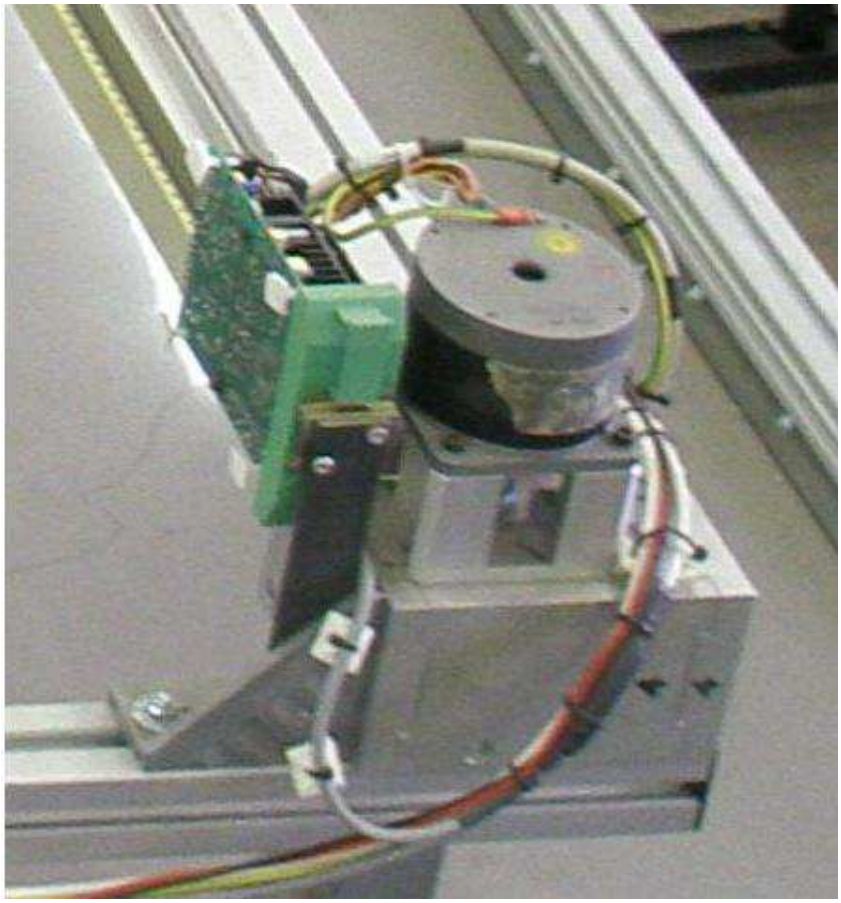

Fig. 39. Stepper motor

The movement along Z consists of moving the arm vertically when the cover plate is moving the cross section. The drive in this case is more difficult: a helical wheel driven by the electric motor engage with a worm. The worm transmits motion to a toothed wheel (represented in green in the next picture) that engage with a rack fixed to the vertical arm.

The link between the worm and the toothed wheel is designed to ensure the irreversible motion. This allows the motor-arm's support when the engine is off.

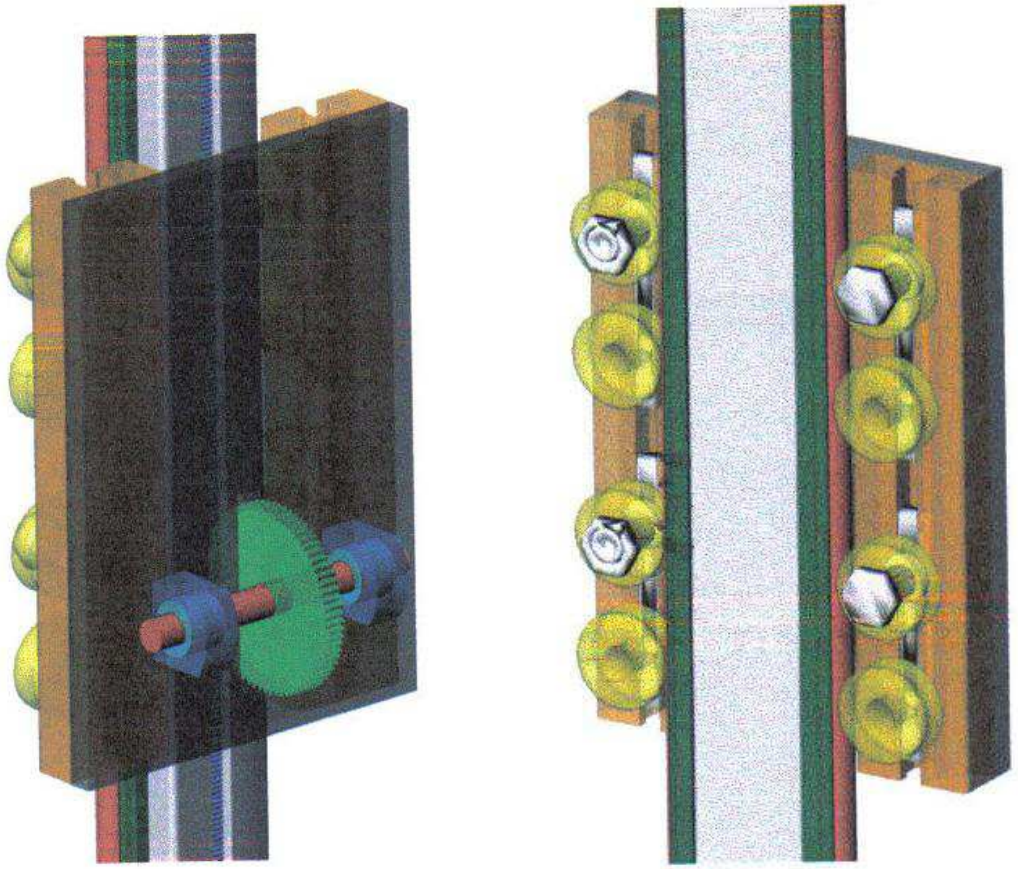

Fig. 40.Special link for Z-axis movement

Operating the robot

The movement is obtained via a command's open chain that can be schematized as follows:

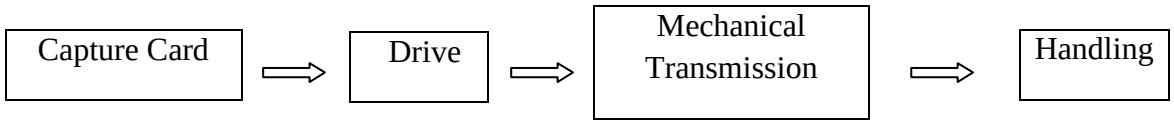

Fig. 41. Movement map

Robot's movement is running by software developed with LabView 8.2. This software interacts with the acquisition card DAQ (Data & Acquisition). The acquisition card generates and sends an electrical pulses' train to the control board, which transform the pulse train in stepper motor's angular rotations.

Stepper motor's angular rotations are transformed into a linear movement through mechanical transmission. This transmission, as it has been explained before, it's different for each axis.

Command's chain is open, so there is a feedback system and a feedback control on the movement. Position's control during the experiment is only available by software, and it's been explained below.

The motor's drive uses 1 control card and 3 pilotage cards. This is shown in the next picture:

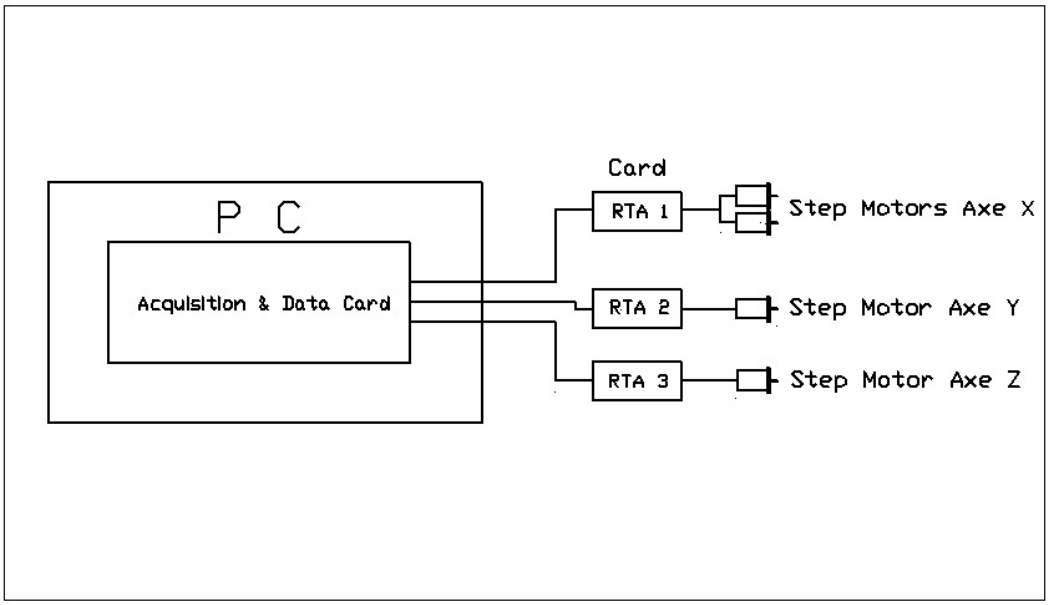

Fig. 42. Control and pilotage cards

Stepper motors are, therefore, electromechanical transducers that convert control electrical impulses in programmable incremental angular rotations. All motor windings are located on the stator, and the rotor is a permanent magnet made of soft iron.

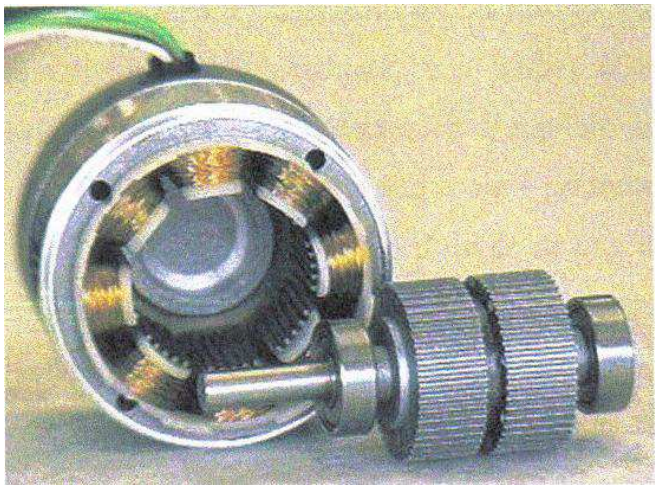

Fig. 43. Step motor

Driver cards, besides convert the pulses driving stepper motor in rotation, manage the dynamics of the motors' movement: speed and acceleration. The cards are RTA series HDG's cards.

Engines are all the same type but based on the workloads to be handled can develop different torque:

- The engines (2 engines) for the X axis develop a 4.8 Nm torque.
- The engines for Y and Z axis develop a 2.8 Nm torque.

It's noted that to move the robot along X axis it's necessary to use two engines because these motors have to do the mobile roof's movement and the arm's movement.

Table 3: Features Stepper motors

		Y, Z motors	***X motors***
Step angle		*1.8º/0.9º*	*1.8º/0.9º*
Precision %		*±0.05*	*±0.05*
Tightening torque	*Unipolar*	*2.2 Nm*	*3.8 Nm*
	Bipolar	*2.8 Nm*	*4.8 Nm*
Rotor inertia		*0.64 kgcm^2*	*1.2 kgcm^2*
Conductors		*8*	*8*
Link details	*Unipolar*	*Yes*	*Yes*
	Bipolar series	*Yes*	*Yes*
	Bipolar parallel	*Yes*	*Yes*
Rated current per phase	*Unipolar*	*4.3 A*	*4.3 A*
	Bipolar series	*3.0 A*	*3.0 A*
	Bipolar parallel	*6.0 A*	*6.0 A*
Resistance per phase		*55 mΩ*	*750 mΩ*
Inductance per phase		*2.1 mΩ*	*3.5 mΩ*
Dimensions	*Length [mm]*	*67*	*94*
	Depth [mm]	*73*	*73*
	Width [mm]	*73*	*73*
	Diameter [mm]	*8*	*8*

9. Probes[15]

Hot-wire anemometers:

Hot wire anemometers use a very fine wire (on the order of several micrometres) electrically heated up to some temperature above the ambient. Air flowing past the wire has a cooling effect on the wire. As the electrical resistance of most metals is dependent upon the temperature of the metal (tungsten is a popular choice for hot-wires), a relationship can be obtained between the resistance of the wire and the flow speed.

Several ways of implementing this exist, and hot-wire devices can be further classified as CCA (Constant-Current Anemometer), CVA (Constant-Voltage Anemometer) and CTA (Constant-Temperature Anemometer). We have always used CTA's. The voltage output from these anemometers is thus the result of some sort of circuit within the device trying to maintain the specific variable (current, voltage or temperature) constant.

Hot-wire anemometers, while extremely delicate, have extremely high frequency-response and fine spatial resolution compared to other measurement methods, and as such are almost universally employed for the detailed study of turbulent flows, or any flow in which rapid velocity fluctuations are of interest.

Probes:

In general, a probe consists of the following:

- Sensor, forming the heating element.
- Sensor supports (prongs or substrate), carrying the sensor and leading current to it.
- Probe body, carrying the sensor supports.
- Connector, providing electrical connection to the probe support or probe cable.

Probes may have one, two or three sensors for use in one-, two- or three-dimensional flows. Each sensor requires its own anemometer bridge.

The sensor may be either a thin wire suspended between the prongs or a thin metal film deposited on an electrically insulating substrate. Film sensors (not used by us) can be cylindrical (fiber-film probes) or non-cylindrical (film probes). Wire sensors (used by us) are used in gases and in non-conducting liquids, while film sensors are primarily designed for use in water and other conducting liquids.

The sensor materials are selected to provide maximum flow sensitivity and highest possible mechanical strength with a minimum of thermal inertia. The size of the sensor and its mounting are selected to give minimal disturbance of the flow.

Most probe types are available with different prong or substrate configurations covering wide variety applications.

Wire probes: Wires are used as sensors in probes for measurements in air and other gases at velocities from a few cm/s up to supersonic velocities. In addition, the may be used in non-conducting liquids at low velocities.

Wire sensors have high flow sensitivity and the highest frequency response. On the other hand, the mechanical strength is limited and they are quite sensitive to particle contamination.

The sensor supports, or prongs, are made of stainless and tapered, providing an end surface of around 0.1 mm in diameter to which the wires are spot welded.

- **55P11:**

It's a single-sensor miniature wire probe.

Miniature wire probes have 5 µm diameter, 1.25 mm long platinum-plated tungsten wire sensors. The wires are welded directly to the prongs and the entire wire length acts as a sensor.

The probe body is a 1.9 mm diameter ceramic tube, equipped with gold-plated connector pins that connect to the probe supports by means of plug-and-socket arrangements.

They are general purpose probes recommended for most measurements in one-dimensional flows of low turbulence intensity. The accuracy of turbulence measurements may be reduced because of interference from the prongs. On the other hand, the more rigid construction makes them more suitable for high speed applications without the risk of self-oscillation. The probes are the cheapest in the Dantec Dynamics program and are straightforward to repair.

Table 4. Techical data for miniature wire sensors:

Medium	Air
Sensor material	Platinum-plated tungsten
Sensor dimensions	5 µm dia, 1.25 mm long
Sensor resistance R20 (approx)	3.5 Ω
Temperature coefficient of resistance (TCR) α 20 (approx.)	0.36%/°C
Max. sensor temperatura	300°C
Max. ambient temperatura	150°C

Max. ambient pressure	Depends on the type of mounting
Min. Velocity	0.05 m/s
Max. Velocity	500 m/s
Frequency limit fcpo (CCA mode, 0 m/s)	90 Hz
Frequency limit fmax (CTA mode)	400 kHz

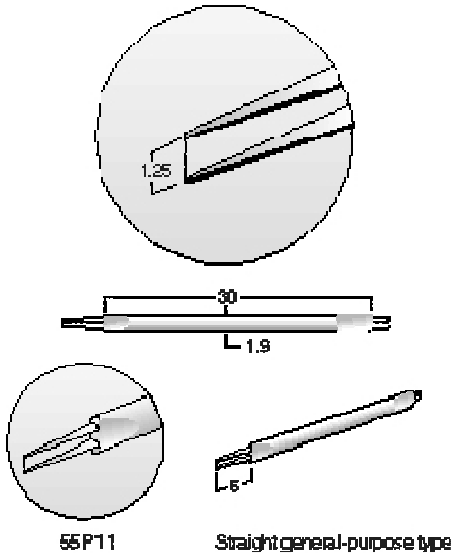

Fig. 44. 55 P11 Probe (Images by Dantec Dynamics)

Fig. 45. 55 P11 Probe (Picture by Davide Francesco De Fazio)

- **55P01:**

It's a single-sensor Gold-plated wire probe.

Gold-plated probes have 5 µm diameter, 3 mm long platinum-plated tungsten wire sensors. The wire ends are copper-plated and gold-plated to a thickness of 15 to 20 µm, leaving an active sensor, 1.25 mm, on the middle of the wire.

The probe body is a 1.9 mm diameter ceramic tube, equipped with gold-plated connector pins that connect to the probe supports by means of plug-and-socket arrangements.

They are designed for measurements in high-turbulence flows of one-dimension. The plating of the ends serves the dual purpose of accurately defining the sensing length and reducing the amount of heat dissipated by the prongs. This results in a much more uniform temperature along the wire than is the case for miniature wires. Another advantage is less flow interference from the prongs at the point of measurement due to the wider prong spacing. Both increase the accuracy at high turbulence levels.

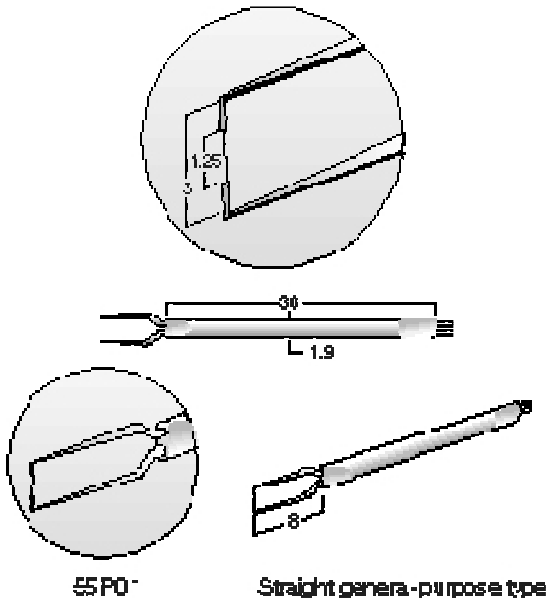

Fig. 46. 55P01 Probe (Images by Dantec Dynamics)

Fig. 47. 55P01 Probe (Picture by Luigi Di Leo)

Single sensor probes use 4 mm. probe supports. We have used the 55H20.

The supports consist of a coupling ring with an internal rubber ring that provides a water- and pressure-tight sealing, and one set of contacts embedded in a cylindrical body that ends in one Teflon-coated cable with detachable BNC connector. Outside probe support diameter is 4 mm.

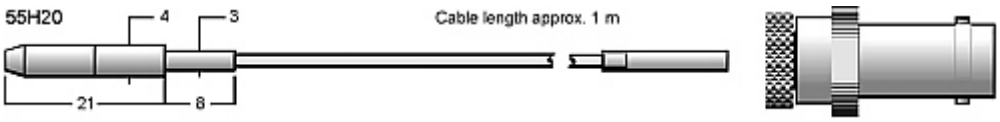

Fig. 48. Probe support 55H20. (Image by Dantec Dynamics)

- **55P51:**

It's a dual-sensor gold-plated wire probe.

Gold-plated wire probes have 5 µm diameter, 3 mm long platinum-plated tungsten wire sensors. The wire ends are copper- and gold-plated to a thickness of 15 to 20 µm, leaving an active sensor, 1.25 mm, on the middle of the wire.

The sensors are arranged in X-arrays, where they form an angle of 90° with one another. The probe body is a 2.3 mm diameter ceramic tube, equipped with gold-plated connector pins that connect to the probe supports by means of plug-and-socket arrangements. Dual-sensor probes have marks (one and two dots) that indicate the sensor number.

The Dual-sensor probes are designed for use in dual-sensor high-turbulence flows. The plating of the ends serves the dual purpose of accurately defining the sensing length and reducing the amount of heat dissipated by the prongs. This results in a much more uniform temperature along the wire than is the case for miniature wires. Another advantage is less flow interference from the prongs at the point of measurement due to the wider prong spacing. Both increase the accuracy at high turbulence levels. All X-probes measure two velocity components simultaneously in turbulent, in stationary dual-sensor flow fields. They provide information for calculation of Reynolds shear stress. The flow vector may not exceed ±45°.

Table 5: Technical data for gold-plated wire sensors:

Medium	Air
Sensor material	Platinum-plated tungsten
Sensor dimensions	5 µm dia, 1.25 mm long The overall wire lenght is 3 mm
Sensor resistance R20 (approx.)	3.5 Ω
Temperature coefficient of resistance (TCR) α 20 (approx.)	0.36%/°C
Max. sensor temperature	300°C
Max. ambient temperature	150°C
Max. ambient pressure	Depends on the type of mounting
Min. velocity	0.05 m/s
Max. velocity	200 m/s
Frequency limit fcpo (CCA mode, 0 m/s)	90 Hz
Frequency limit fmax (CTA mode)	400 kHz

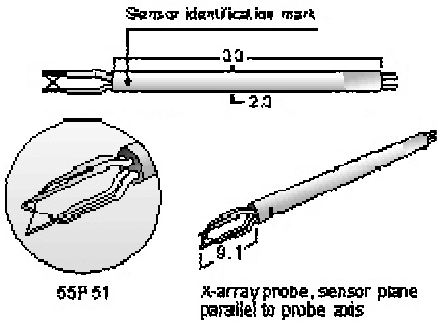

Fig. 49. 55P51 Probe (Images by Dantec Dynamics)

Dual sensor probes use 6 mm. probe supports. We have used the 55H24.

There are three probe support types available for dual-sensor probes: short, long straight and long right-angled. The supports consist of a coupling ring with an internal rubber ring that provides a water- and pressure-tight sealing, and two sets of contacts embedded in a cylindrical body that ends in one or two Teflon™ -coated cables with detachable BNC connectors.

Outside support diameters is 6 mm. The cables on dual-sensor supports are marked with one and two rings indicating the connector number corresponding to the sensor number on the probe.

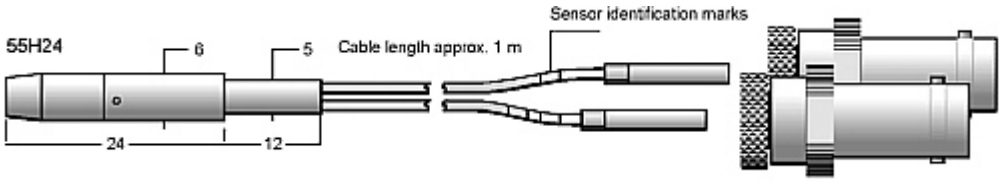

Fig. 50. Probe support 55H24 (Image by Dantec Dynamics)

Fig. 51. 55P51 Probe (Image by Luigi Di Leo)

Hot-wire calibrator:

The Dantec Dynamics Hot-Wire Calibrator is a simple, but accurate, device for 2-point calibration of most hot-wire probes used with Constant Temperature Anemometers. The calibrator produces a free jet, where the probe is placed during calibration. It requires a normal pressurized air supply and is able to set velocities from 0.5 m/s to 60 m/s.

It is primarily designed to provide two-point calibrations of standard wire probes, but can also be used for multi-point calibrations. By combining two sets of measured velocity-voltage values with a generic uni-curve transfer function it is possible to create a calibration function for an actual probe, which is valid for the entire velocity range.

Fig. 52. Calibrator (Images by Luigi Di Leo)

10. Compressed air line to the calibration process

The calibration system requires that the compressed air has some specific characteristics. These features are given by the manufacturer to limit the measurement uncertainty and to prolong the calibrator and probe CTA useful life. These are the requirements:

1. Flow over 400 Std l/min
2. Supply pressure between 6.5 and 8.5 bar.
3. Air quality PNEUROP 6611 Class 1

The system was designed to supply air compressed to the calibrator, using the air system already present in DiMeG's laboratory. In particular, the line comes from the laboratory's circular distribution. On the line were fitted valves and filters to bring the compressed air to the cleanliness' desired level.

Table 6: Air quality PNEUROP 6611 Class 1[14]

Particle size	*< 0.1 [e]*
Particle density	*< 0.1 [mg/m^3]*
Pressure dew point	*-40ºC*
Oil content	*< 0.01 [mg/m^3]*

**http://www.duncanrogers.com/literature/bekoflow_manual.pdf*

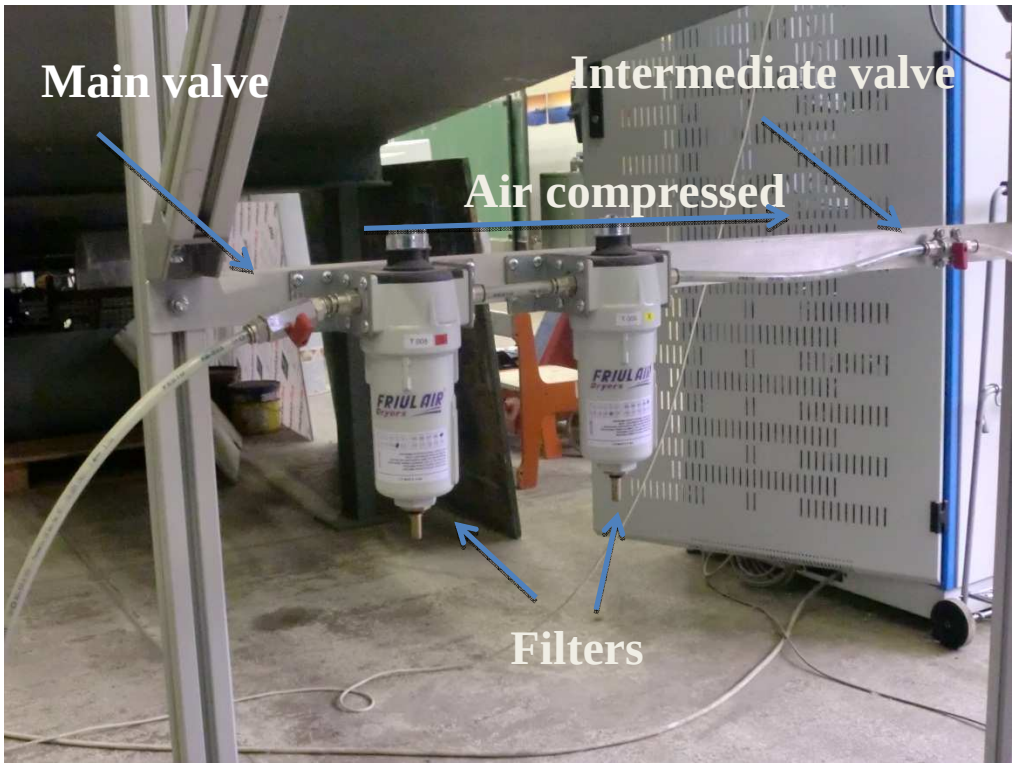

Fig. 53. Filters system

Fig. 54. DiMeG's air compressed system

As it's showed the system has two filters type powder/oil FRIULAIR with the following features:

Table 7: Friulair filters

Coarse Filter	
Code	*FT S 008*
Flow	*850 Std l/min*
Connections	*G $^{3}/_{8}$''*
Cartridge	*TS008*
Weight	*0,77 Kg*
Fine Filter	
Code	*FT X 008*
Flow	*850 Std l/min*
Connections	*G $^{3}/_{8}$''*
Cartridge	*TS008*
Weight	0,77 Kg

The first filter, coarse filter (Series S) can remove particles down to 1 micron, including oil and liquid, and it's used as a Grade X pre-filter. The air, after pass this filter, has a maximum residual oil: 0.1 mg/m^3. The fine filter (Series X) is a separator filter, which can remove oily and extremely small particles down to 0.01 micron (maximum residual oil: 0.01 mg/m^3).

At the end of the filtration system the oil-free air respect the characteristics required for the calibrator's proper functioning. The system also includes a main valve, whose task is to intercept the compressed air drawn from DiMeG's system, and a valve that is open when the calibration test must be done.

At the star of the compressed air system's circuit, a dryer (Friulair DFE 11) is used to eliminate the water content in this air. It ensures a 0ºC dew point.

11. Software – LabView

In order to handle all the avaliable tools such as the robot, we have to use software designed to work in a laboratory, this is Labview.

LabVIEW is a graphical programming environment; it is the most used by scientist and engineers all over the world.

Benefits of Graphical Programming

Like most people, engineers and scientists learn by seeing and processing images without any need for conscious contemplation. Many engineers and scientists can also be characterized as “visual thinkers,” meaning that they are especially adept at using visual processing to organize information. In other words, they think best in pictures. This is often reinforced in colleges and universities, where students are encouraged to model solutions to problems as process diagrams. However, most general-purpose programming languages require you to spend significant time learning the specific text-based syntax associated with that language and then map the structure of the language to the problem being solved. Graphical programming with G provides a more intuitive experience.

G code is typically easier for engineers and scientists to quickly understand because they are largely familiar with visualizing and even diagrammatically modeling processes and tasks in terms of block diagrams and flowcharts (which also follow the rules of data flow). In addition, because dataflow languages require you to base the structure of the program around the flow of data, you are encouraged to think in terms of the problem you need to solve. For example, a typical G program might first acquire several channels of temperature data, then pass the data to an analysis function, and, finally, write the analyzed data to disk. Overall, the flow of data and steps involved in this program are easy to understand within a LabVIEW diagram.

VI’s of the experiment

In this experiment two VI are necessary, one to handle the robot, and move it all over the gallery, and another one to turn on the fan and the servo of the rotor.

The next picture shows the block of the VI to handle the robot.

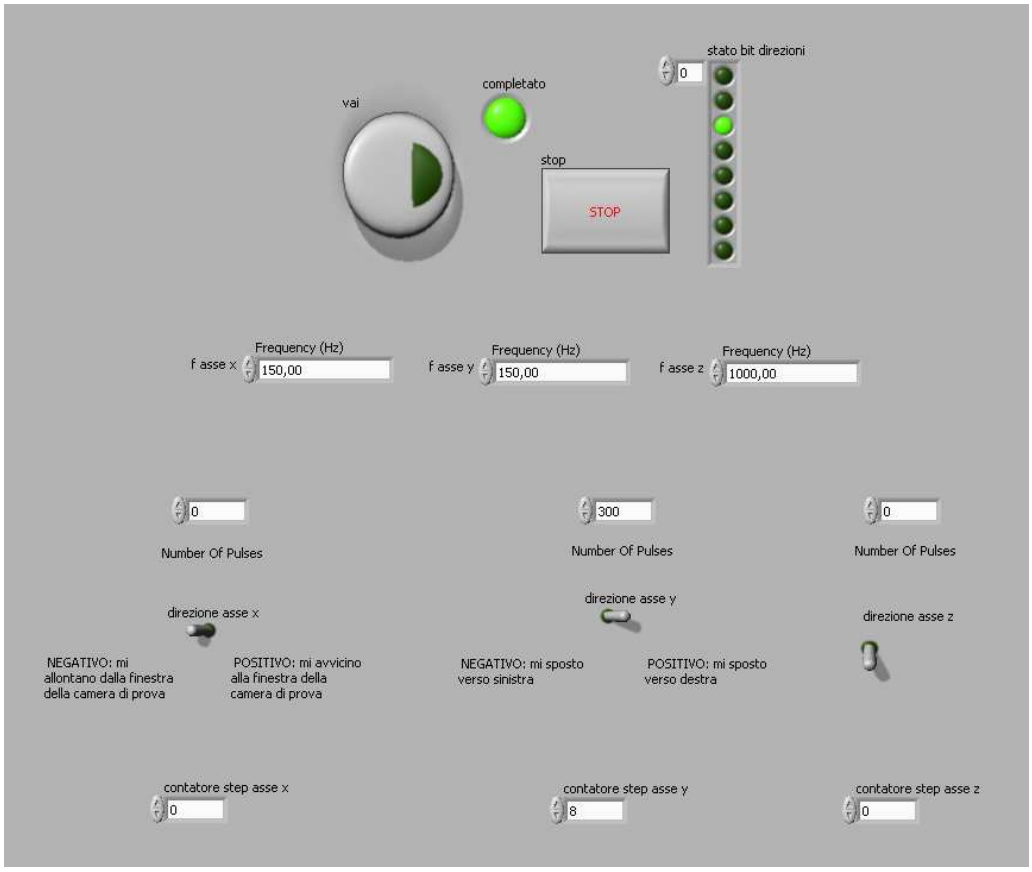

Fig. 55. Robot panel control

The big button in the left part is used to start the movement of the robot, the green light next to it shows if the movement is finished. There is a button to stop the movement.

Under these 3 buttons there are other 3, that can be used to modify the frequency of the engines of the robot, in order to avoid any mistake we recommend not to change these frequencies.

Below, there are the scores where we write the number of the steps that we want to, moreover it's possible to change the sense with the buttons of flashlight shape.

There are three scores more in the below part to know how many times we have clicked the button of movement.

The next pictures show the graphical diagram of the block before.

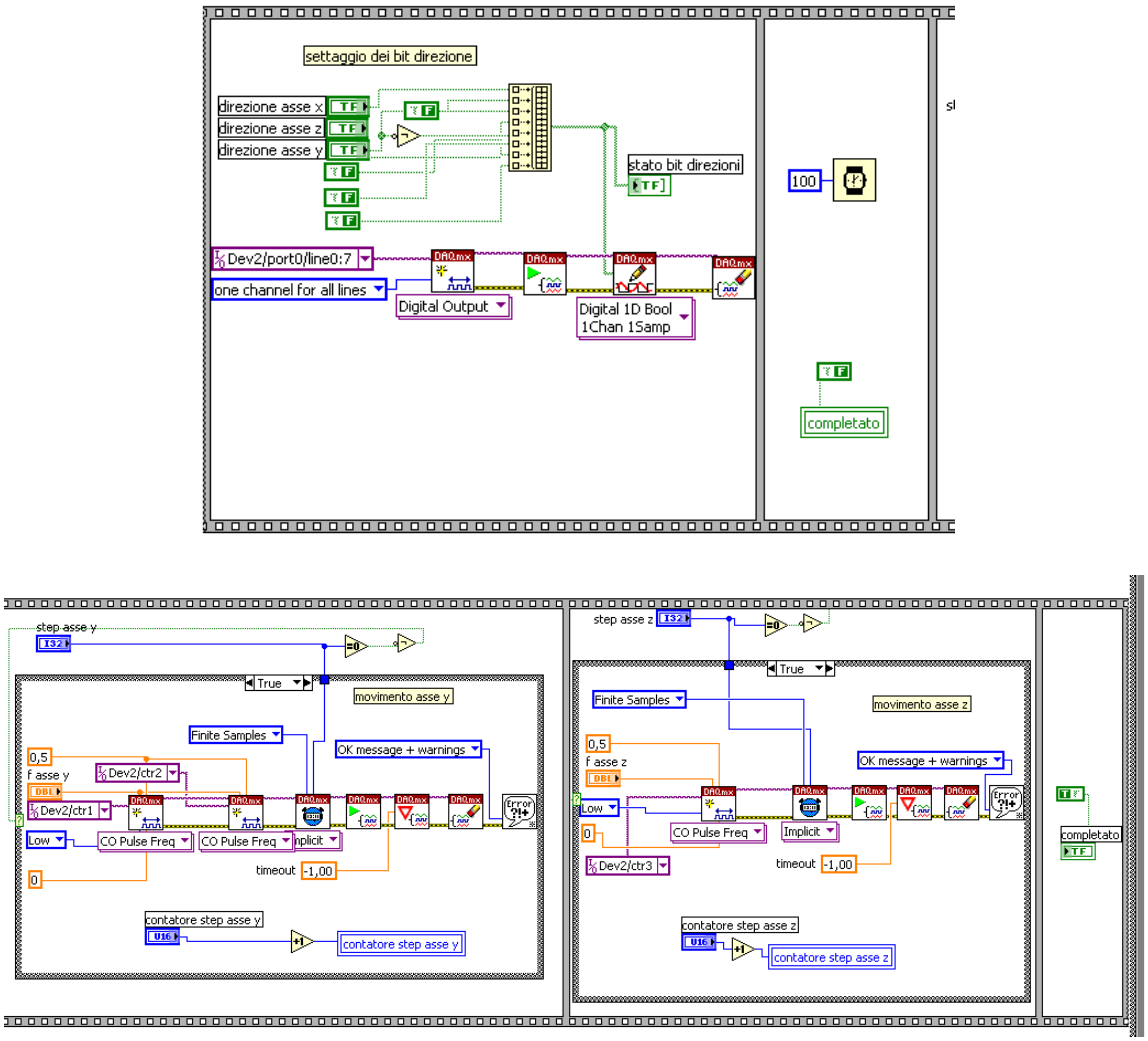

Fig. 56. Robot VI's block diagram

The next pictures show the VI to handle the fan, the servo and the process to get the information.

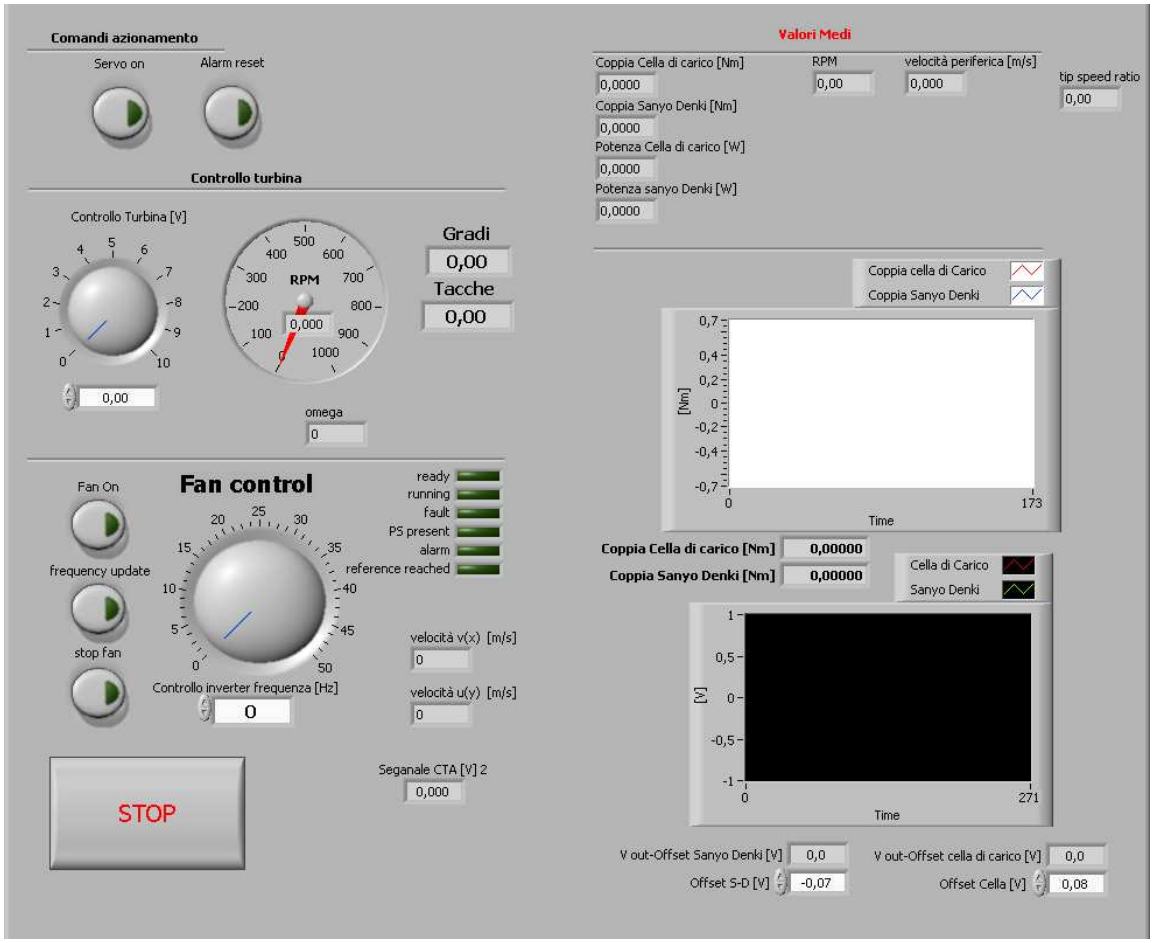

Fig. 57. Fan Panel control

On the upper left part we have the buttons to activate the servo and the light of alarm that warn in case of any risk.

Under these signs, we have the rotor control; we can give the speed that we want to the rotor trough the servo.

On the left below part we have the buttons to handle the fan, we can give the necessary speed.

The graphics in the right side give information about the torque that servo is suffering according with the time.

This is the window to get the information, To start the process we have to click the button of acquisition and the button of stop to finish the process.

The minimum number of turns is 100, when this number is reached; the light in the center of the window becomes brighter.

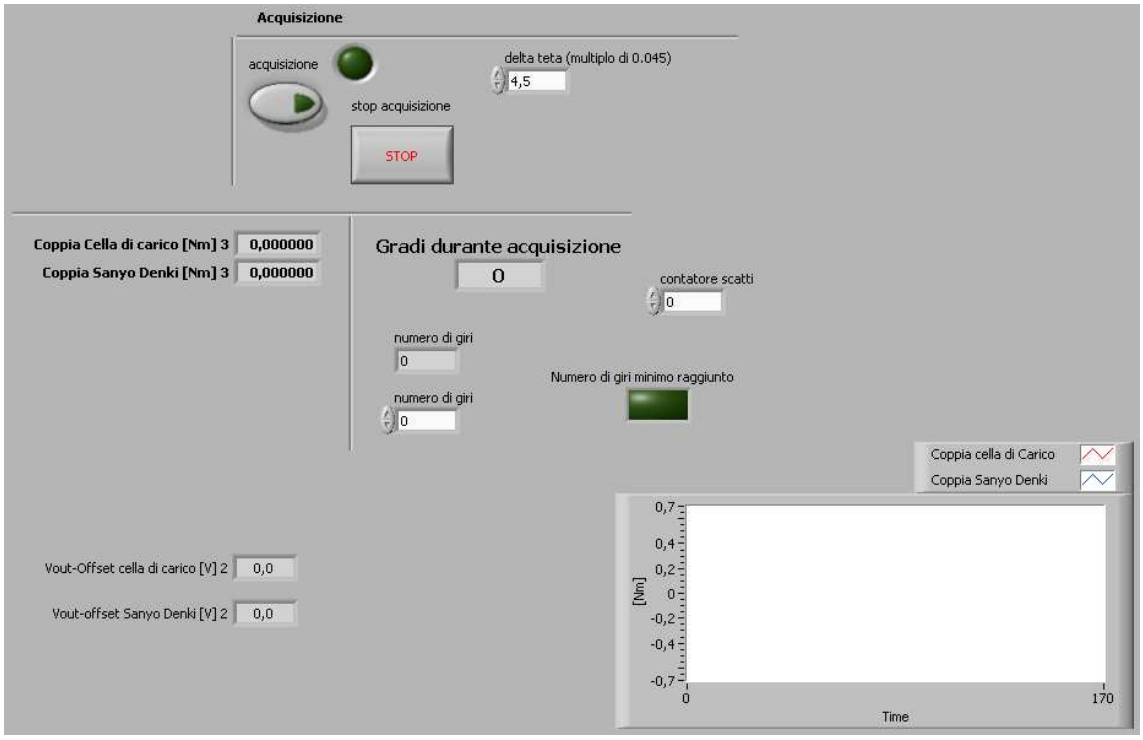

Fig. 58. Acquisition Panel control

12. Calibration Procedures

Calibration procedure single-sensor probe

The calibration procedure is necessary to establish a relationship between the fluid's velocity we want to measure and the output volt of the hot wire probe. This consist of exposing the probe to a set of fluid's known speed (U_i) and record the corresponding voltage (E_i). The best interpolation points (E_i,U_i) is obtained by the transfer function that will be used to convert the voltage data into velocity data.

During the calibration, ambient temperature is important too. However, if the measurement is done following probe's calibration, temperature changes will not affect too much in transfer function's polynomial coefficients.

Operations required in calibration procedure:

I. Power up the system:

- Switch on the next key until you can see the message "load protected", and after that switch on the power strip:

Fig. 59. Power strip

- It's necessary also to switch on the power strip that is behind Rack PC, to power Sanyo-Denki motor.
- Switch on Acquisition Card pressing the button 1 and after, for a few seconds the button number 2:

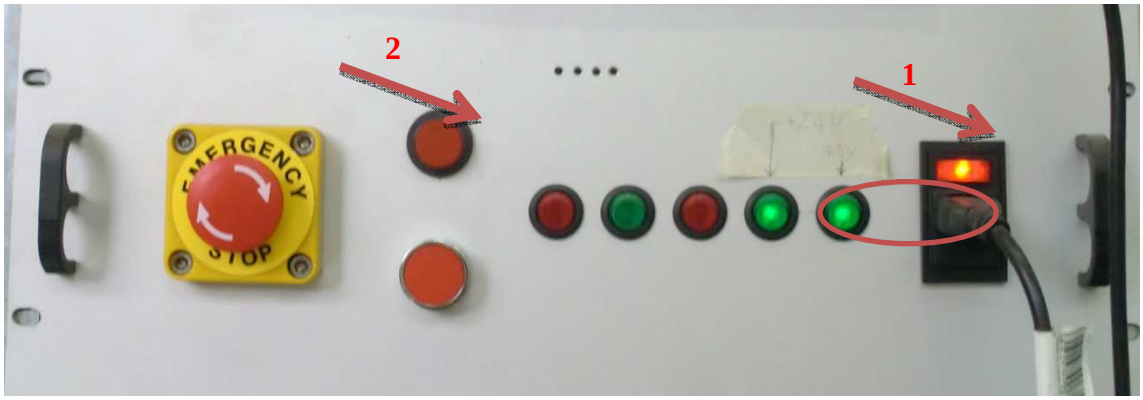

Fig. 60. Acquisition card (The green lights will be switch on)

II. Calibration unit

Take the calibration unit Dantec 54H10 Hot Wire Calibrator and put it inside the test chamber in the horizontal direction, taking care the pivot shafts are perfectly perpendicular to the test chamber edge and then, mount the port probe bracket

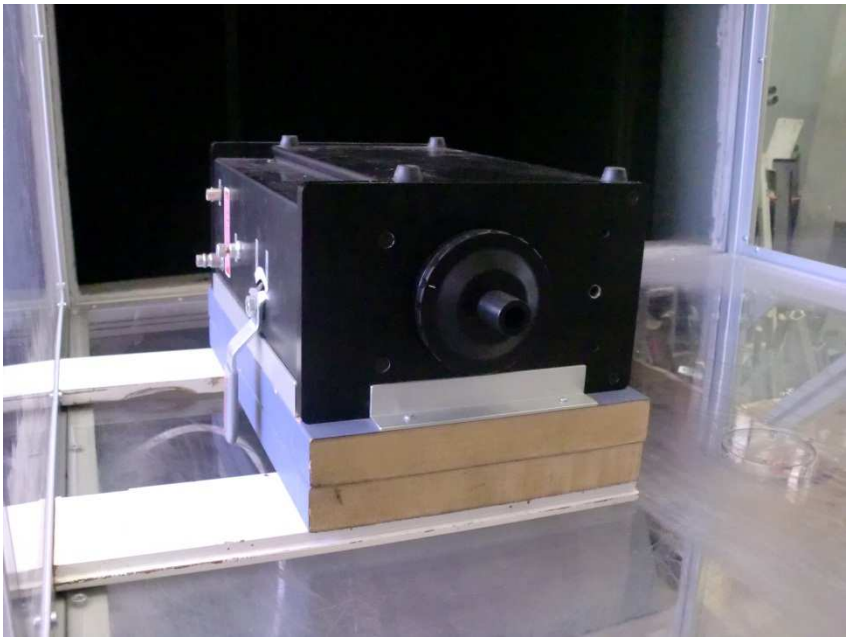

Fig. 61. Calibrator

- Connect the Rilsan hose, quick fit, to the calibrator to take the compressed air into calibrator.

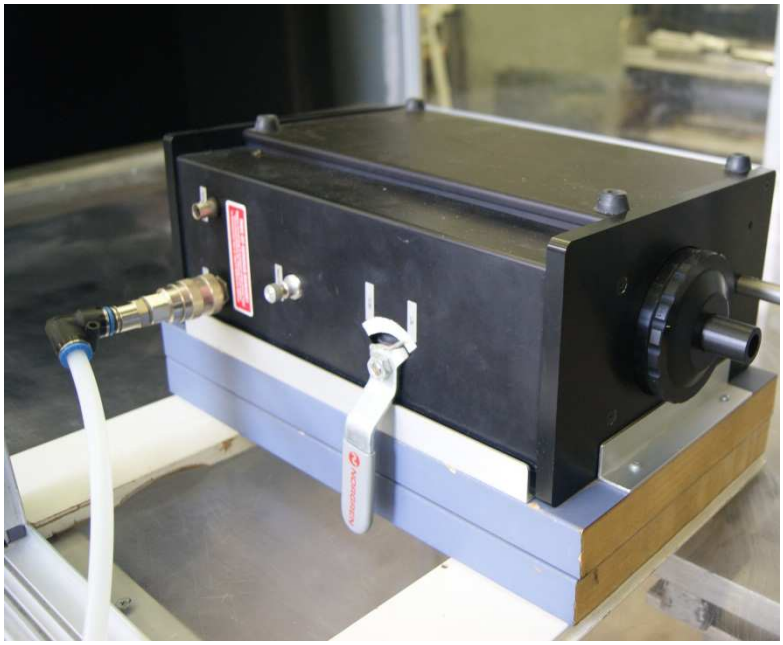

Fig. 62. Calibrator with Rilsan hose

- Open the main valve and the intermediate valve located below test chamber

Fig. 63.Air filters

III. Probe assembly

- First of all, it's needed to make sure that Dantec's frame system is completely shut down. After, connect the termocouple cable BNC to the module "Temp Probe", in the frame.

Fig. 64. Frame

- In the case that the port is connected to 2D probe 55H24 (55R51) for 2 channels coming out from the robot arm, present in the test chamber, disconnect the channel I cable in robot's arm, to use it with monodimensional probe.

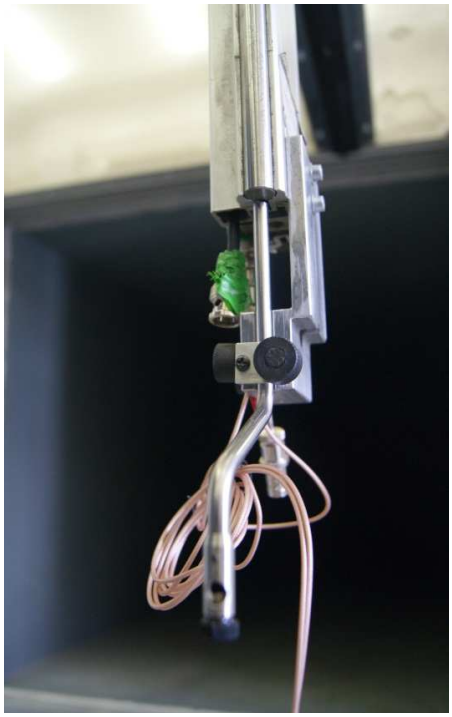

Fig. 65. Robot arm

- Connect the probe holder 55H20, the unidimensional probe holder, to the channel I in the robot arm, via BNC cable.
- Mount the probe holder into the calibrator's probe bracket.
- Mount 55P01 probe into the probe holder carefully because probes are fragile elements.

  (In the next picture it's showed everything mounted but the probe)

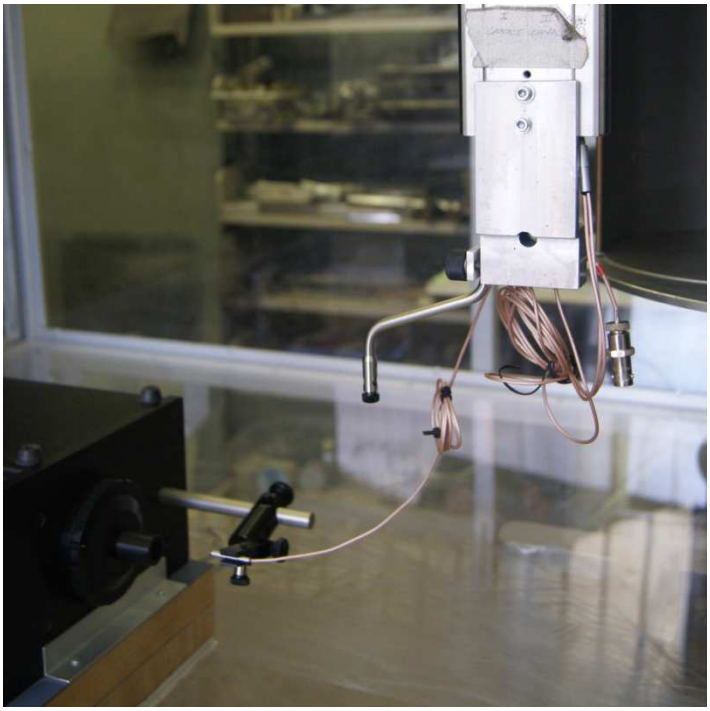

Fig. 66. Everythong mounted for the calibration

- It's necessary to position the probe at nozzle's center, however, it doesn't require high accuracy because calibrator is able to ensure a uniform velocity flow over the entire noozle's surface.

Fig. 67. Nozzle's center

***IMPORTANT:**

Only after connecting all cables and insert the probe in its support, turn on the frame, with power button on the frame's back.

Fig. 68. Frame

Before start working with the PC insert USB key that comes with Streamware software inside PC's USB port, and after, start the program.

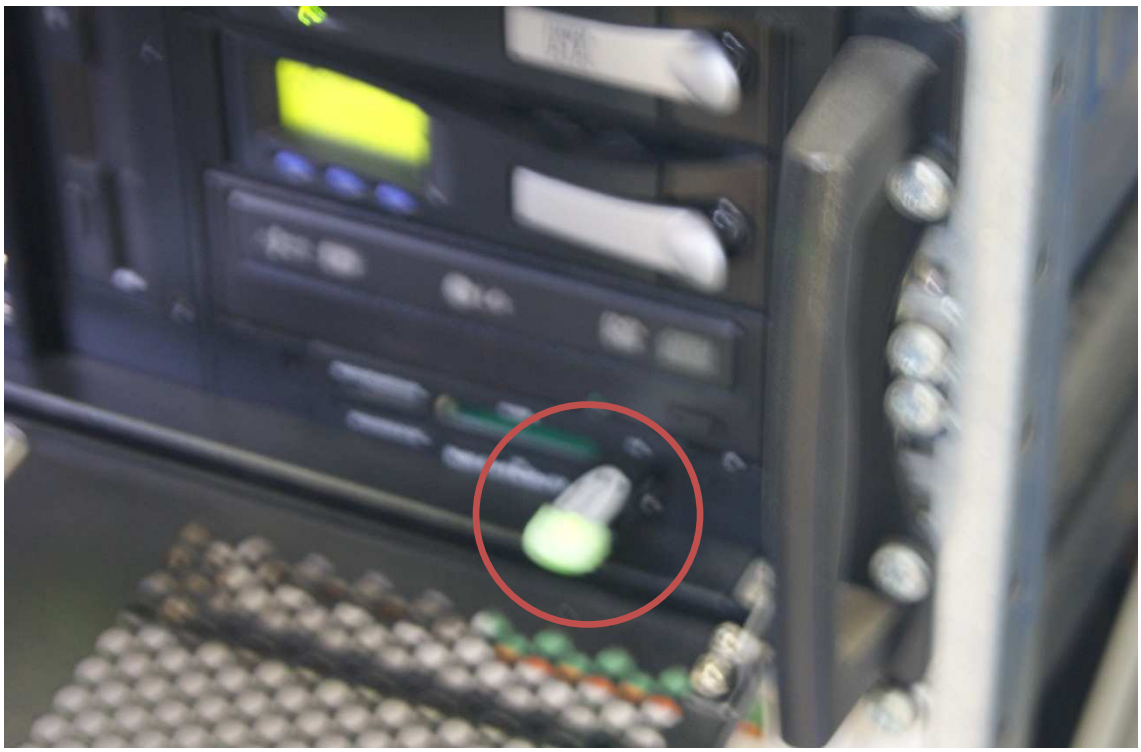

Fig. 69. USB Key

IV. Software instructions

- Open StreamWare software, it has a shortcut in the PC's desktop, this is the program we use to do the calibration.

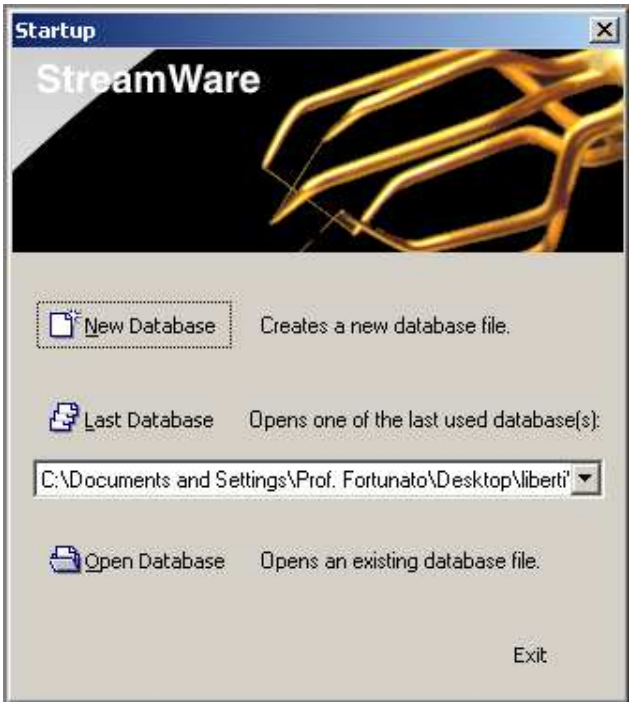

- Select "New Database" and type the name for the project, then assign to a New Project ID Project name:

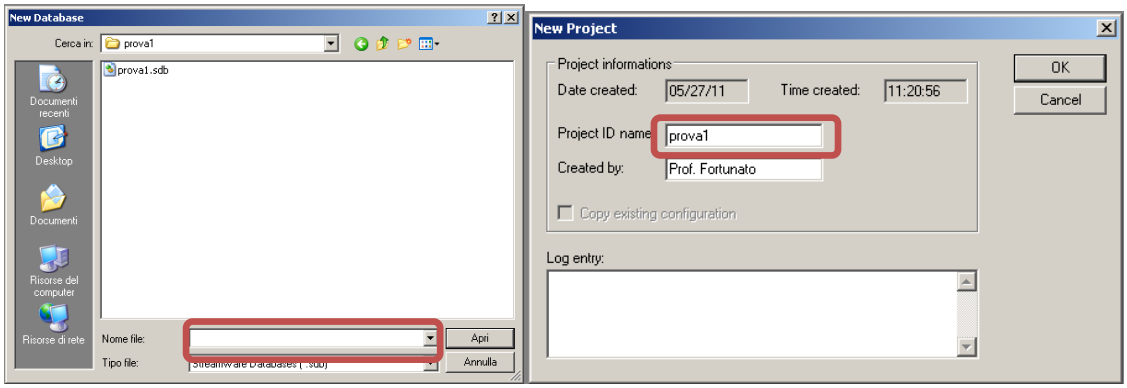

- The program will ask you: "Select A/D board?". Press *Yes* and select the capture card: *NI PCI-6024E*

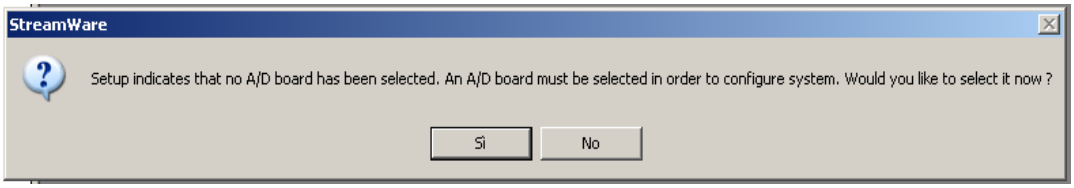

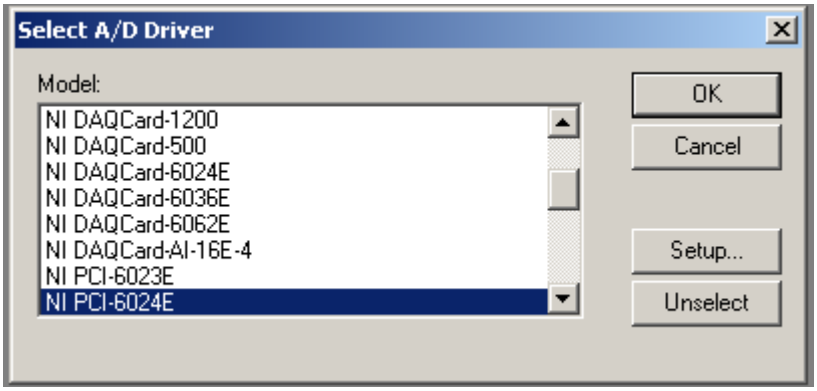

- Continue with system's configuration by setting the components:
  - Select the frame and select the COM 1 port
  - Choose the probe type, single-sensor, and the particular model among those available, the last on the list "valori modificati".
  - Select probe support: 55H20
  - Select cable length: 20 m (A866)

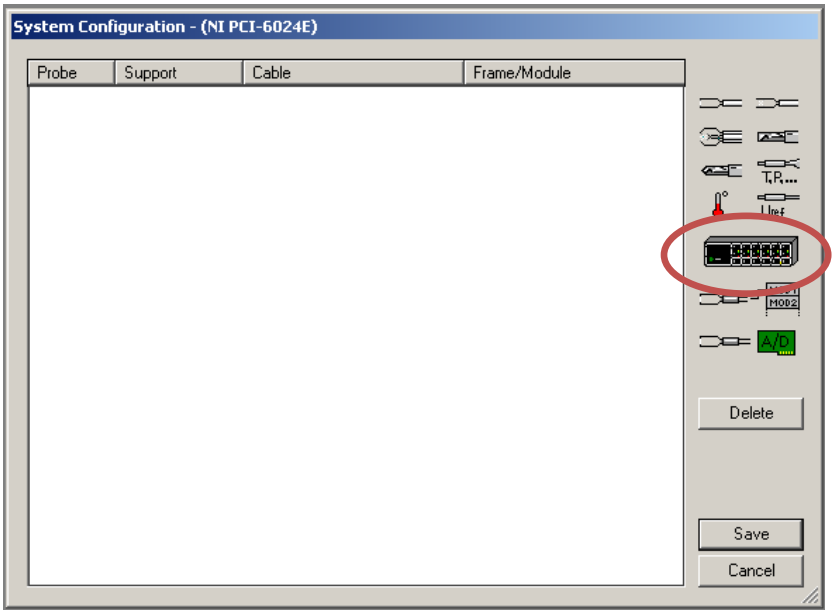

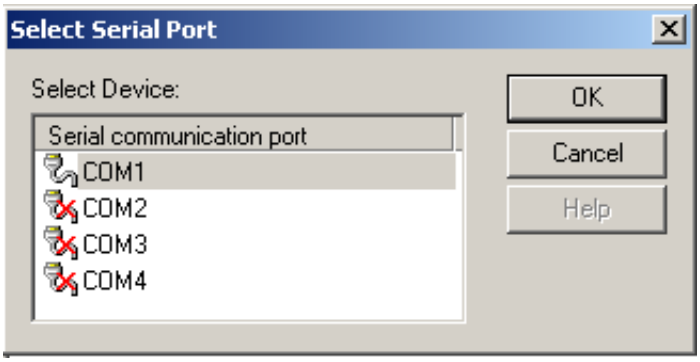

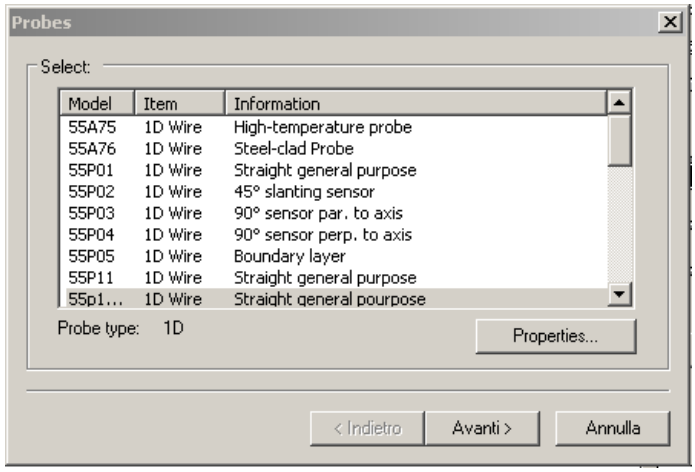

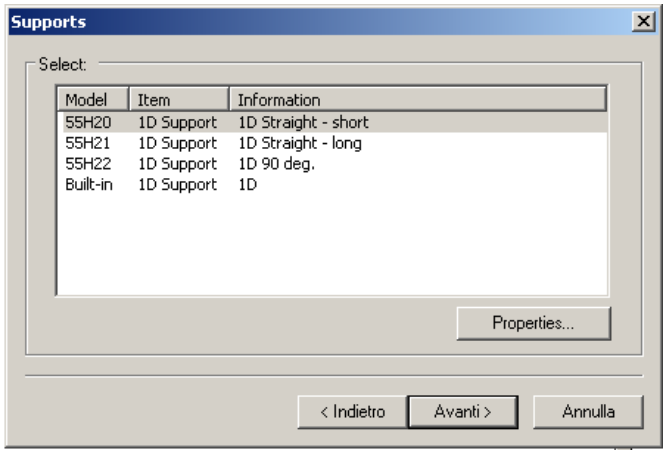

- After select all characteristics, in the window we must see the next picture:

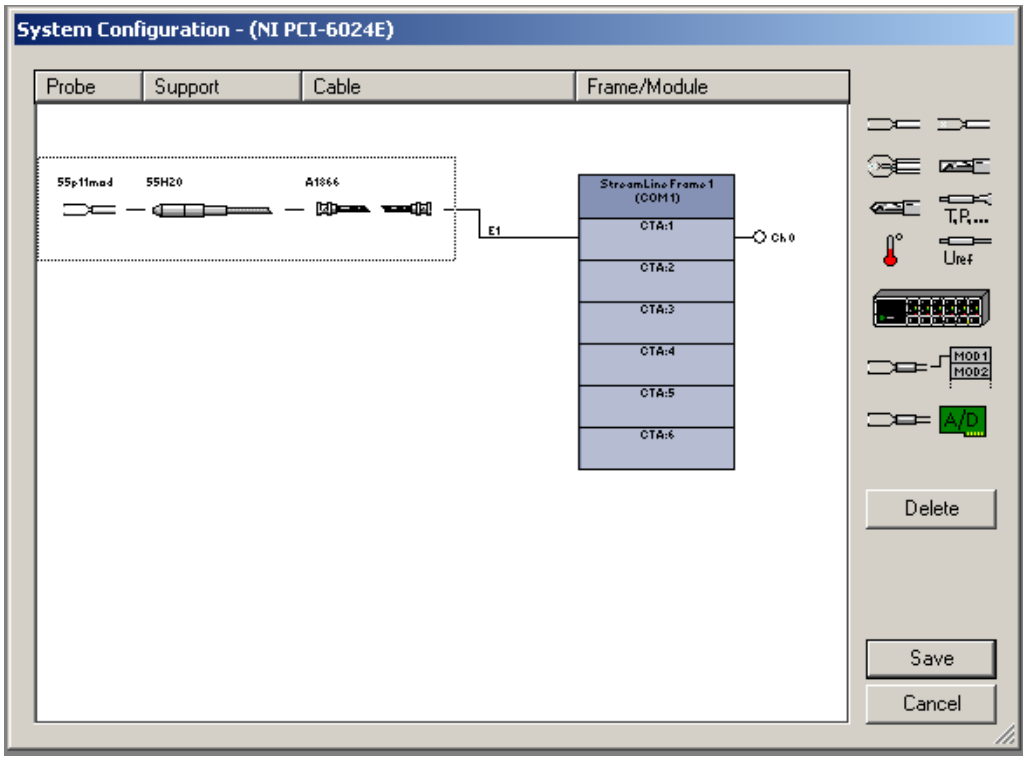

- Select “Save”

- The system, after the configuration, performs automatic hardware setup, which will allow him to balance the Wheatstone bridge inside the frame before the velocity measurements.
- Select “Set Overheat” and, in the next window, “Autobalance”. The system will balance according to the temperature value read by the thermocouple.

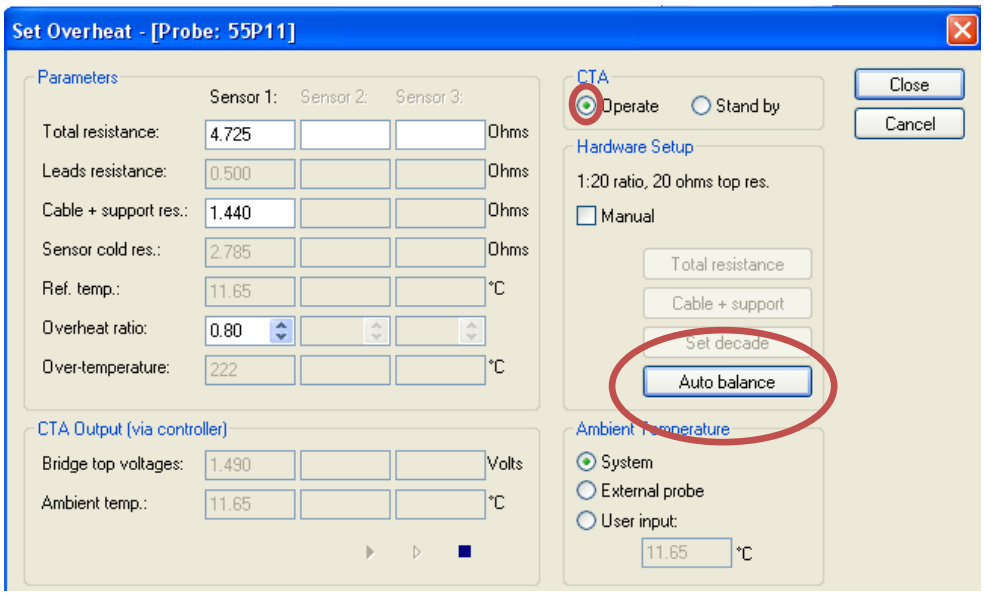

- When the system finishes “Autobalance” operation, we must change the CTA to “Operate” mode, making active the probe (this will also cause the green light comes on frame’s module)
- Press “Play” button to read the voltage value measured.

IMPORTANT:
If you want to know probe’s voltage and temperature through other software (like LabView) it’s necessary stop reading through Streamware software (pressing “stop” button in “Set Overheat” window) because the communication channel capture card can only be used by one software at the same time.

- Open the Excel sheet “Spreadsheet for Hot-wire calibrator” that comes with the calibration unit, activate the macro and click the tab on the way “Two Point mode”

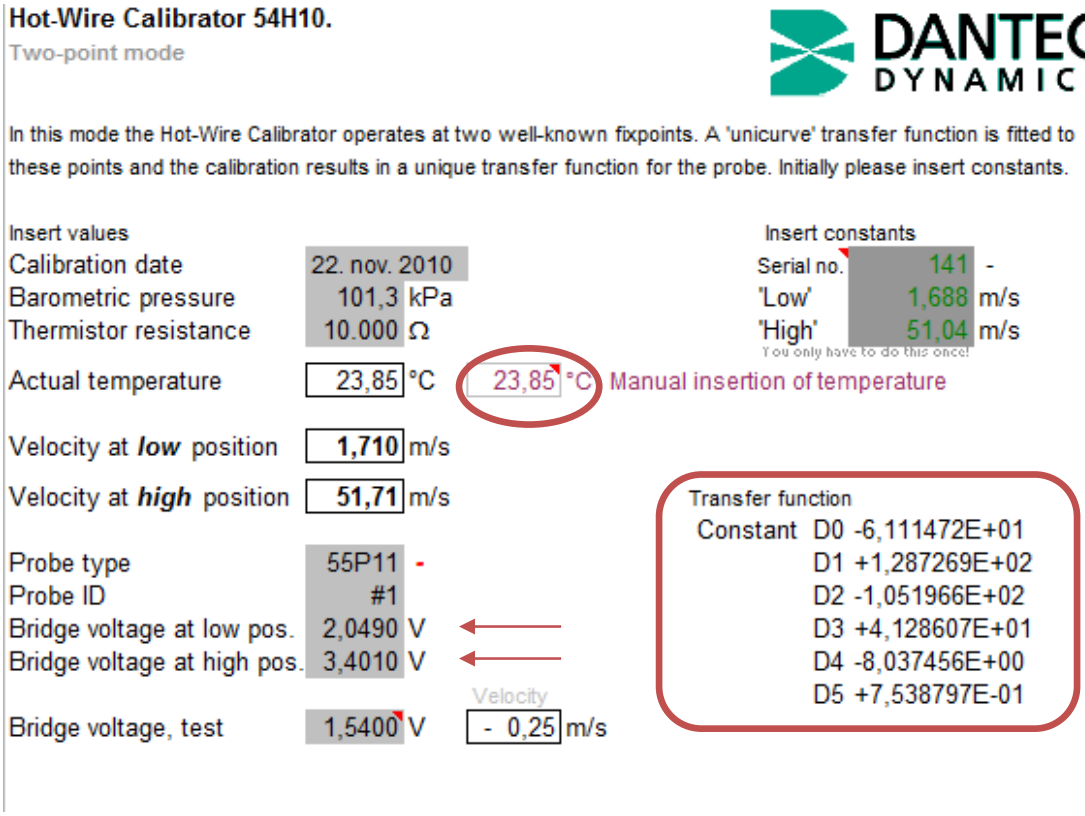

Fig 70. Spreadsheet for Hot-wire calibrator

1. Insert the temperature measured by the thermocouple [ºC]
2. Insert the voltage measured by the probe with the valve positioned in "Low Position" on the calibrator.
3. Insert the voltage with the valve positioned in "High Position"

- The spreadsheet will return the value of the six coefficients that must be used to plot the curve, enabling the transition from the voltage to those of speed. With these coefficients can be derived with high accuracy rate each velocity in the calibrator's range (speed range 1.688-51.04 [m/s], standard temperature). Outside this range, accuracy and precision in speed's calculation, falls quickly.

Fig. 71. Calibrator in high position

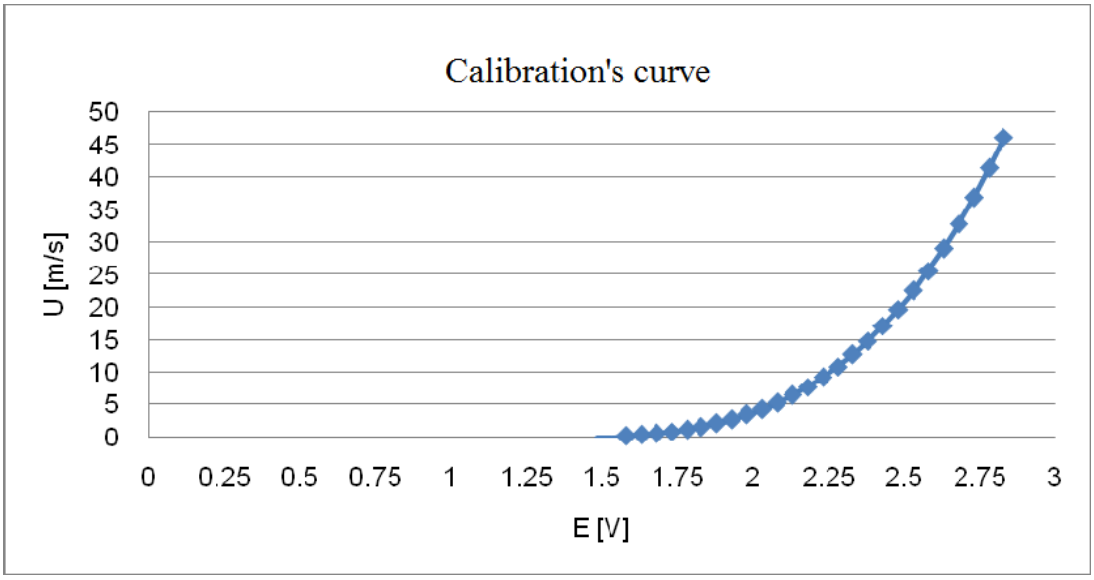

Fig. 72. Calibration's curve

After these operations, we have finished the single-sensor probe calibration.

Calibration procedure dual-sensor probe

After calibration of the single-sensor probe is finished, it's possible to calibrate the dual-sensor probe.

Using the single-sensor probe still in place, we evaluate the voltage [V] at some intermediate points, by placing the control valve's knob at the two intermediate points on the calibrator.

Fig. 73. Calibrator and intermediate points

Once you know the coefficients of the calibration curve obtained from Spreadsheet file with single-sensor probe, and using the following formula, we must consider the speed U [m/s] even in the middle just acquired, that are known in their respective voltage values.

$$U = D_0 + D_1E + D_2E^2 + D_3E^3 + D_4E^4 + D_5E^5$$

Table 8: Voltage and speed table

Control valve position	*Voltage Value E [V]*	*Speed U [m/s]*
1 – Low	E_1	U_1
2	E_2	U_2
3	E_3	U_3
4 - High	E_4	U_4

Now the values are known for speed, even in intermediate positions, values that will later get to know the calibration curve's constants for the dual-sensor probe.

- Once you switch off the frame, remove the probe from probe holder and disconnect the BNC cable from the robot arm.
- Connect the probe holder (55H24) by dual-sensor probe to the BNC cable channel, then mount the port probe bracket on the calibrator by repeating the procedure like with single-sensor probe.
- After assemble the dual-sensor probe (55R51) to probe holder, you can turn on the frame, insert the USB key and open Streamware software.
- We must repeat the hardware configuration, like we did for the single-sensor probe:
    - "New Database"
    - Insert a name for the project
    - Insert a name for Project ID Name
- At the "Select A/D board?" question, press yes and select the capture card: NI PCI 6024E. You can then select the system's components:
    - The frame and the port COM 1
    - The probe type (dual-sensor) and among the models: 55R51

- Probe support: 55H24
- Cable length: 20 metres (A1866)

- Finally, system will ask you for two default values (0.400%), press “yes” without change these values. At the end you’ll have to select “End”, and “Save”.

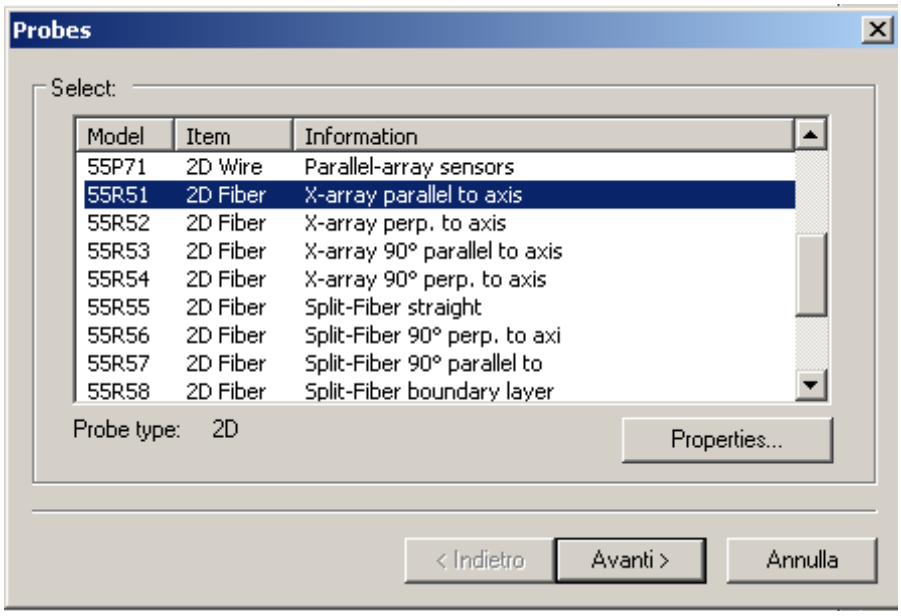

- Select “Set Overheat” and, in the next window, “Autobalance”. The system will balance according to the temperature value read by the thermocouple.

- When the system finishes “Autobalance” operation, we must change the CTA to “Operate” mode, making active the probe.

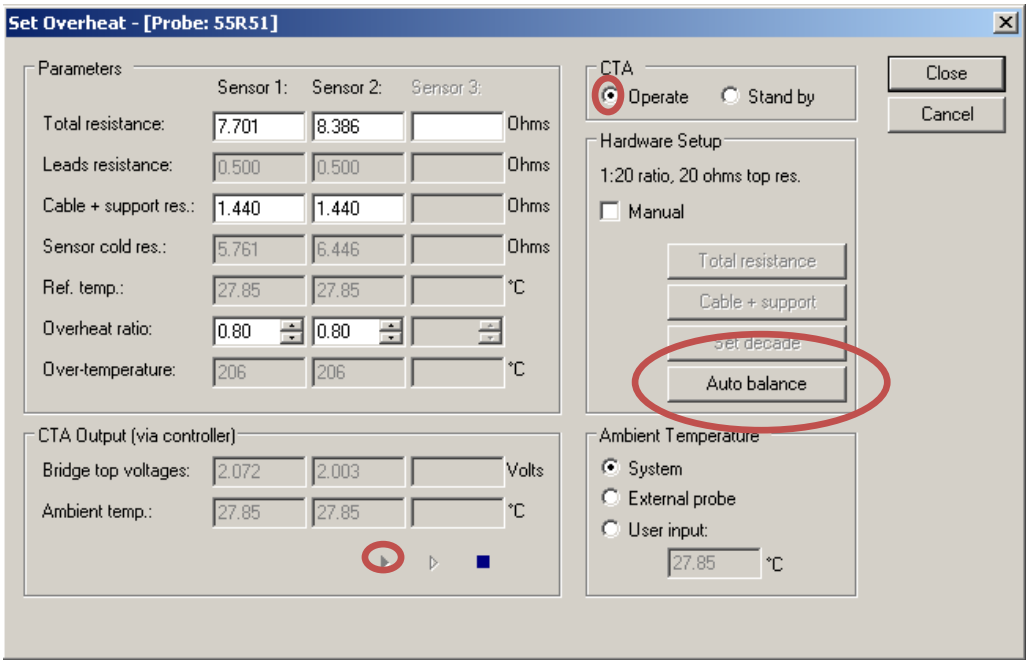

- Complete a voltage's reading across the probe at the 4-point 2D previously considered, obtained by varying the knob's angle, and create a table like this:

Table 9: Voltage table

Position knob	*Voltage channel 1 E[V]*	*Voltage channel 2 E[V]*	*Vel. U[m/s]*
1 - Low	E_1 (ch1)	E_1 (ch2)	U_1
2	E_2 (ch1)	E_2 (ch2)	U_2
3	E_3 (ch1)	E_3 (ch2)	U_3
4 - High	E_4 (ch1)	E_4 (ch2)	U_4

- At the end of voltage reading, close the Set Overheat.

- From the main menu screen Streamware software, press "*Setup*", and then select "*Velocity calibration*", in the next window set number points = 4, and entered: "*Maximum Velocity*" and "*Minimum Velocity*" in these points.

- After pressing "Ok" you will get a new template in which you must enter the both channels' voltage of the 2D probe and its speed (calculated previously with the single-sensor probe) for all 4 points, by pressing the "update" at the end of every post.

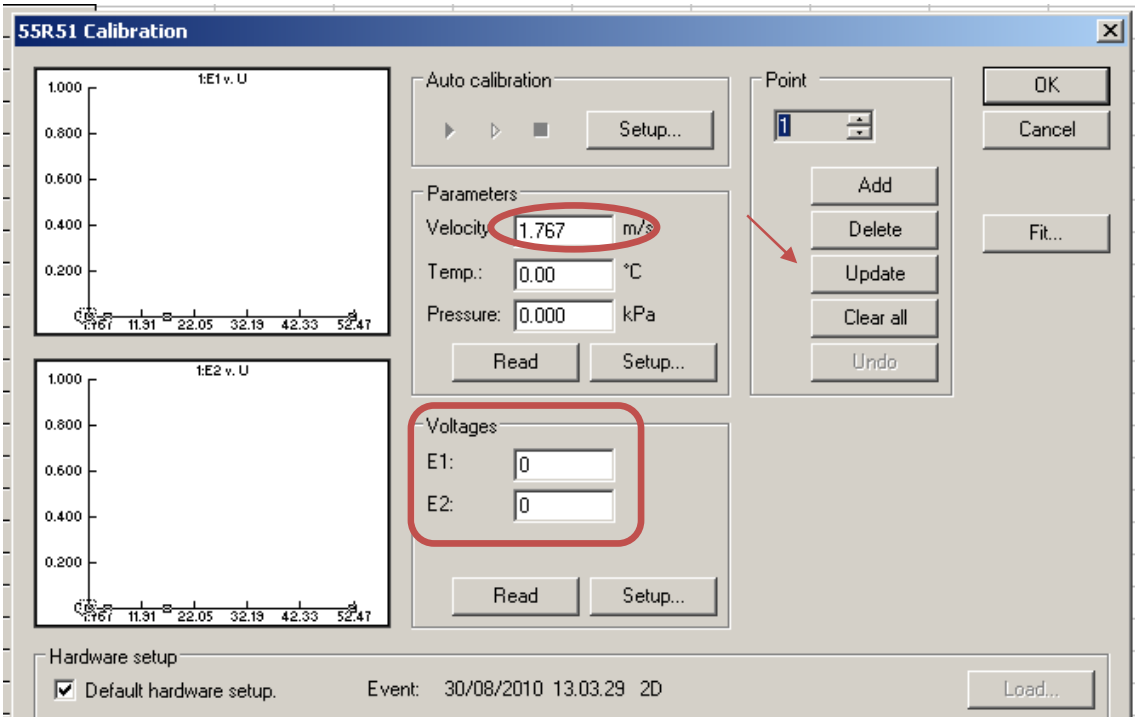

- Once you have entered all the tension values, press "fit", which will give you access to another menu, where you can obtain the coefficients.
- Select "Curve fit", and, in the next window, select "Polynomial" and specify 3rd order.

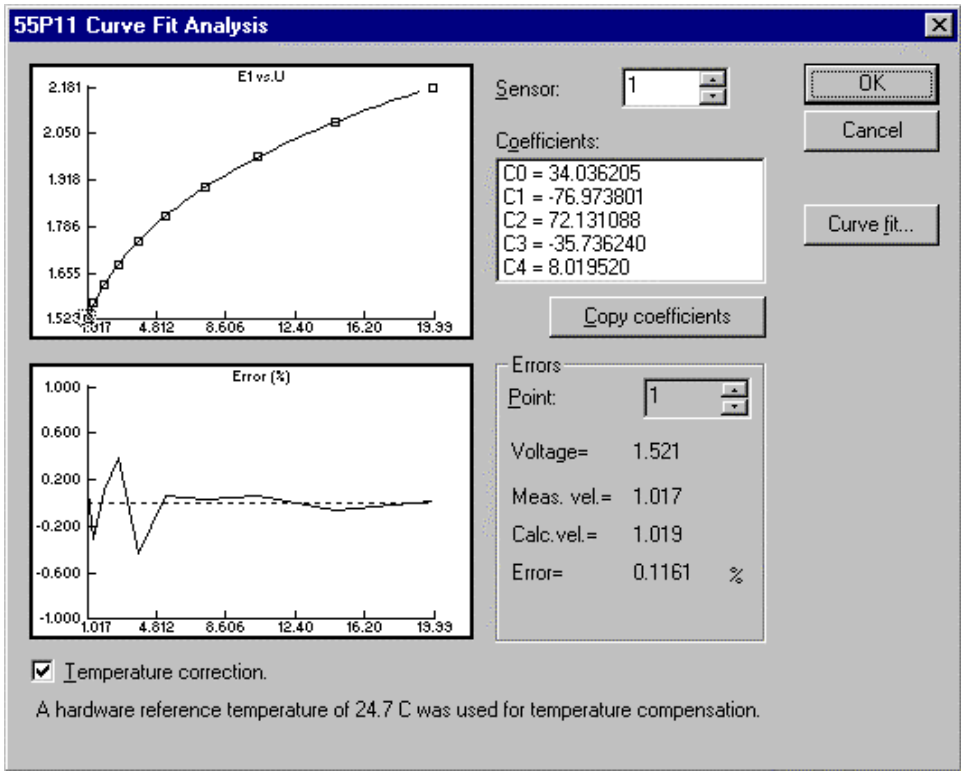

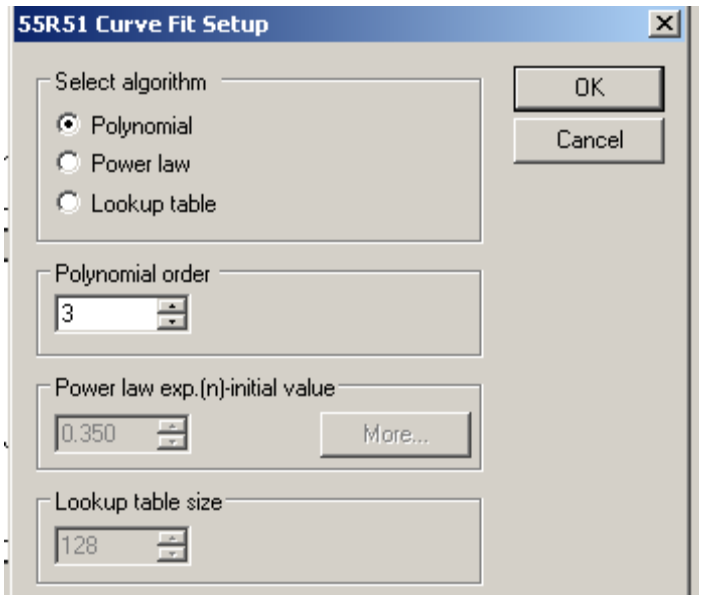

You will get out the 8 calibration curve coefficients, 4 for one channel and 4 for the other channel, to be used in dual-sensor VI in LabView during the test.

Channel 1	***Channel 2***
C_0(ch1)	C_0(ch2)
C_1(ch1)	C_1(ch2)
C_2(ch1)	C_2(ch2)
C_3(ch1)	C_3(ch2)

$$U_{ch1} = C_0(ch1) + C_1(ch1)\,E_{ch1} + C_2(ch1)\,(E_{ch1})^2 + C_3(ch1)\,(E_{ch1})^3$$

$$U_{ch2} = C_0(ch2) + C_1(ch2)\,E_{ch2} + C_2(ch2)\,(E_{ch2})^2 + C_3(ch2)\,(E_{ch2})^3$$

Once you get the 8 coefficients, the calibration procedure is finished.

13. Inlet velocity profile

The first thing we did before start to take measurement was to find a mesh, which defines the points where we have to put the robot's arm. We had to do it upstream the turbine, as far away as possible from the turbine.

We decided that our mesh will have 8 cells in the vertical axis and 8 cells in the horizontal axis, and it will occupy the maximum area possible, in order to evaluate what happens in every point of the test chamber. Then the velocities have been measured in the cell vertices.

In order to compute the cell velocity, we perform the average of the velocities measured at its four vertices, and this will be the cell velocity.

The mesh we have made is a symmetrical mesh, and because of robot construction we can't measure in the first 200 mm from the roof, because the robot arm has a support in which probe is mounted and this make the probe can't upload more.

Finally we obtained the next mesh:

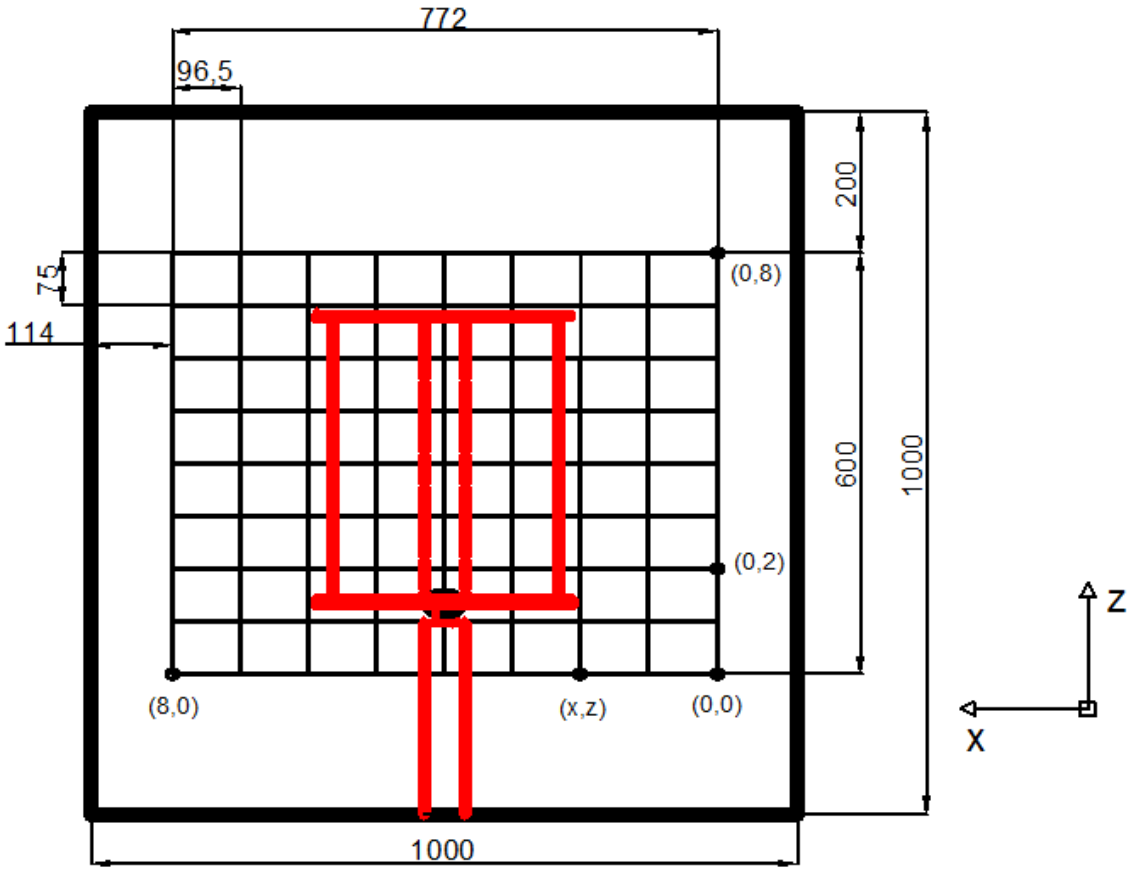

Fig. 74. Vertical mesh

Using the single-sensor probe

Later we decide to measure with the single-sensor probe to look for differences between the two probes and to see how it could have influence in the results we take.

To make this we calibrate with the single-sensor probe and we entered the coefficients we obtain in LabView's Panel Control after modifying our VI.

To do this comparison we decided to measure with the following conditions:

- Rotor spin: 300 rpm
- Fan frequency: 8 Hz

Environmental conditions:

- Measurement Data: 16/02/2011
- Room temperature: 14.35 ºC

With this probe and these conditions we have obtained the following results:

- Velocity x-axis
- Flow 8x8
- Flow 4x4

Coefficients obtained from the calibration that we have entered in the VI:

- -157.9763
- 369.6913
- -338.8060
- 152.6232
- -34.99667
- 3.633029

- **Velocity x-axis [m/s]**

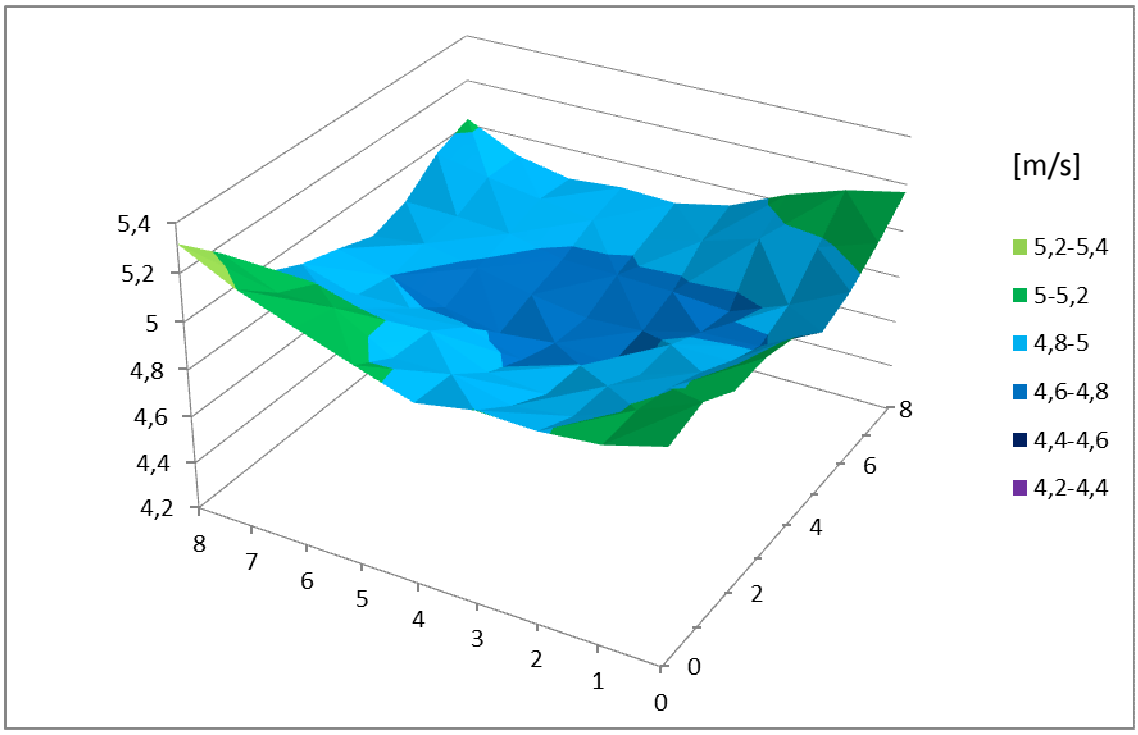

- **Flow 8x8 [m^3/s]**

Cross-section of each cell: 0.0072375 m^2

Total flow: 2.26231412 m^3/s

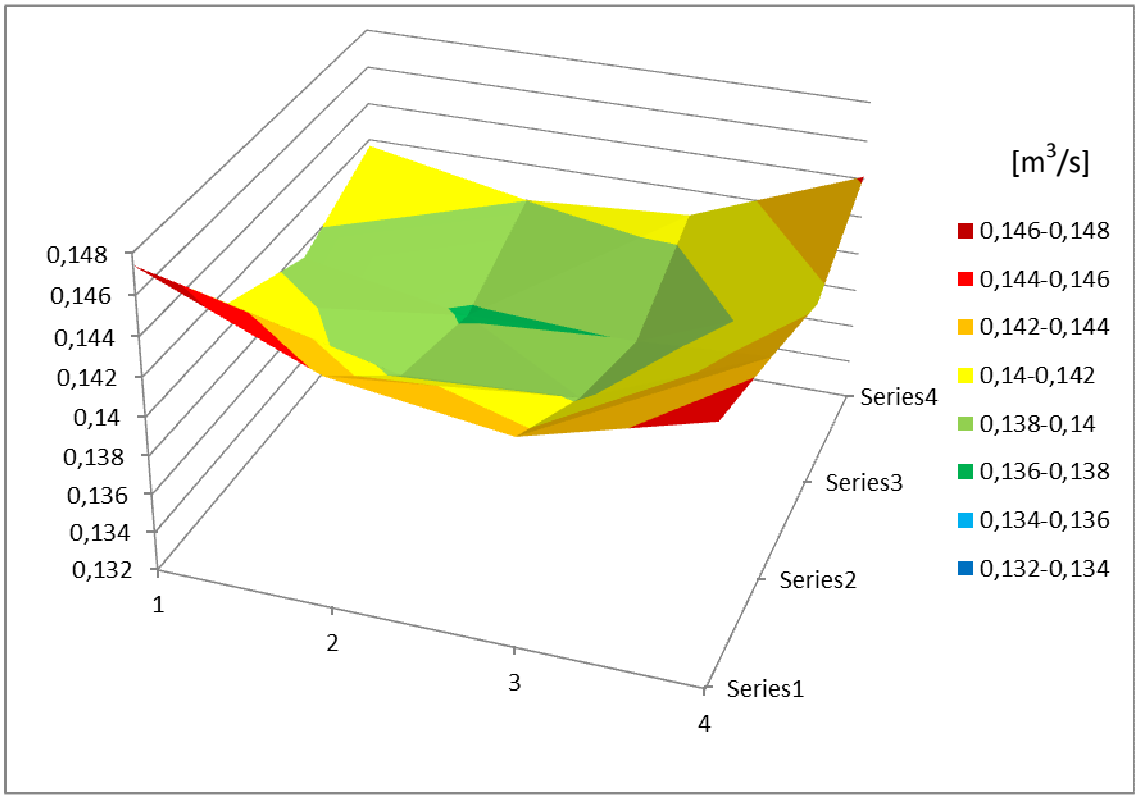

- **Flow 4x4 [m^3/s]**

  Cross-section of each cell: 0.02895 m^2

  Total flow: 2.265724615 m^3/s

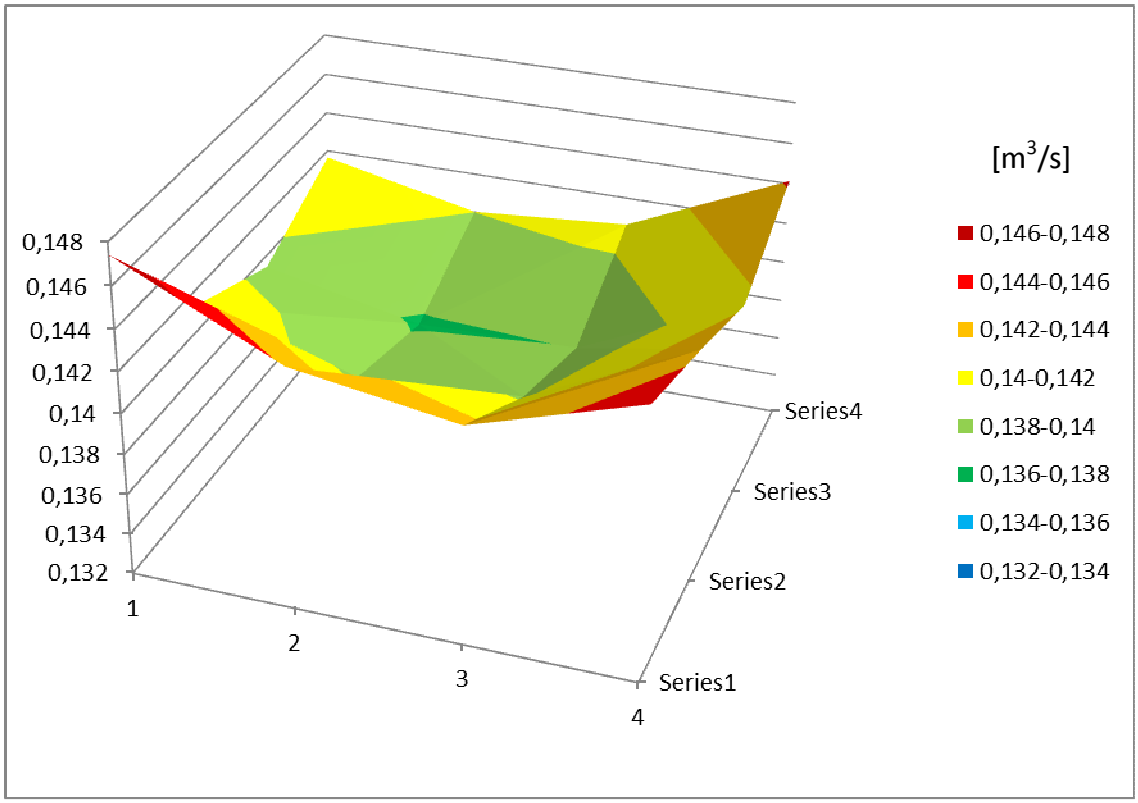

- **Comparison of flow:**

Now we can compare how different is to use a 8x8 mesh or to use a 4x4 mesh:

- Total flow 4x4: 2.265724615 m^3/s
- Total flow 8x8: 2.26231412 m^3/s

So we can observe that the difference between calculate the flow wit a 8x8 mesh or do it with the 4x4 mesh is *0.010015%*.

14. Relation between air flow and wind velocity at a reference point

Our goal is getting a relationship between the wind velocity at a reference point and the air flow at the entrance of the wind tunnel. The point chosen to find a mathematical relationship between wind velocity and flow through the tunnel is the 4_8, central higher point of the mesh. The mesh is placed at the entrance to the test chamber in a vertical plan.

We use the same mesh with which we perform the comparison of data between the one-dimension probe and two-dimension probe. We saw that the difference in the calculation of flow using a mesh of 81 points (8x8 cells mesh) or 25 (5x5 cell mesh) is negligible; that's why we chose to use the 4x4 mesh for our study.

On March 2nd and 4th 2011 we took data in the wind tunnel at the Dipartimento di Ingegneria Meccanica e Gestionale of Politecnico di Bari. Also we use data obtained at 300 rpm and 8 Hz on February 16th 2011.

We take data with the Savonius rotor velocity at 200 rpm and fan frequency at 6, 8 and 10 Hz, Savonius rotor velocity at 300 rpm and fan frequency at 6 and 10 Hz and Savonius rotor velocity at 400 rpm and fan frequency at 6, 8 and 10 Hz.

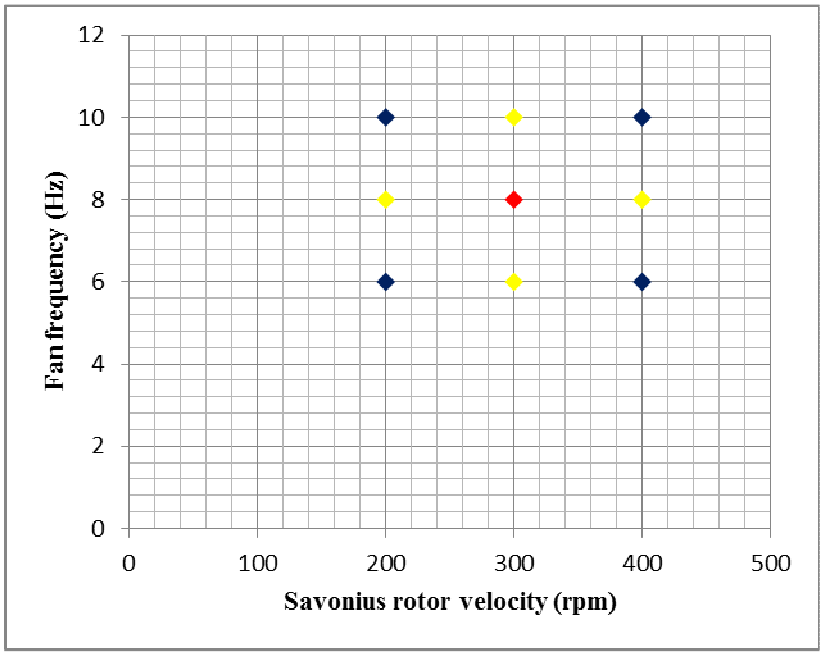

Fig. 75. Configurations measure and measures date

Red marker indicates measurement made on February 16th 2011, yellow markers indicate measurements made on March 2nd 2011 and blue markers indicate measurements made on March 4th 2011.

Table 10: Summary of key data obtained:

Date	Savonius rotor velocity (rpm)	Fan frequency (Hz)	Wind velocity in 4_8 (m/s)	Experimental air flow (m^3/s)
March 4th 2011	200	6	3.62721435	1.67193418
March 2nd 2011	200	8	4.82885089	2.25399075
March 4th 2011	200	10	6.50199396	3.01631349
March 2nd 2011	300	6	3.62871805	1.70158314
February 16th 2011	300	8	4.9577675	2.265724615
March 2nd 2011	300	10	6.11403048	2.86276719
March 4th 2011	400	6	3.6183527	1.7086327
March 2nd 2011	400	8	4.9717405	2.32385722
March 4th 2011	400	10	6.34426417	2.94808629

We observe very little variations of wind velocity and air flow when the Savonius rotor velocity changes. In the following charts we have graphed wind velocity and experimental air flow versus fan frequency. Blue, yellow and red markers indicate fan frequencies at 6, 8 and 10 Hz respectively.

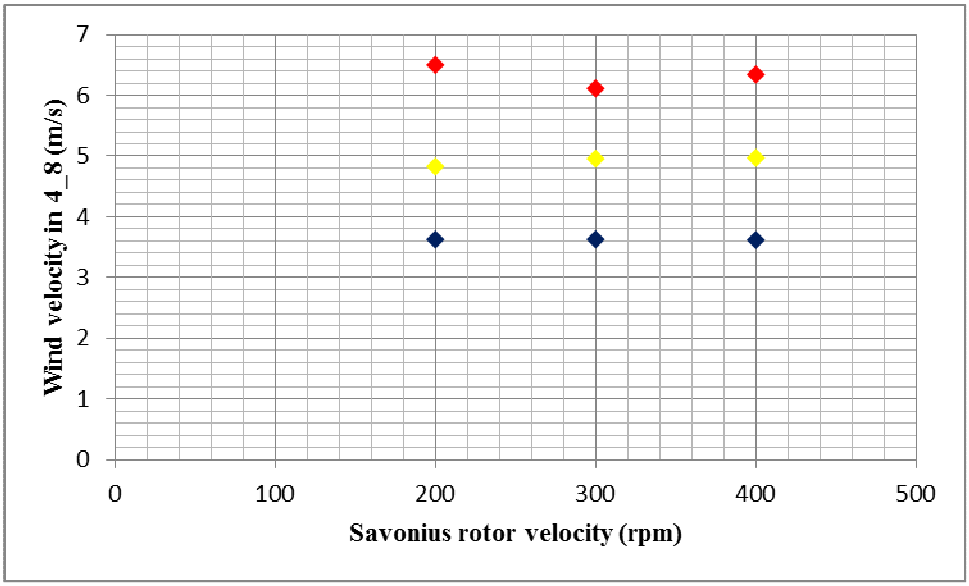

Fig. 76. Relation between velocity measure in 4_8 and Savonius velocity

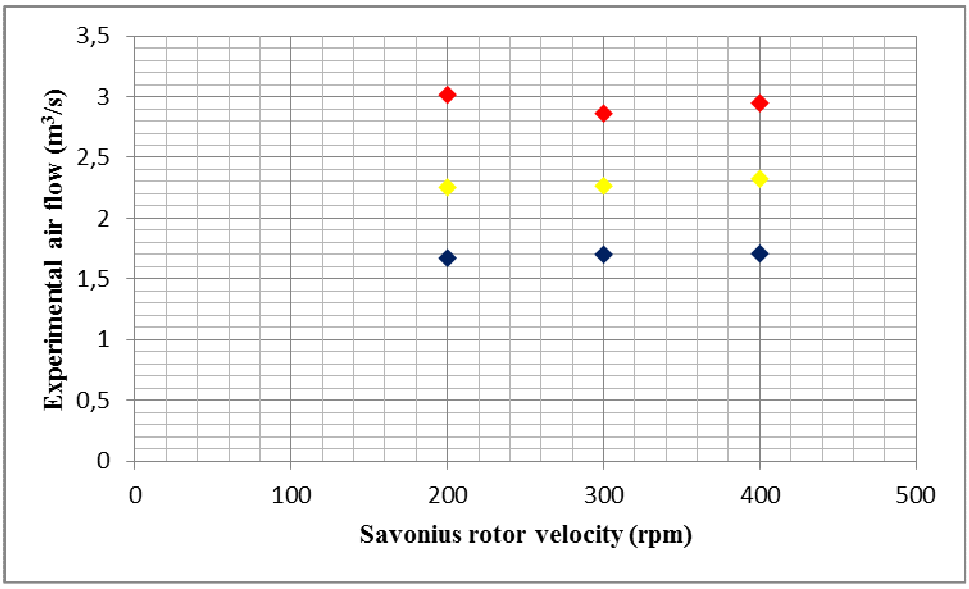

Fig. 77. Experimental air flow respect Savonius velocity

For this reason we find that the relationship to calculate the flow rate is directly proportional to the velocity chosen at the reference point (4_8). To arrive this point from the starting point we must move the robotic arm 777 mm in z-axis (positive), 799 mm in y-axis (negative) and 386 mm in x-axis (negative).

That is the representation of the experimental air flow versus the wind velocity at the point 4_8 independent of fan frequency and Savonius rotor velocity.

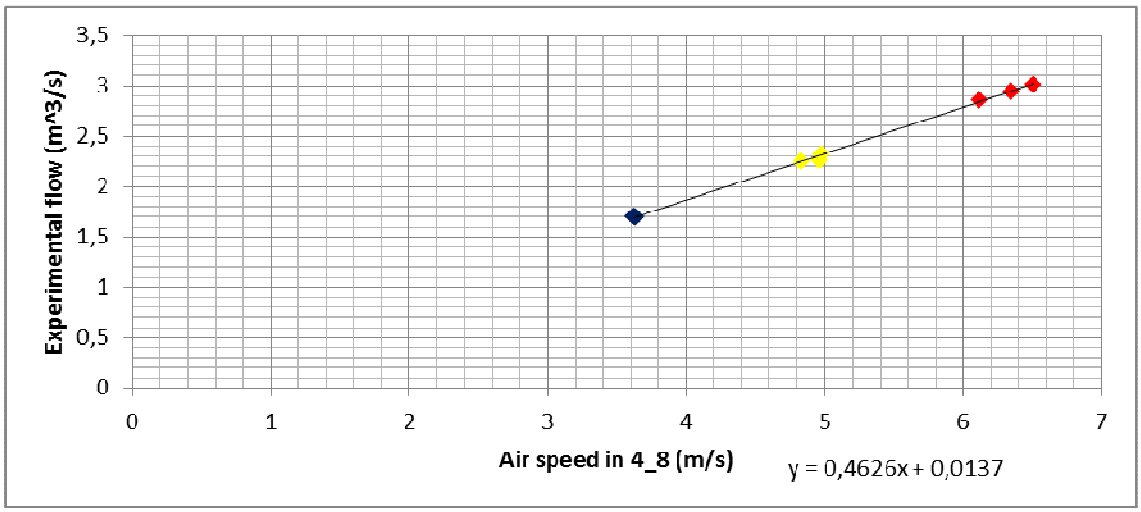

Fig. 78. Experimental air flow respect wind velocity in 4_8 point

Markers blue, yellow and red represent fan frequencies at 6, 8 and 10 Hz respectively.

This graph clearly shows the linear relationship between wind velocity at the point chosen (4_8) and the experimental air flow calculated as the sum of flow through the 25 mesh cells.

Obviously, this linear relationship would pass through the point of coordinates (0,0) because if wind velocity in 4_8 is 0 m/s then the experimental air flow will be 0 m^3/s. So we try the data as a line through the origin to find a mathematical relationship of the form y = ax.

In this case, taking into account the method of least squares approximation of experimental data:

$$a = \sum_{i=1}^{n} (x_i y_i) / \sum_{i=1}^{n} (x_i^2)$$

where "a" is the slope of the line through the origin, "x" is the wind velocity in point 4_8 and "y" is the experimental air flow through the mesh.

Thus using the data in the table above attached

a = 0.465254417

We calculate analytically the flow with the wind velocity in the point 4_8 and the slope. The data are shown below:

Wind velocity in 4_8 (m/s)	Analytical air flow (m^3/s)
3.62721435	1.687577509
4.82885089	2.24664422
6.50199396	3.025081429
3.62871805	1.688277112
4.9577675	2.306623243
6.11403048	2.844579705
3.6183527	1.683454587
4.9717405	2.313124243
6.34426417	2.951696947

In the following table we can see the experimentally calculated air flow, the analytically calculated air flow and the percentage difference between them.

Experimental air flow (m^3/s)	Analytical air flow (m^3/s)	Variation (%)
1.67193418	1.687577509	+0.94
2.25399075	2.24664422	-0.33
3.01631349	3.025081429	+0.29
1.70158314	1.688277112	-0.78
2.265724615	2.306623243	+1.81
2.86276719	2.844579705	-0.64
1.7086327	1.683454587	-1.47
2.32385722	2.313124243	-0.46
2.94808629	2.951696947	+0.12

The difference between the calculated flows is always less than 2% and we believe that the linear approximation we have found is more than satisfactory.

15. Analytical calculation of the air flow out of the study mesh

We start from the next mesh that has been used in previous studies.

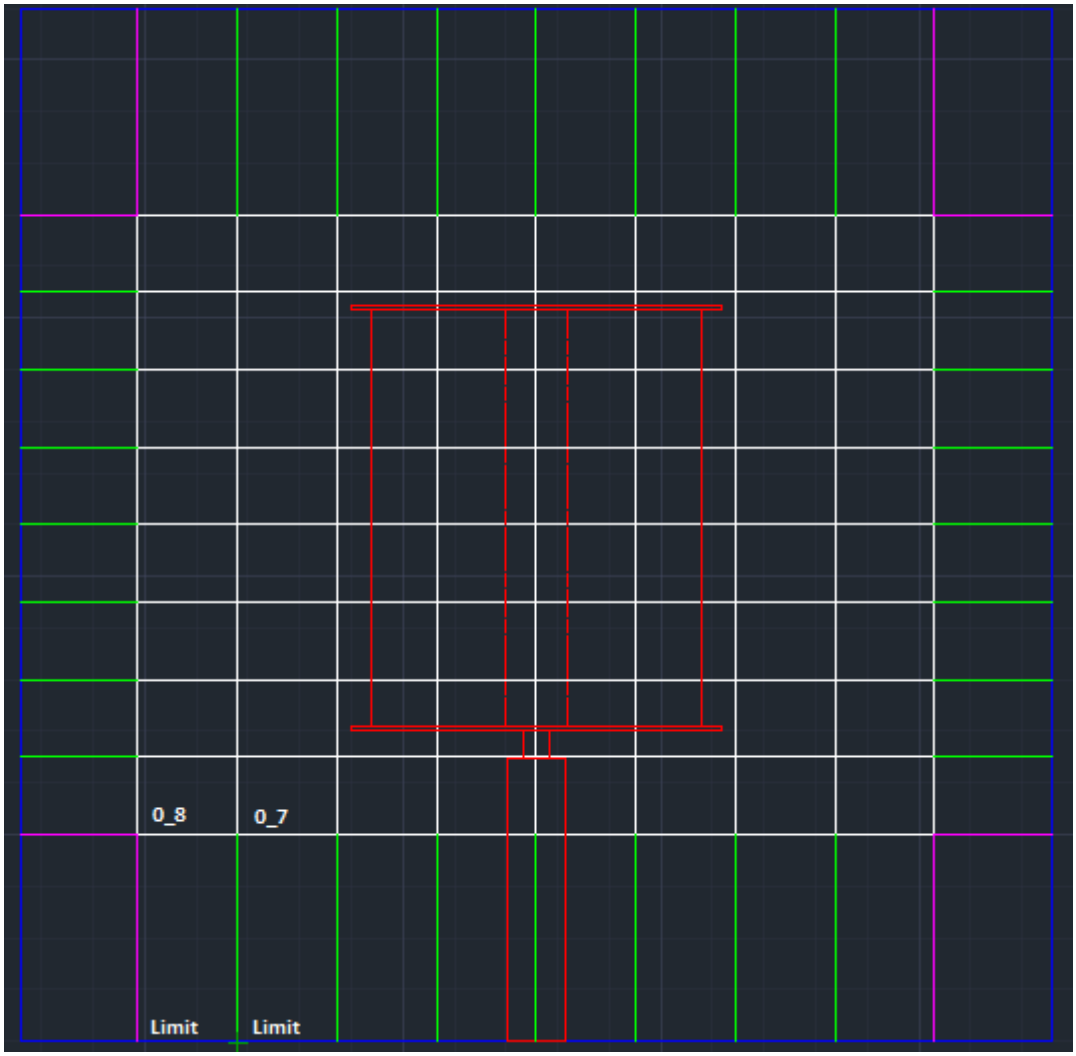

Fig. 79. Schematic of the test chamber. (Own elaboration.)

This mesh has different areas. White lines represent areas of the test chamber where it is possible to measure wind velocity with the dual-sensor probe. Blue lines are the limits of the test chamber where we assume null wind velocity as shown in the chart below:

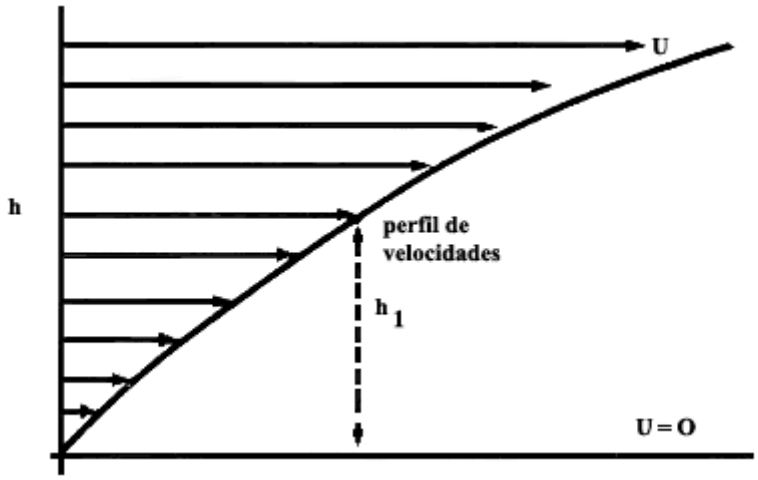

Fig. 80. Speed profile of a gas in a rectangular section.
Made by Instituto Latinoamericano de Comunicación Educativa

The green lines show us the area outside the mesh and the linear trend of the wind velocity. See explanatory graphic.

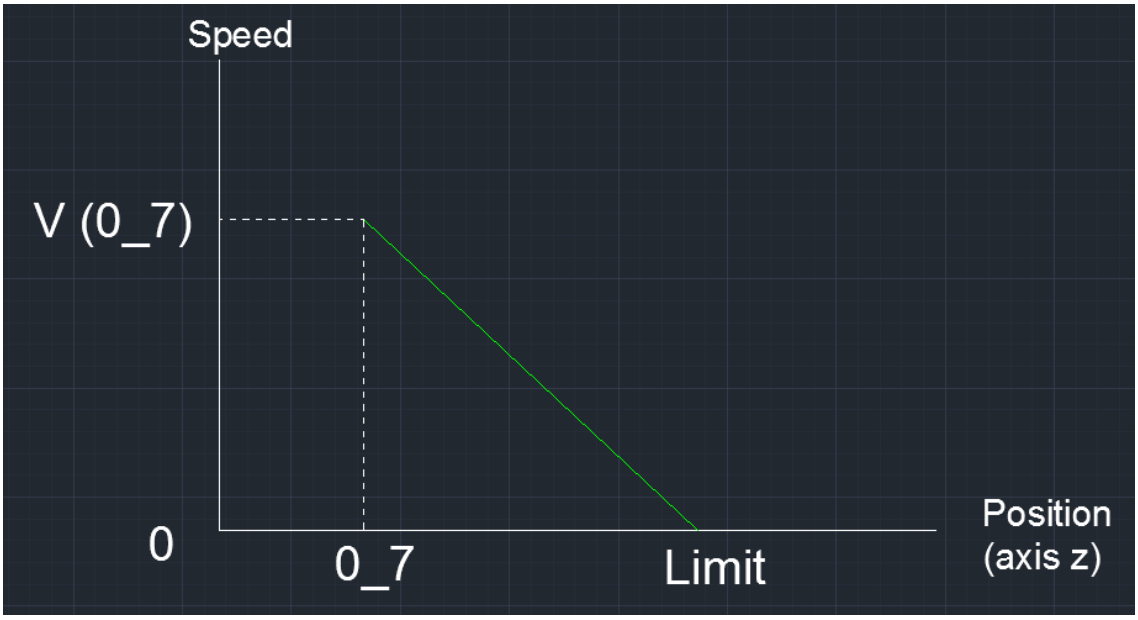

Fig. 81. Linear trend of the wind velocity profile. Own elaboration.

And finally the purple lines indicate areas near the corners of the screen where we consider that the wind velocity will follow a curve trend due to the proximity of two different null speed zones (a vertical and a horizontal wall).

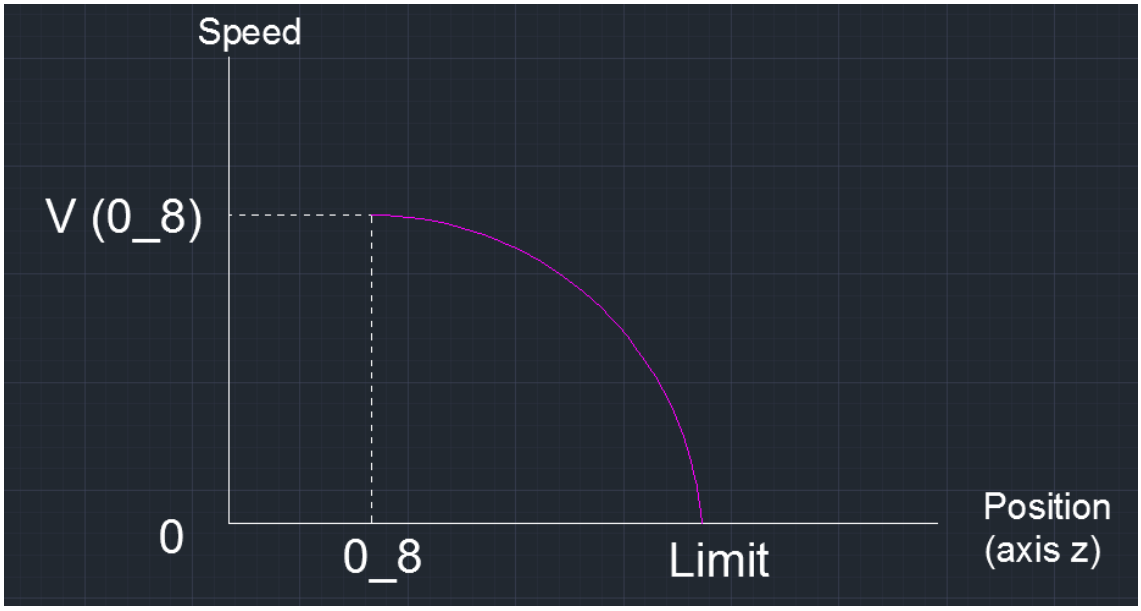

Fig. 82. Curve trend of the wind velocity profile. (Own elaboration).

To find the value of wind velocity outside the measurement mesh we divide the space into a total of 1000 rectangular cells of the same area.

We interpolate the intermediate values (green) between the value of the limit of the mesh and the wall of the test chamber.

To know the values of wind velocity out of the mesh in positions close to the corners we make the average of a double interpolation; one in the direction of x-axis and another in the z-axis direction. Data for this average are referenced in red and yellow colors in the image shown below.

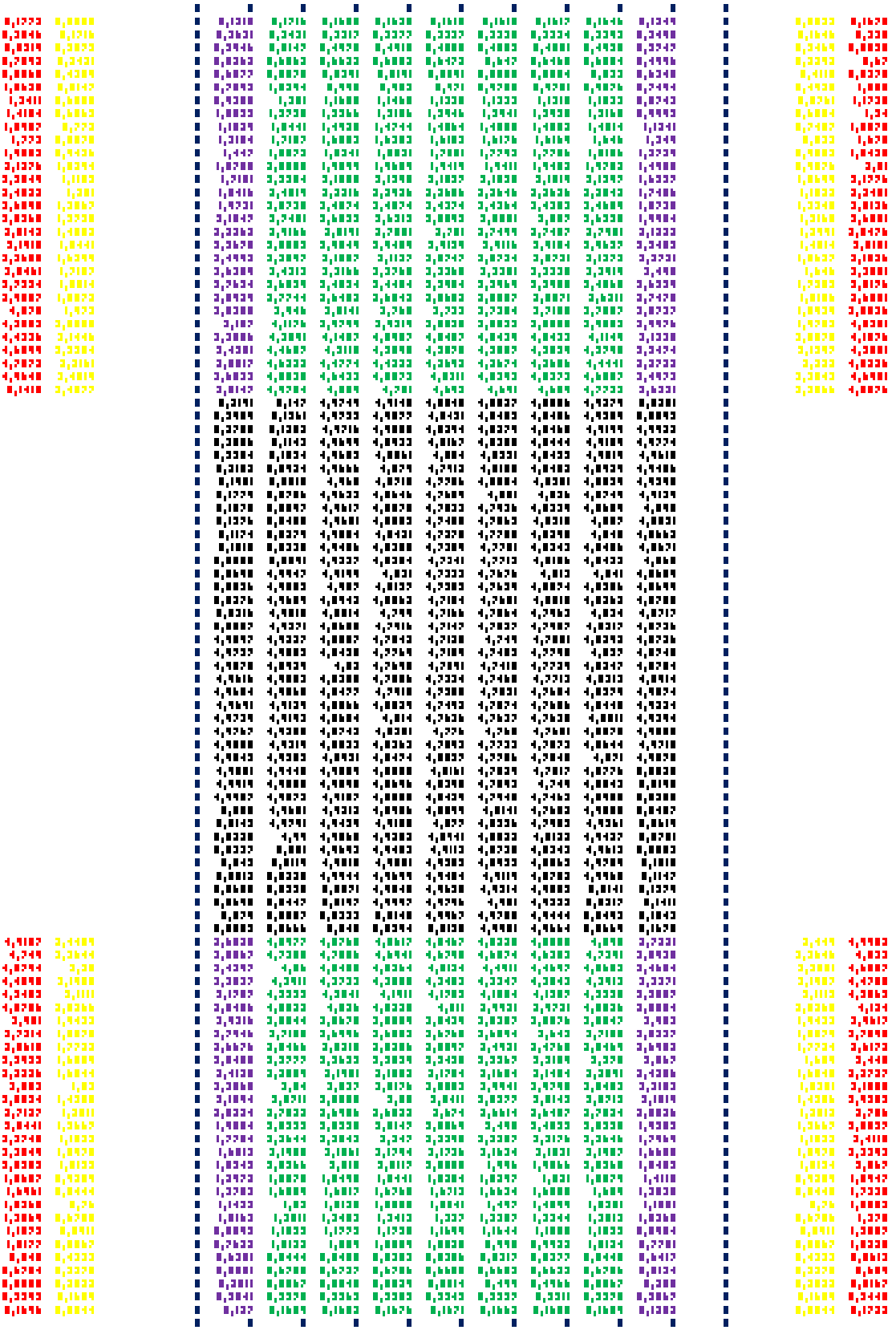

Fig. 83. Display configuration data (300 rpm, 8 Hz) schematically colored as in the drawing of the mesh and its surroundings. (Own elaboration).

Black color identifies data measured with dual-sensor probe. Blue marks the limits of the test chamber where the wind velocity is zero. Green identifies the linear trend from the inside of the mesh to the limit of the test chamber. Purple identifies the curve trend of wind velocity from the corners of the mesh to the limit of the test chamber.

The red and yellow numbers are values which have served to calculate the curve trend.

With these data, and considering that all cells have the same area, the velocity diagram (in the central point of every cell) representation is proportional to flow representation.

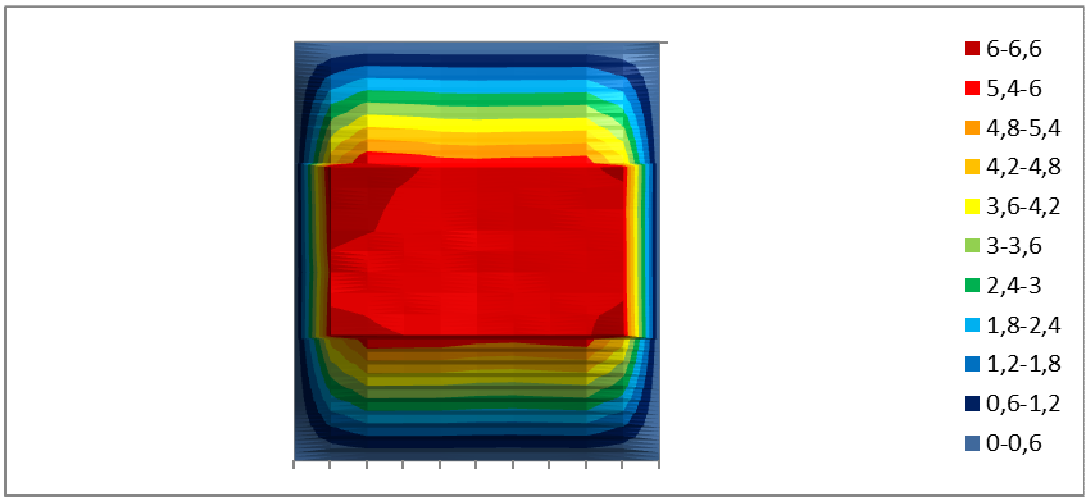

Fig. 84. Front view of the configuration flow (300 rpm, 8 Hz) through the vertical plane at the entry into the test chamber. (Own elaboration)

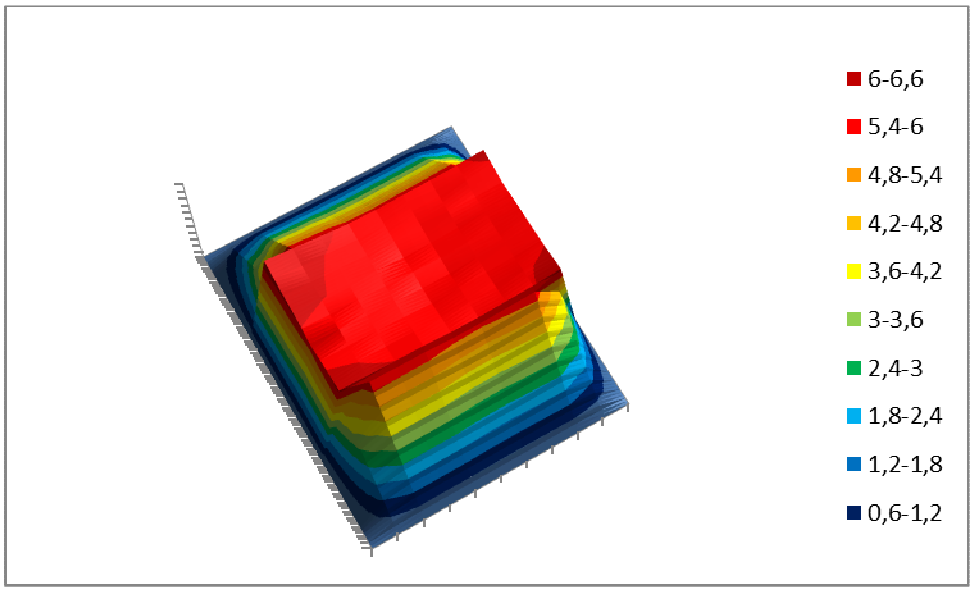

Fig. 85. Oblique view of the configuration flow (300 rpm, 8 Hz) through the vertical plane at the entry into the test chamber. (Own elaboration)

The study was performed for all possible combinations of 200 rpm, 300 rpm and 400 rpm with 6 Hz, 8 Hz and 10 Hz. Following are the data:

Configuration (rpm, Hz)	Flow through the mesh (m^3/s)	Total flow (m^3/s)	Flow out of the mesh (%)
200, 6	1.672	2.252	25.75
200, 8	2.254	3.022	25.41
200, 10	3.016	4.071	25.92
300, 6	1.702	2.273	25.12
300, 8	2.266	3.045	25.58
300, 10	2.863	3.837	25.38
400, 6	1.709	2.299	25.66
400, 8	2.324	3.105	25.15
400, 10	2.948	3.974	25.82

With these data we conclude that between 25 % and 26% of the air flow passes through the plane of measures out of the mesh.

The mesh occupies 46.32% of area measurement plane and through the mesh passes about 75% of air flow.

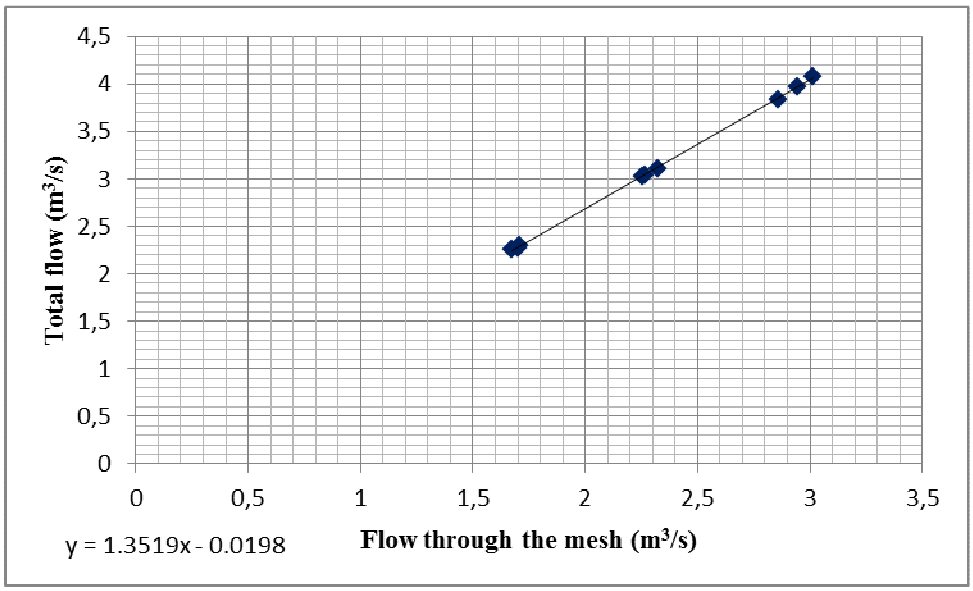

Fig. 86. Relation between total flow and flow through the mesh

The linear relationship between total air flow and air flow through the mesh is evident.

Using a least squares approximation we conclude that to calculate the total flow that drives the fan we must simply multiply the measured flow through the mesh (calculated by experimental method or by analytical method from the wind velocity at a particular point of the mesh as explained above) by a factor; in this case is 1.3519. It gives us a very high accuracy so that we consider it a very good approximation.

16. Analysis of the wind flow behind the rotor

To do this point we designed a new mesh:

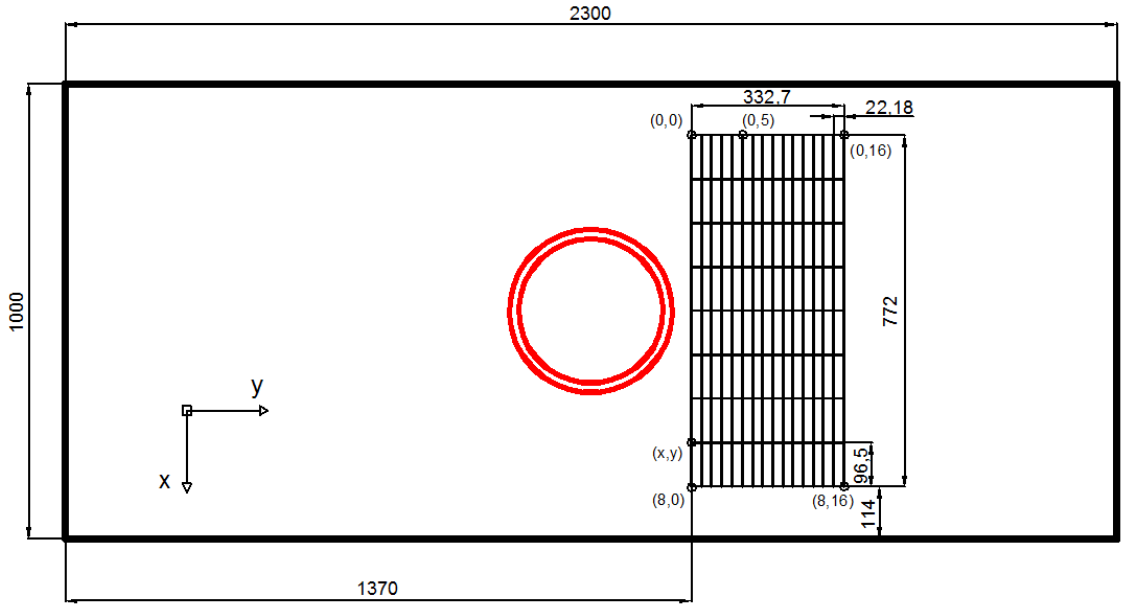

Fig. 87. Horizontal mesh

In our horizontal mesh the coordinate system follows the logic of movement of the robot. So, we work with the x-axis and y-axis being our notation (x-axis, y-axis). If we see the mesh from above the (0_0) is on the right side near the rotor and (8_16) is on the left side away from the rotor.

CONDITIONS OF THE EXPERIMENT

The fan spins with a frequency of 8Hz and the turbine with a speed of 300 rpm, the sensor takes data every 4.5 grades of the turbine rotation. If the turbine has a speed of 300 rpm, the turbine takes 0.2 seconds in spinning around so the sensor takes a data every 0.0025 seconds. We get data for about 105 turns, so get approximately 8400 data in each point.

SUMMARY OF THE MEASUREMENT PROCESS

First of all, it is necessary to put the robot in a starting point.

We put the robot in the reference position we have explained in the part of process of measurement. From there we have to move 532 mm along the window, going away from the turbine, 772 mm in the perpendicular direction in the same plane than the before movement, it means going away from the point where we watch the experiment. Moreover it is necessary raise the robot up 447 mm because the measurement must be done in the half height of the turbine.

If we carry out this process, the robot will be in the point (0_0). From here we can start to take information, the net has 17 points streamwise and 9 points in the transversal direction.

The distance among the points in the transversal direction is 96.5 mm, and the distance among the points along the window is 22.18 mm.

AVERAGE OF ALL VALUES IN THE MAP

This graphic shows the average of all data taken in each point:

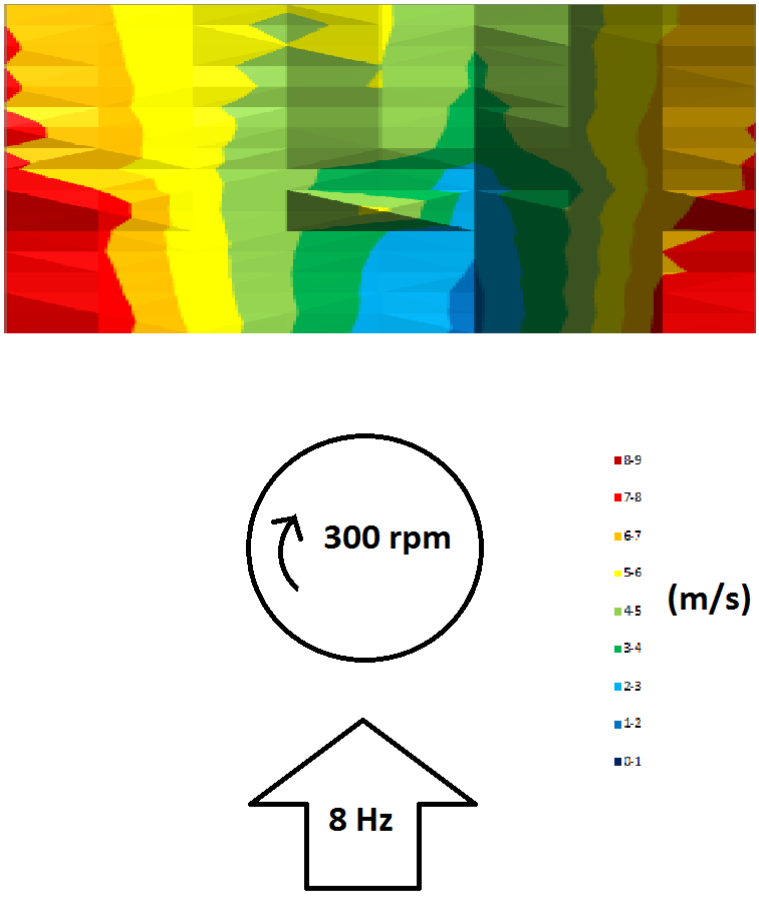

Fig. 88. Average velocity map

With this graphic we realize that the left part of the flow goes faster, the lack of symmetry is produced because of the spin of the turbine, this spin goes from the right side to the left side, it means that it spins counterclockwise.

To know the turbulences of the flow we take the variance, this graphic shows the variance in each point.

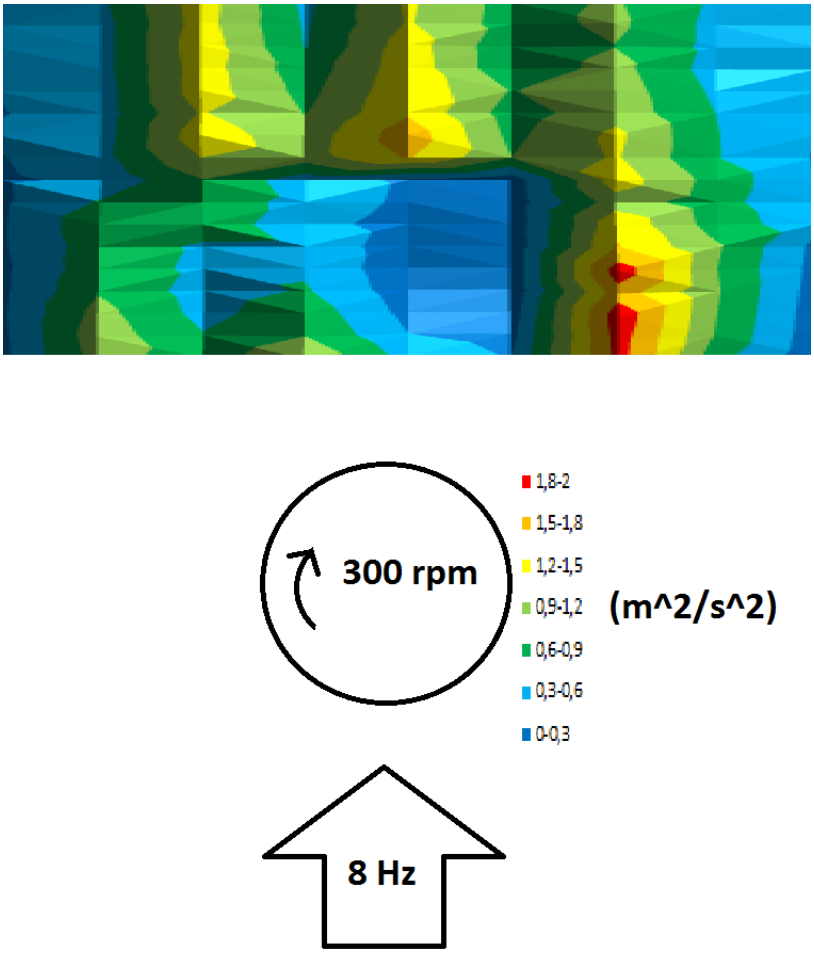

Fig. 89. Variance map

Here we see that the turbulence is low in the part next to the window, there is some turbulence in the middle of the corridor, this is because there is a change in those points with the time.

EVOLUTION OF ANY COLUMN WITH THE TIME

If we analyze the evolution in any column according with each 4.5 grades it means 0.0025 seconds. We realize that the small increases in the speed move away from the turbine.

This graphic shows the evolution of the column 8.

Any line represents a point of the column, (8_0)(8_1)(8_2)(8_3)…etc.

There are 17 lines because each line represents a point in a column and there are 17 points of measurement.

In the horizontal axis it is represented the degrees that the turbine has turned, therefore we can say also that represents the time.

In the vertical axis it is represented the speed of the flow.

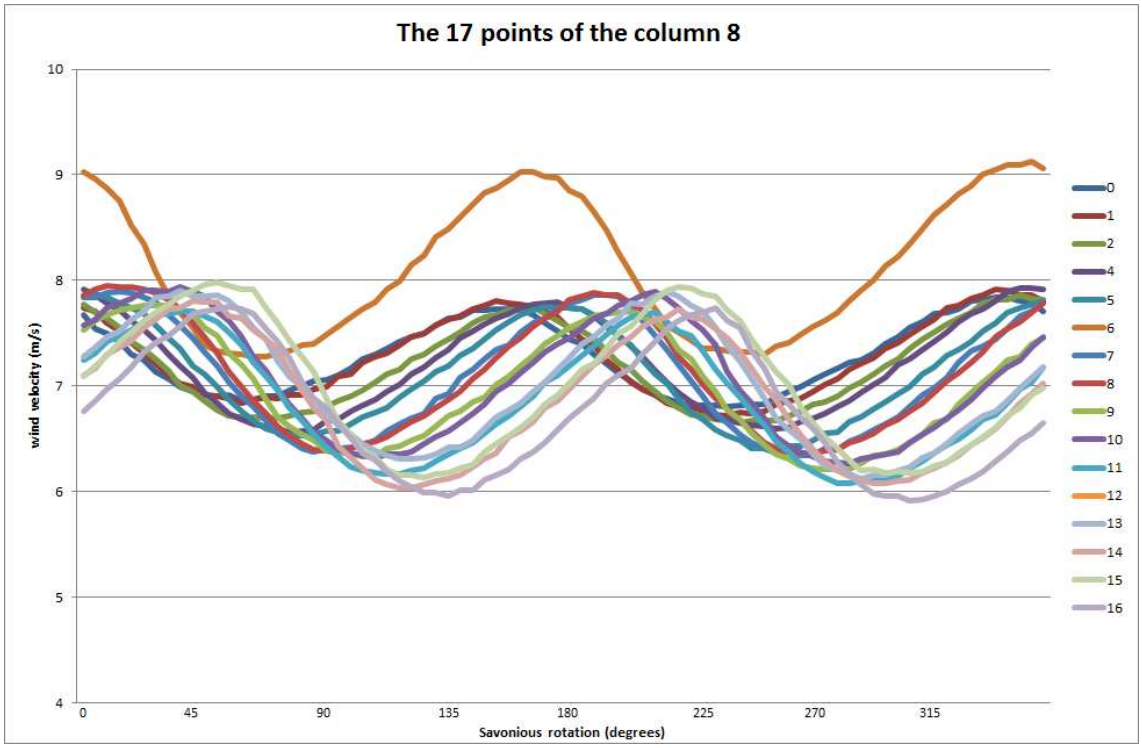

Fig. 90. Evoultion of all points colum 8

We can see that everything that happen in the point (8_1) happen a bit later in the point (8_2), and later in the rest of the points of the column, for example if one point reach the maximum value in the position of 135 degrees the point next to it will reach the maximum for 139,5.

We can see that some lines are over other lines because they are taking their values almost at the same time.

The point 6 has a higher velocity but its evolution is according with this fact.

We can see that some lines are over other lines because they are taking their values almost at the same time.

This fact is regular in the parts near the window but not in the central area.

This graphic shows the evolution of the column 4, as we see the central area has more turbulence, and we can't even appreciate the delay of the velocity in any point.

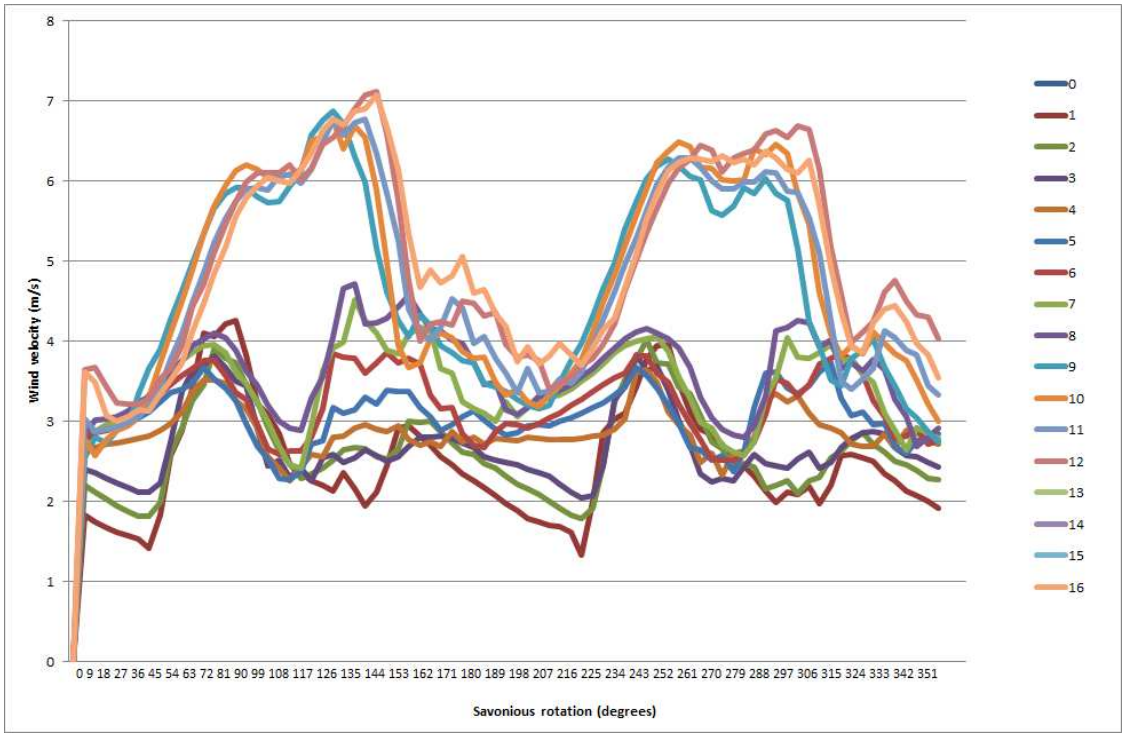

Fig. 91. Evolution of all points colum 4

Evolution of the whole area behind the rotor

The Savonius rotor sometimes produces effects behind itself such as increases of the velocity in common areas.

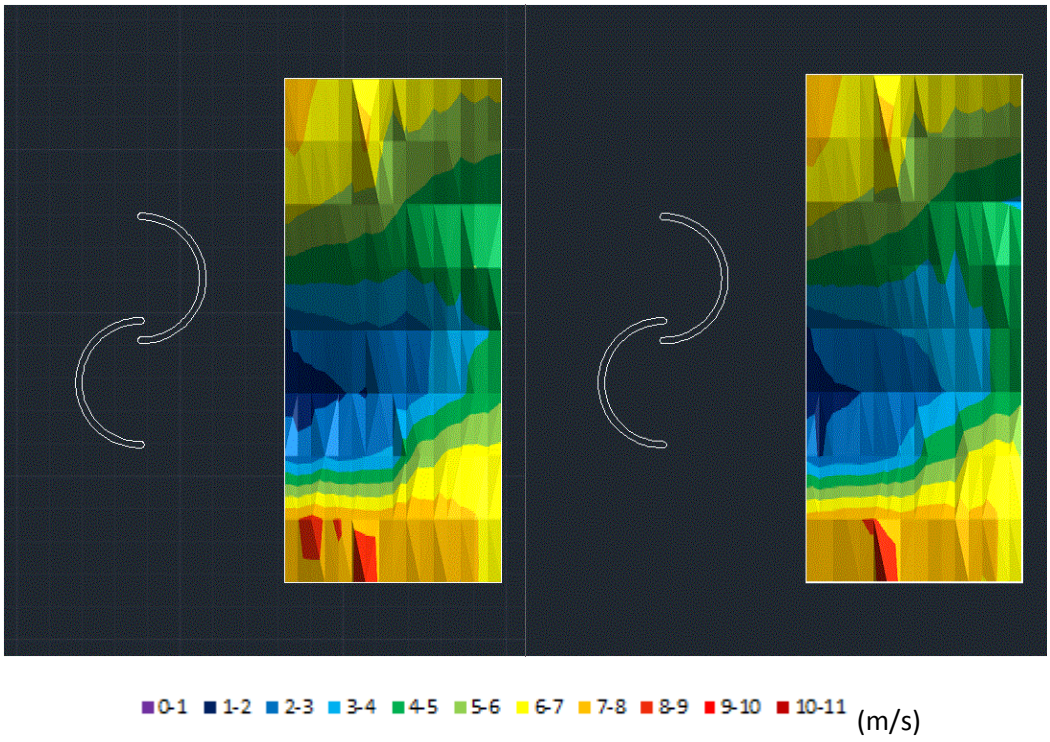

Fig. 92. These graphics are in the moment 0, and in the moment 180, we can see that map of velocities is almost the same.

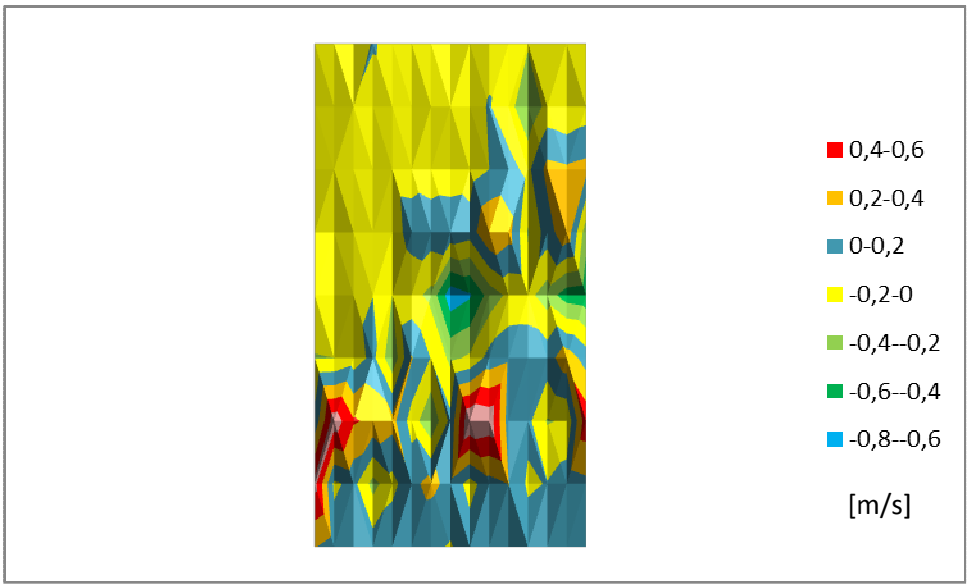

Fig. 93. Comparison between graph 0º and graph 180º

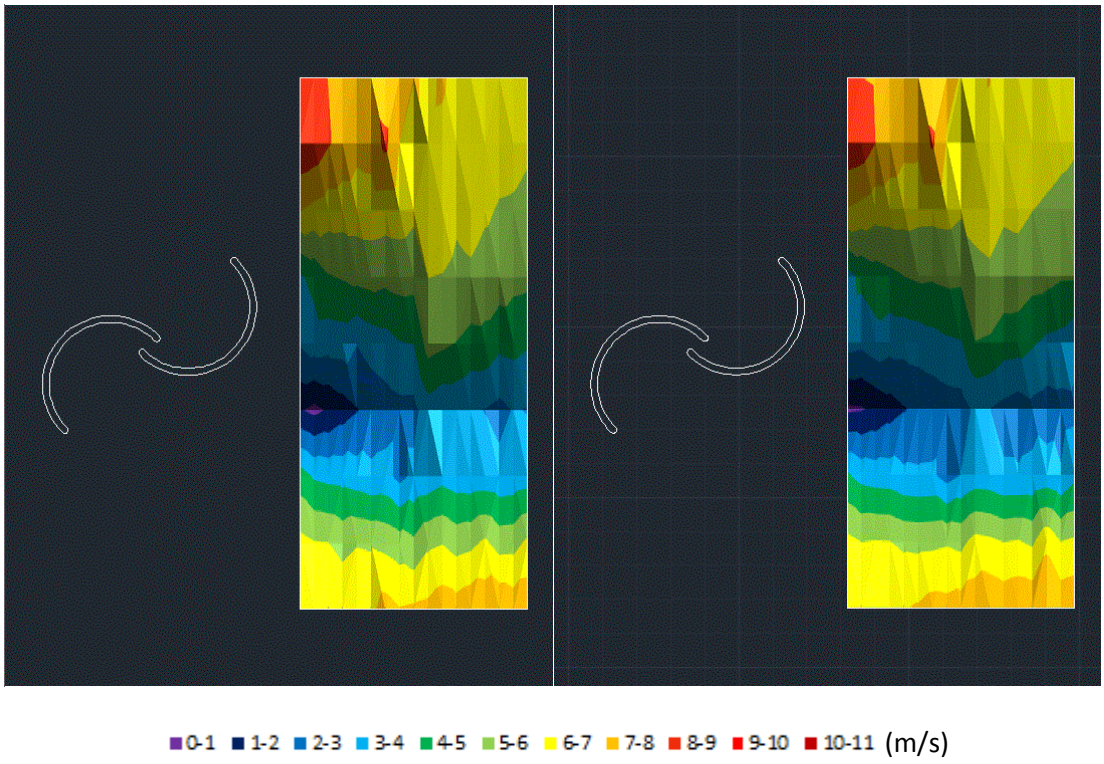

Fig. 94. These graphics are of the moment 45 and 225.

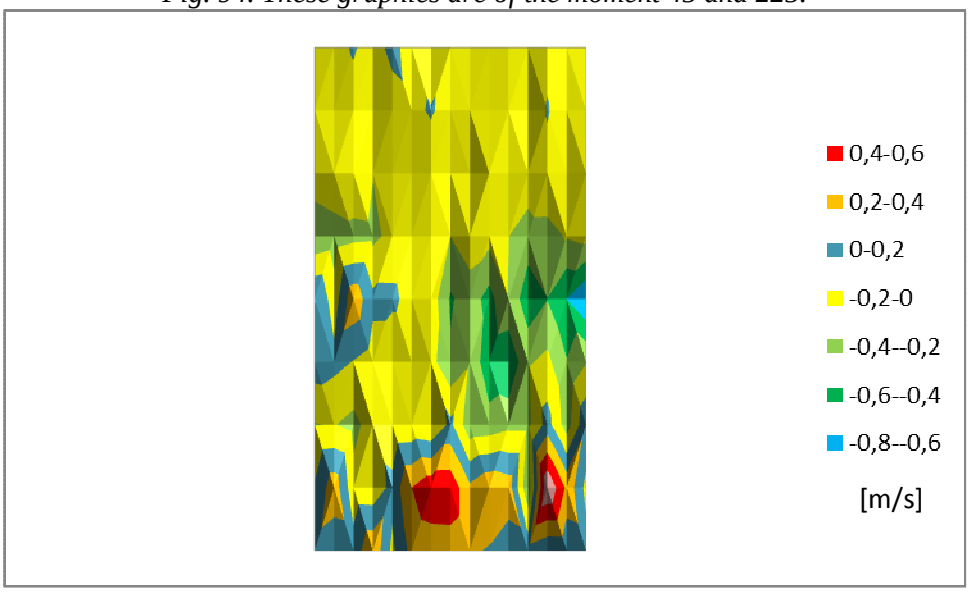

Fig. 95. Comparison between graph 45º and graph 225º

With these two examples we see that the velocity of the wind repeats its value each 180 degrees, but it does not mean that the situation is the same because the torque of the servo is different as we explain in the following point.

COMPARISON BETWEEN VELOCITY AND TOTAL TORQUE BEHIND THE ROTOR

At first glance seems that every 180 degrees the situation repeats. It's obvious if we see 0 degrees and 180 degrees charts or any other couple of graphs separated 180 degrees.

But doing a study about the torque we conclude that both situations are not exactly the same.

To calculate the total torque we use the Sanyo-Denki Torque and the multiplication of angular acceleration times the moment of inertia of the Savonius rotor.

$$TT = T_{S-D} + I\alpha$$

TT = Total torque (Nm)

$T_{S\text{-}D}$ = Sanyo-Denki torque (Nm)

I = Savonius inertia momento = 0.350695127 Kgm^2

α = Smoothed angular acceleration (m/s^2)

The moment of inertia of this Savonius rotor was calculated by Luigi Di Leo in 2010. We use 0.350695127 Kgm^2.

The system does not provide us the value of the angular acceleration. That's why we calculate it through the calculation of angular velocity because the system gives us the value of the time between every measure that represents 4.5 degrees.

$$\omega = \frac{\Delta\theta}{\Delta t} = \frac{\theta_{i+1} - \theta_i}{\Delta t} = \frac{4.5}{\Delta t}$$

And to calculate the angular acceleration.

$$\alpha = \frac{\Delta\omega}{\Delta t} = \frac{\omega_{i+1} - \omega_i}{\Delta t}$$

If we represent the angular acceleration we have this graph.

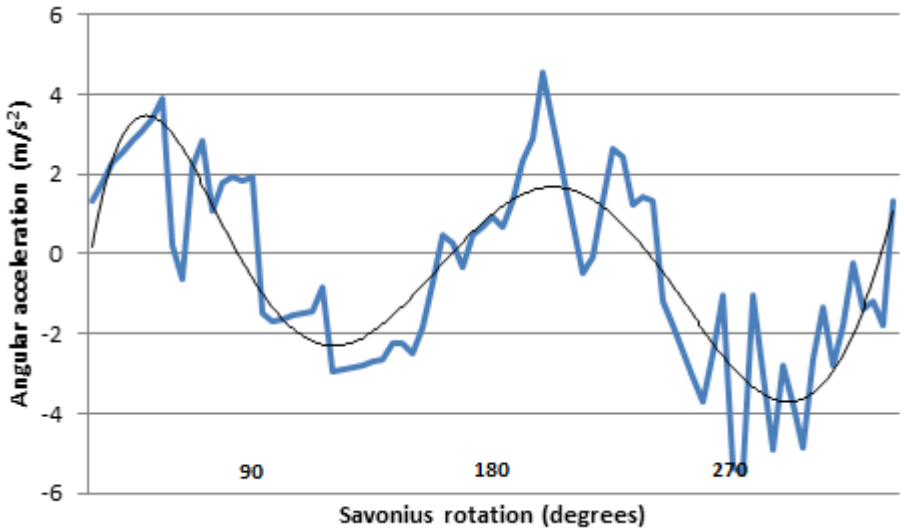

Fig. 94. Evolution of the angular acceleration versus the Savonius rotation

The black line represents the smoothed angular acceleration. We use this data to avoid big steps in the acceleration.

We calculate the total torque and represent it in a radial graph.

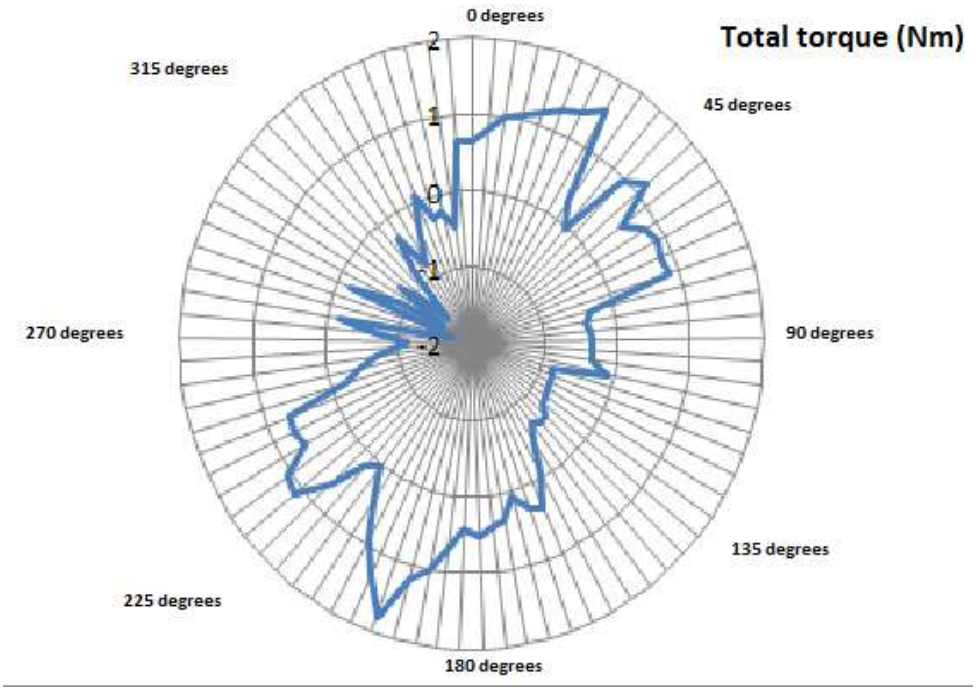

Fig. 95. Evolution of total torque versus Savonius rotation in a radial graph

It’s clearer if we represent it in a linear chart.

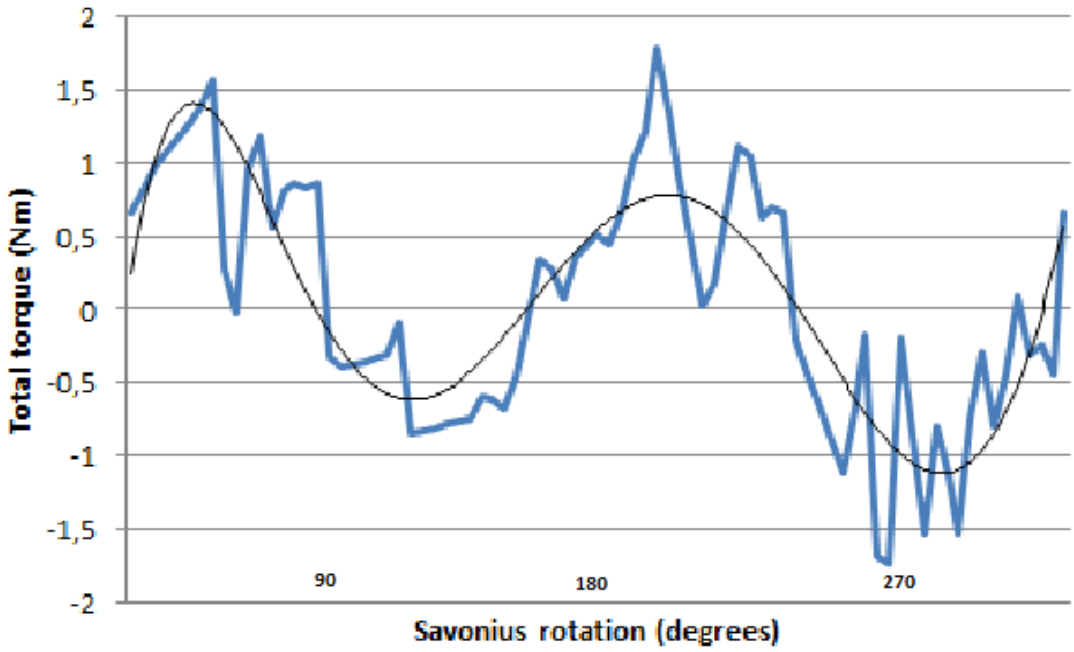

Fig. 96 Evolution of total torque versus Savonius rotation in a linear graph

Now we clearly say that every 180 degrees the situation is not exactly the same. In the velocity video we couldn’t see these changes of torque. We see that, for example, at 0 and 180 degrees the torque is not the same. This thing happens with all cases.

17. Bibliography

Articles:

1.- “Wind tunnel tests on a Savonius rotor” by A.J. Alexander and B.P. Holownia. Journal of Industrial Aerodynamics, 1978.
2.- “Experimental investigations on single stage modified Savonius rotor” by M.A. Kamoji, S.B. Kedare and S.V. Prabhu.
3.- “Experimental study of a Savonius-Darrieus wind machine” by R. Gupta, R. Das and K.K. Sharma.
4.- “Wind tunnel tests on a three-stage out-phase Savonius rotor” by T. Hayashi, Y. Li, Y. Hara and K. Suzuki.
5.- “Wind tunnel performance data for two- and three-bucket Savonius rotors” by B.F. Blackwell, R.E. Sheldahl and L.V. Feltz. 1977.
6.- “Optimum design configuration of Savonius rotor through wind tunnel experiments” by U.K. Saha, S. Thotla and D. Maity. Journal of Wind Engineering and Industrial Aerodynamics, 2008

Books:

7.- “Energía eólica” by Miguel Villarrubia. Grupo Editorial CEAC, Spain, 2004
8.- “Guía completa de la energía eólica” by José Mª Fernández Salgado. AMV Ediciones, Spain, 2011.

Thesis:

9.-“Caratterizzazione sperimentale di una turbine eolica in galleria del vento” by D.F. De Fazio. Politecnico di Bari, Italy, 2009.
10.-“Progettazione, realizzazione e analisi sperimentale di un rotore Savonius” by L. Di Leo. Politecnico di Bari, Italy, 2010.
11.-“Investigation of the Savonius-type Magnus wind turbine” by N. Komatinovic. Technical University of Denmark. 2006
12.-“Ottimizzazione aerodinamica tramite CFD di una turbine eolica ad asse vertical” by E. Leucci. Politecnico di Milano, Italy, 2010.
13.-“Caratterizzazione sperimentale in galleria del vento di una turbine eolica” by N. Manzari. Politecnico di Bari, Italy, 2008.

Others:

14.-“Compressed air applications manual” by Beko.
15.-“Dantec Dynamics information about constant temperature anemometry”
16.-“Bolletino ufficiale della Regione Puglia, 03/08/2007”

Annex

Θ= 0º
(Rotor, Fan) (300 rpm, 8 Hz)
Wind from left to right

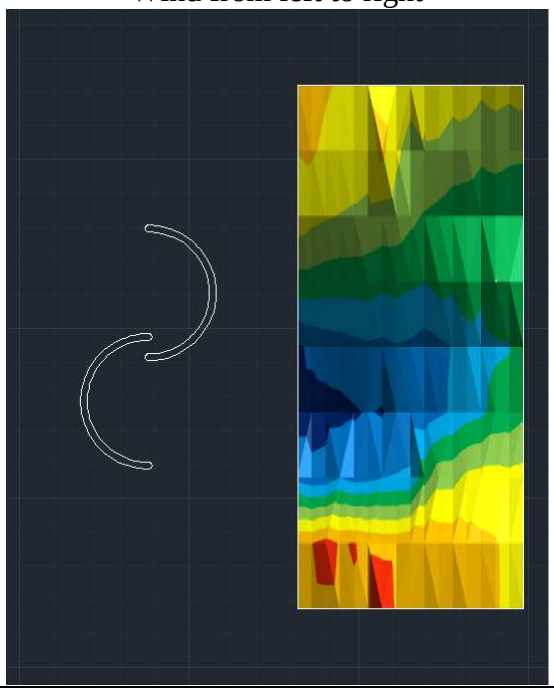

Θ=18º
(Rotor, Fan) (300 rpm, 8 Hz)
Wind from left to right

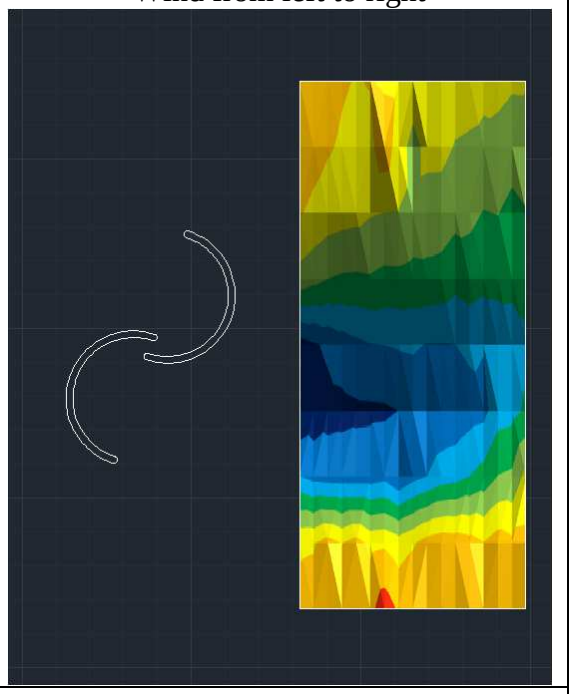

Θ=36º
(Rotor, Fan) (300 rpm, 8 Hz)
Wind from left to right

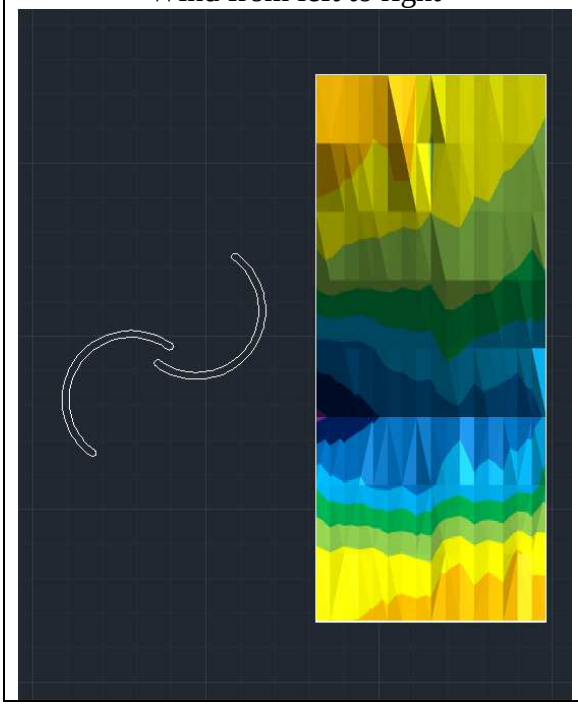

Θ=54º
(Rotor, Fan) (300 rpm, 8 Hz)
Wind from left to right

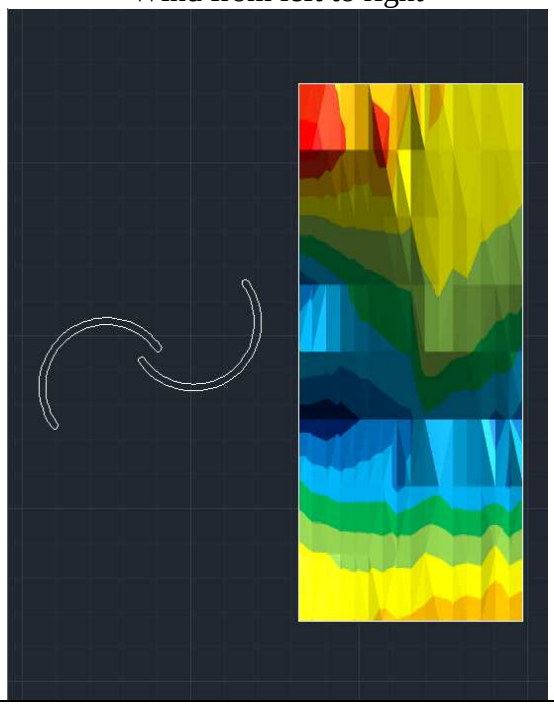

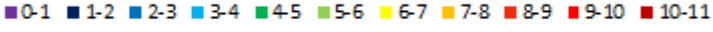

(m/s)

ϴ=72º
(Rotor, Fan) (300 rpm, 8 Hz)
Wind from left to right

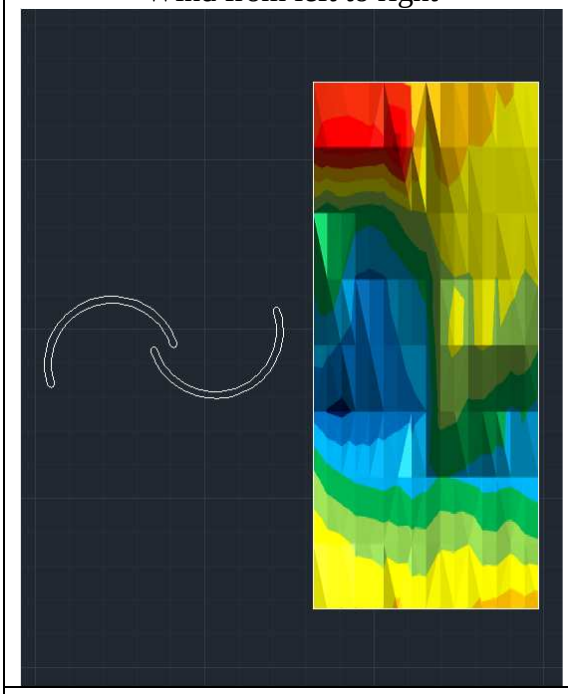

ϴ=90º
(Rotor, Fan) (300 rpm, 8 Hz)
Wind from left to right

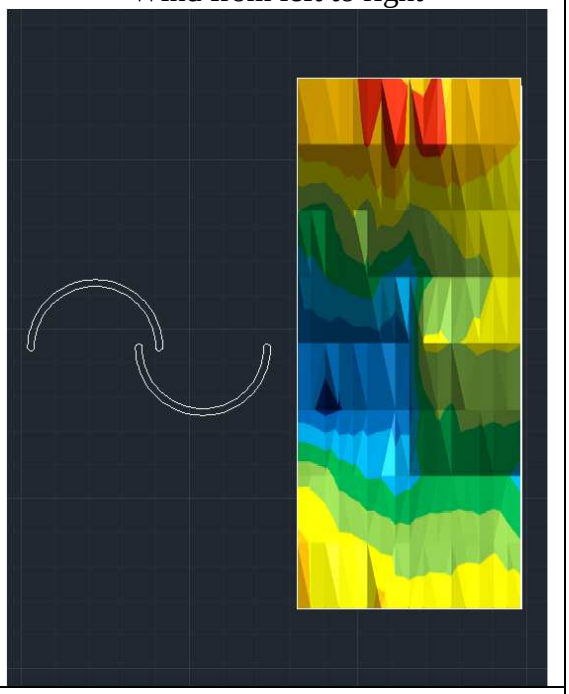

ϴ=108º
(Rotor, Fan) (300 rpm, 8 Hz)
Wind from left to right

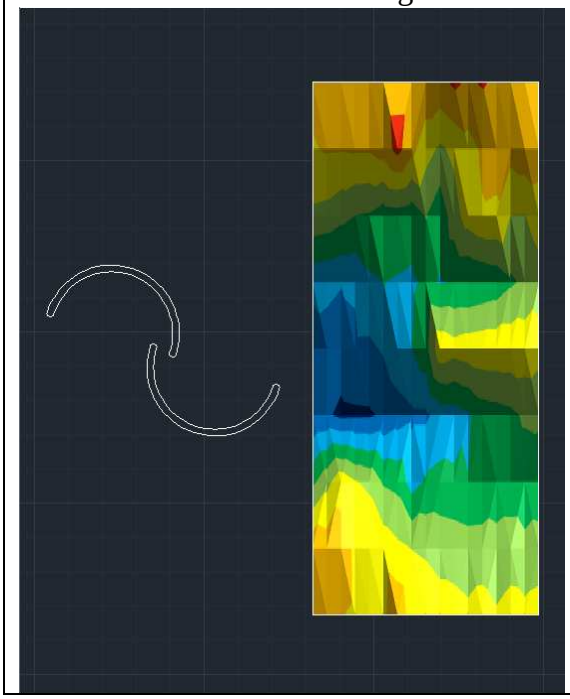

ϴ=126º
(Rotor, Fan) (300 rpm, 8 Hz)
Wind from left to right

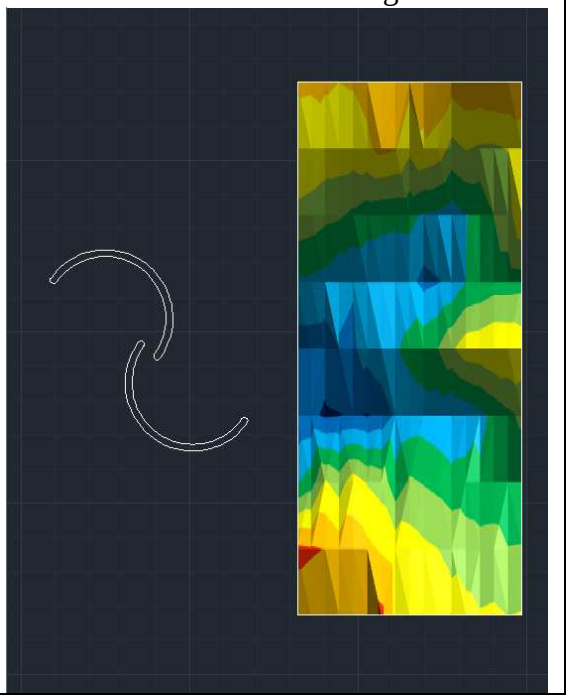

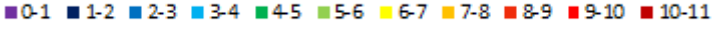

(m/s)

ϴ=144º
(Rotor, Fan) (300 rpm, 8 Hz)
Wind from left to right

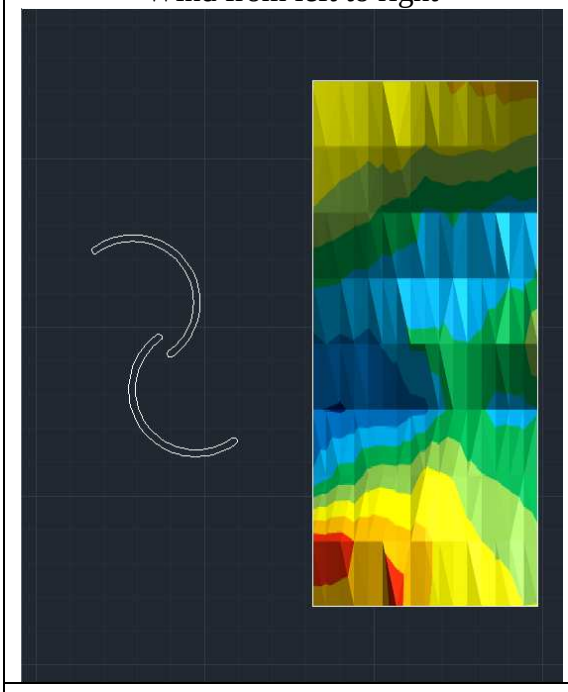

ϴ=162º
(Rotor, Fan) (300 rpm, 8 Hz)
Wind from left to right

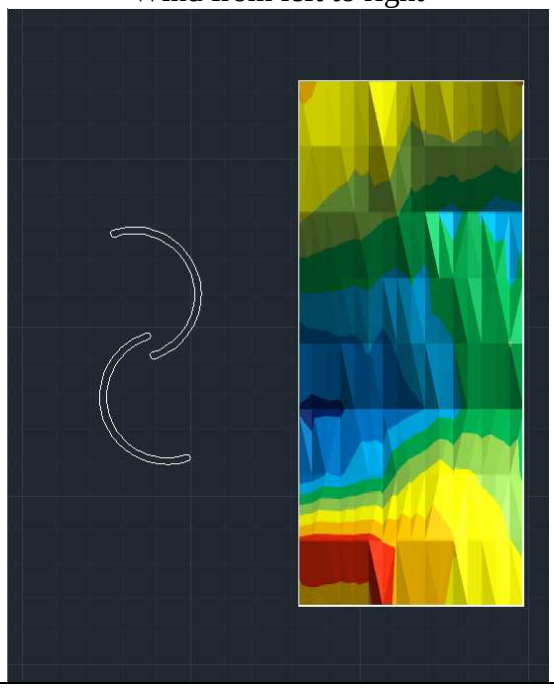

ϴ=180º
(Rotor, Fan) (300 rpm, 8 Hz)
Wind from left to right

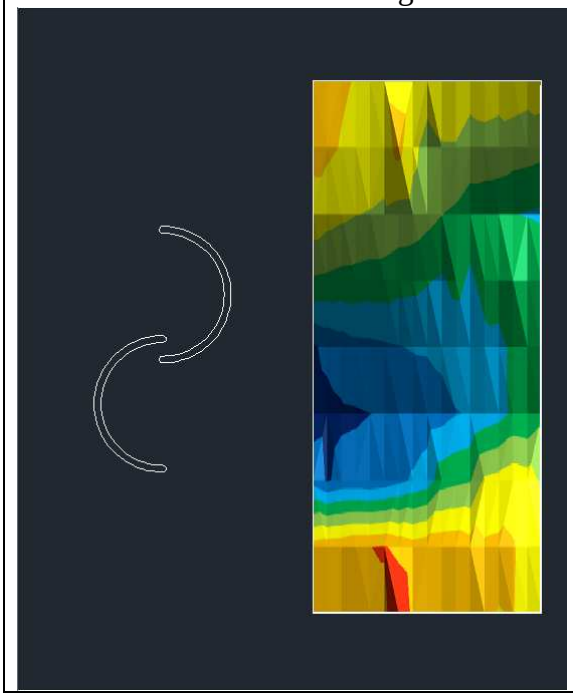

ϴ=198º
(Rotor, Fan) (300 rpm, 8 Hz)
Wind from left to right

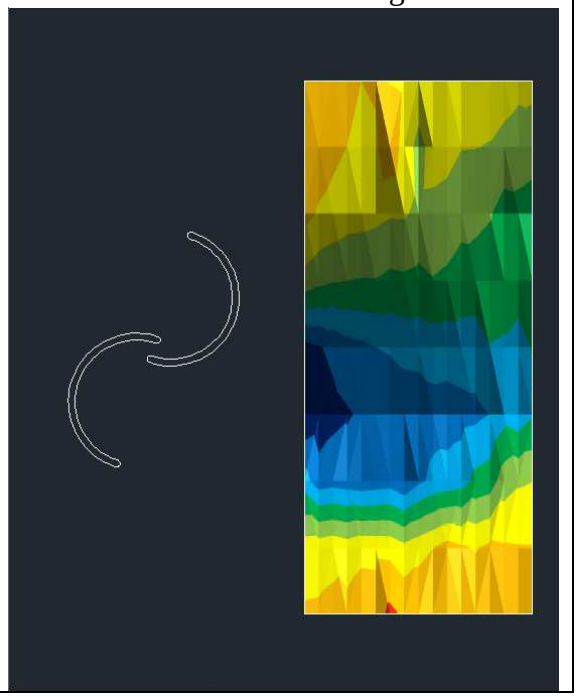

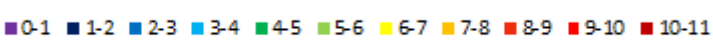

(m/s)

ϴ=216º
(Rotor, Fan) (300 rpm, 8 Hz)
Wind from left to right

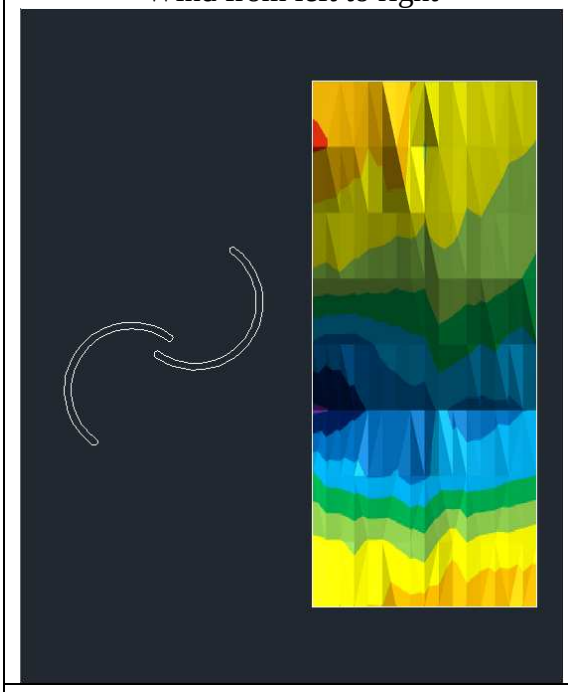

ϴ=234º
(Rotor, Fan) (300 rpm, 8 Hz)
Wind from left to right

ϴ=252º
(Rotor, Fan) (300 rpm, 8 Hz)
Wind from left to right

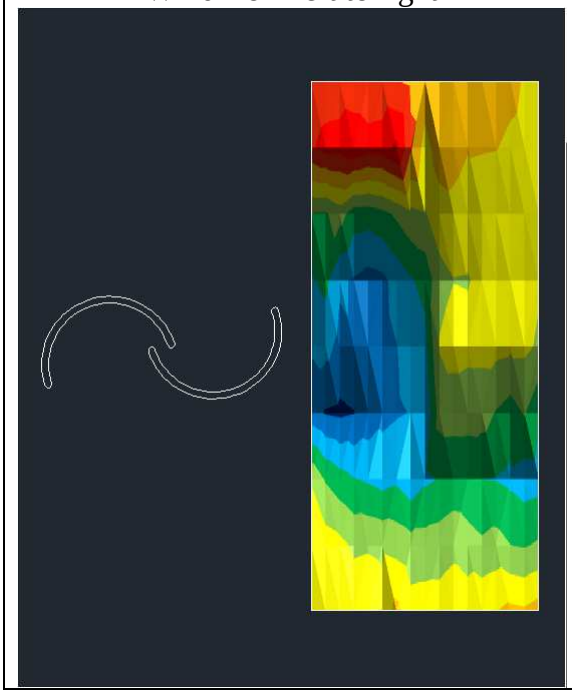

ϴ=270º
(Rotor, Fan) (300 rpm, 8 Hz)
Wind from left to right

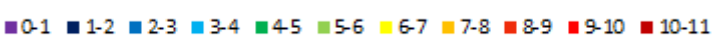

(m/s)

Θ=288º
(Rotor, Fan) (300 rpm, 8 Hz)
Wind from left to right

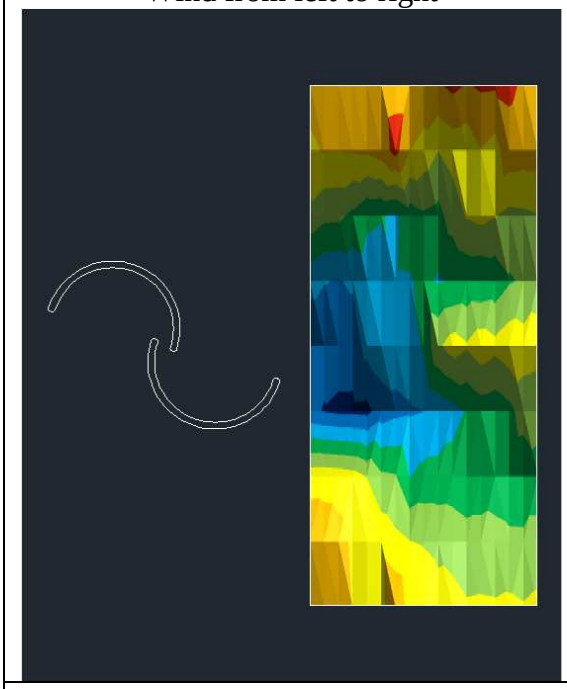

Θ=306º
(Rotor, Fan) (300 rpm, 8 Hz)
Wind from left to right

Θ=324º
(Rotor, Fan) (300 rpm, 8 Hz)
Wind from left to right

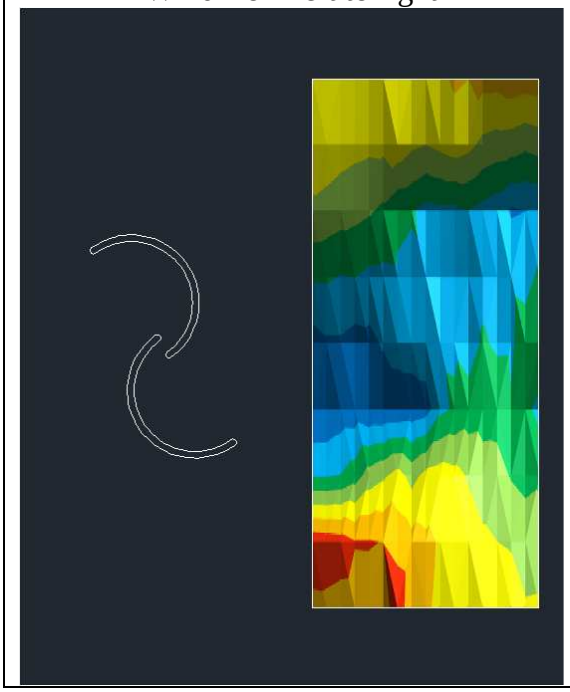

Θ=342º
(Rotor, Fan) (300 rpm, 8 Hz)
Wind from left to right

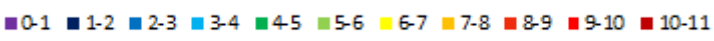

(m/s)

ANALYSIS OF THE FLOW AROUND A SAVONIUS ROTOR

Final Project in Renewable Energies

Supervisor: Prof. Ing. Marco Torresi

Writer: Jose María Jaurrieta Zarranz

INDEX

- Why did I choose this project?
- Wind energy
- Equipment
- Experiments:
  - Inlet velocity profile
  - Relation between flow rate and wind velocity at a reference point; and flow out the mesh
  - Analysis of the flow behind the rotor

Green energy in Europe

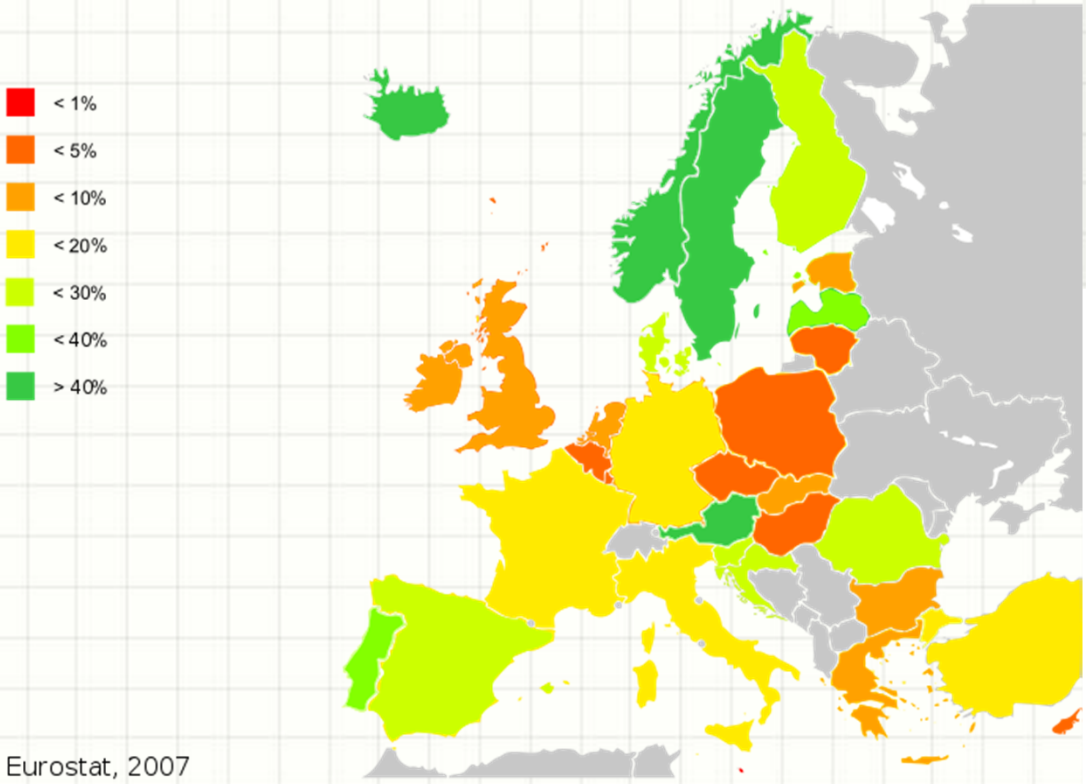

Eurostat, 2007

Wind energy

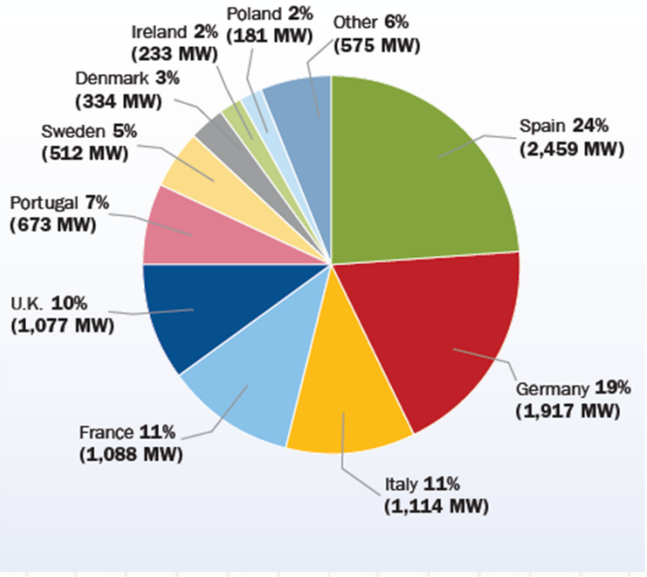

ENERGY IN EUROPE

NEW INSTALLED CAPACITY AND DE-COMMISSIONED CAPACITY IN EU 2009 IN MW. TOTAL 25,963 MW

FIGURE 1.2

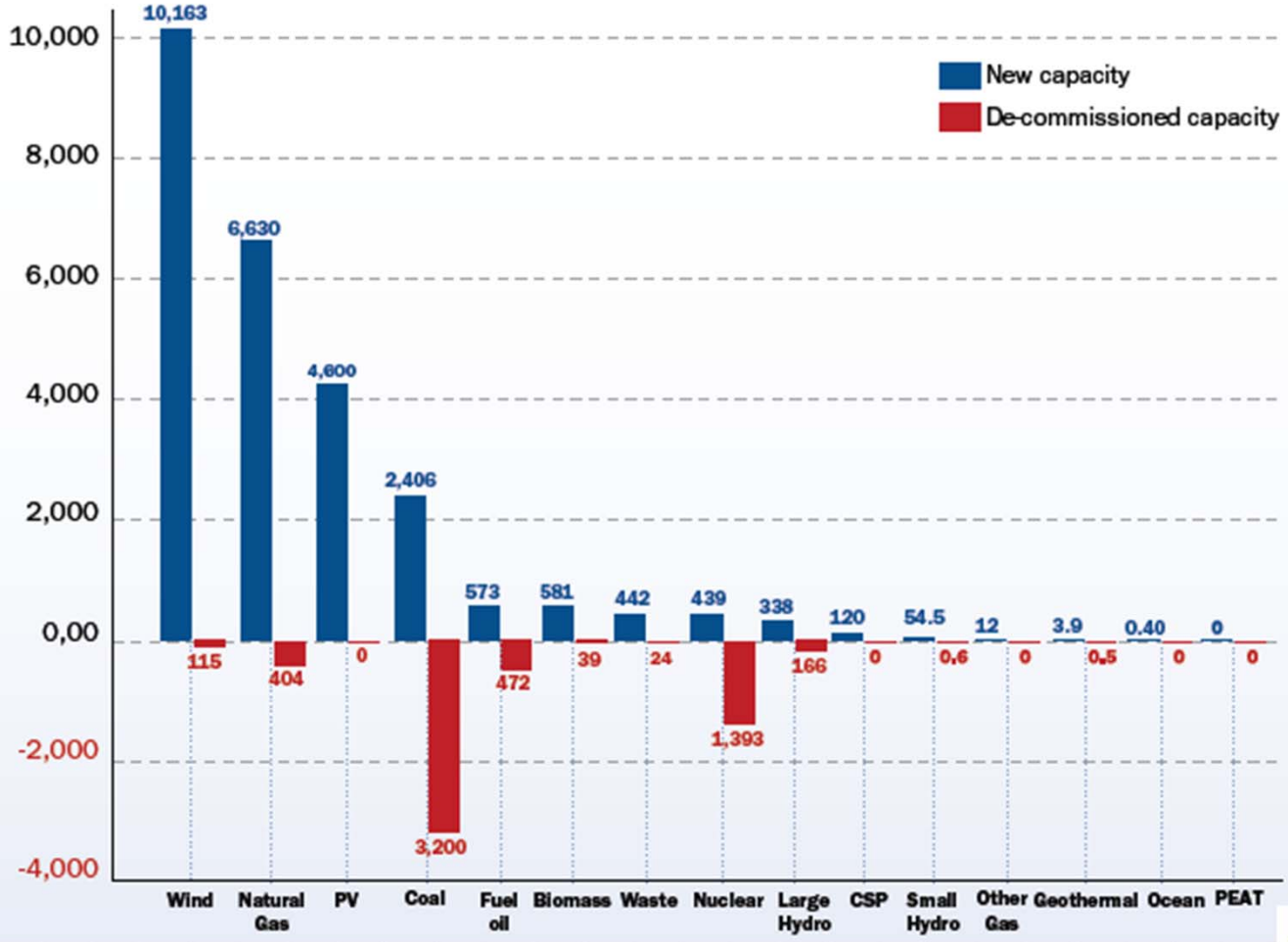

WIND ENERGY IN SPAIN AND ITALY

Spain

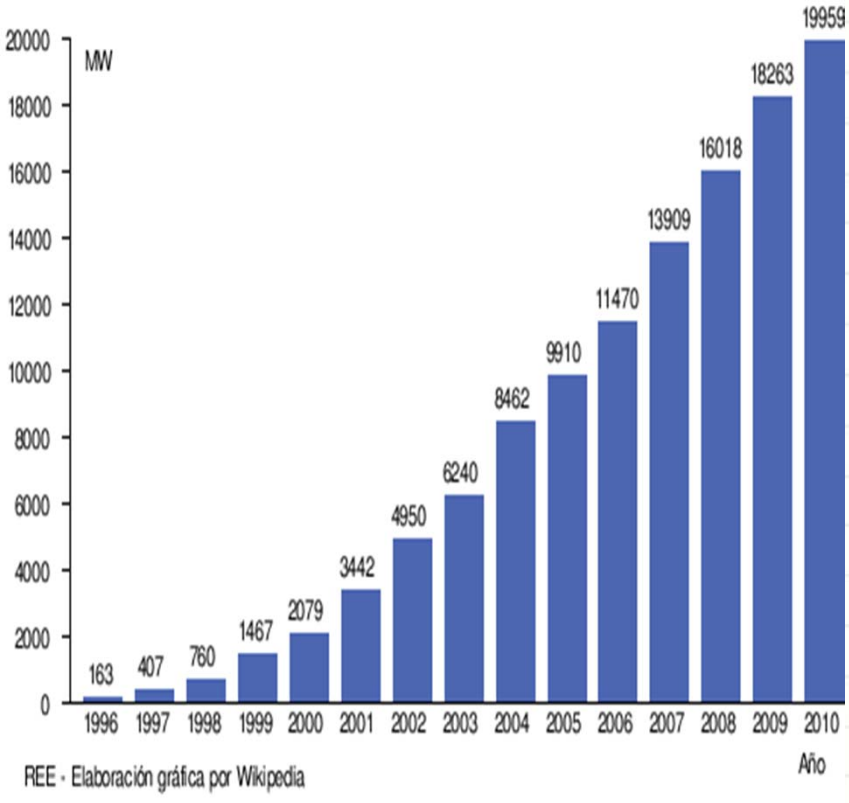

Italy

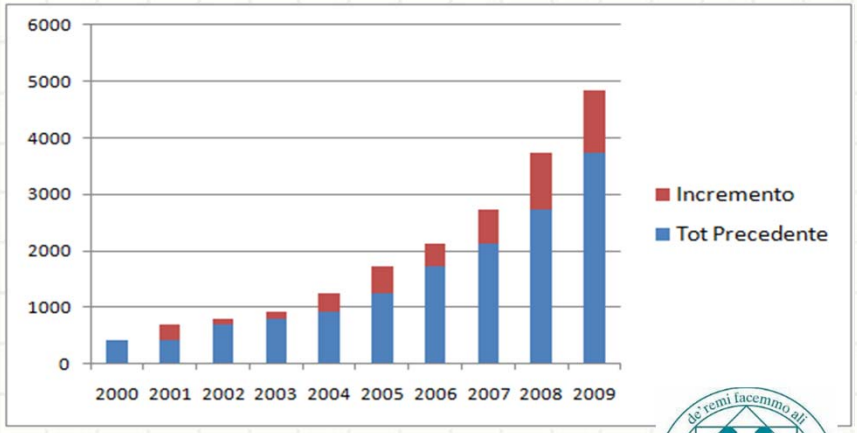

DIFFERENT TYPES OF ROTORS

HAWT Rotors

VAWT Rotors

- Darrieus

- Savonius

EQUIPMENT

SAVONIUS ROTOR

TEST CHAMBER AND ROBOT

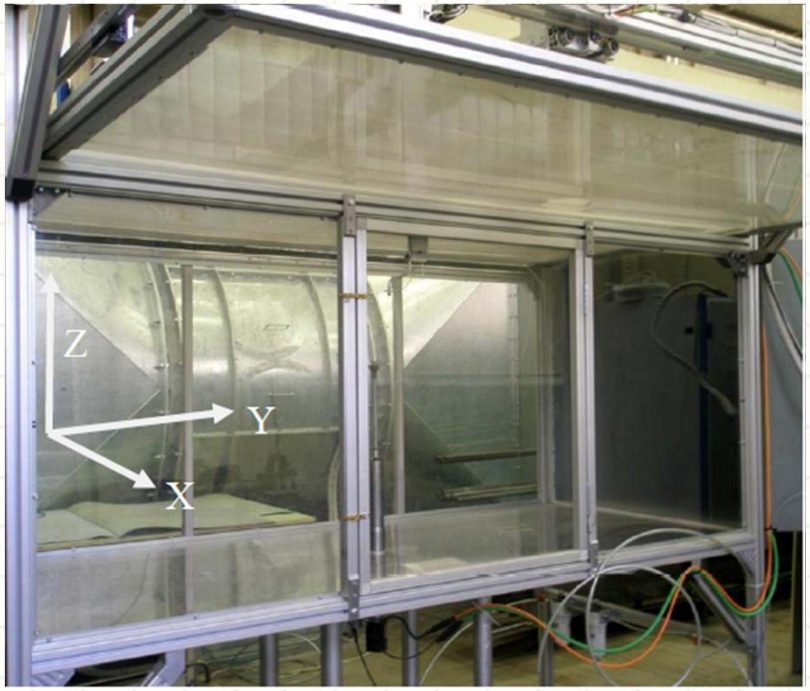

EQUIPMENT

WIND GALLERY

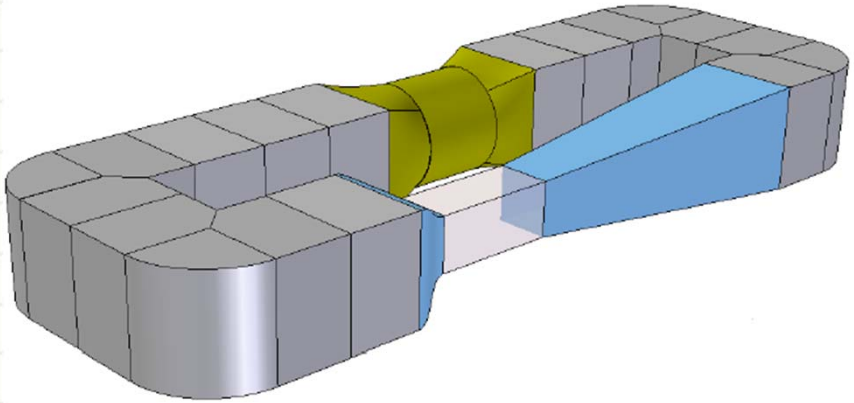

FAN

PROBE

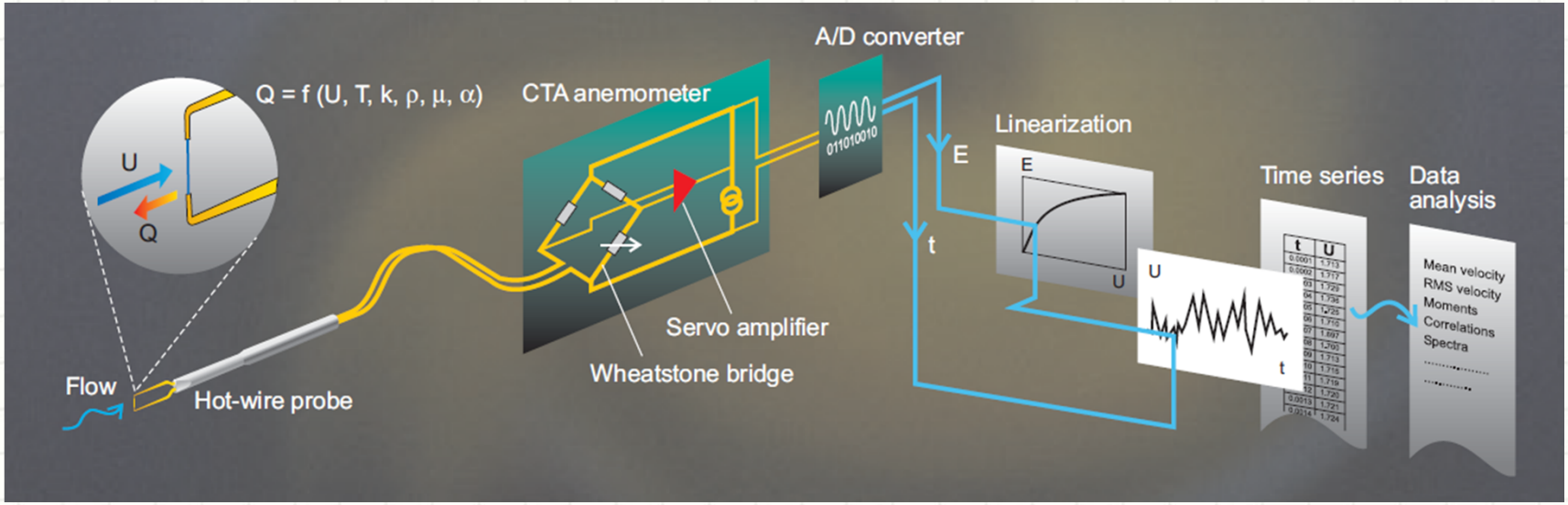

SINGLE-SENSOR:

EXPERIMENTS

- INLET VELOCITY PROFILE

- RELATION BETWEEN FLOW RATE AND WIND VELOCITY AT A REFERENCE POINT; AND FLOW OUT THE MESH

- ANALYSIS OF THE FLOW BEHIND THE ROTOR

MESH

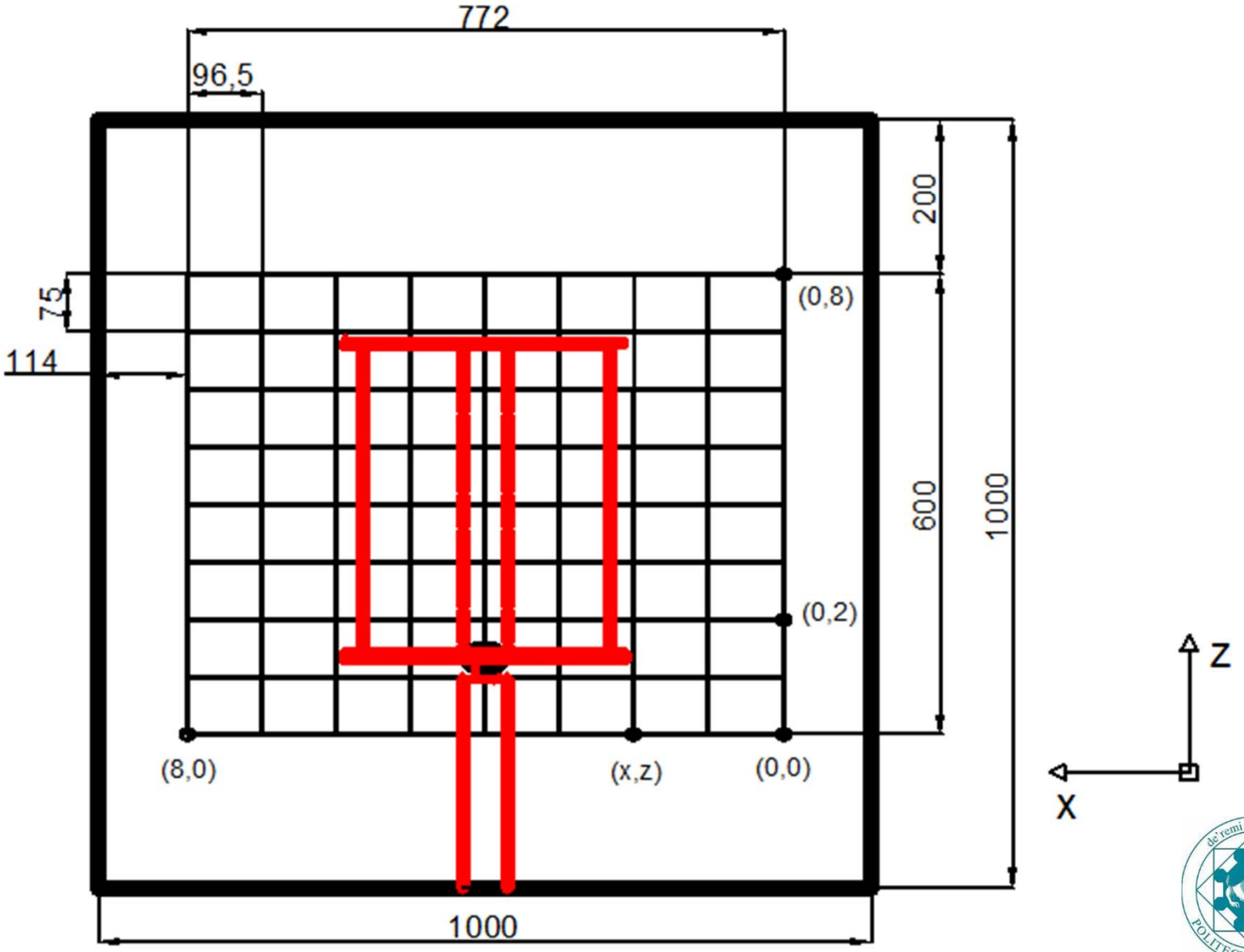

General Parameters

300 rpm, 8 Hz

Average Velocity

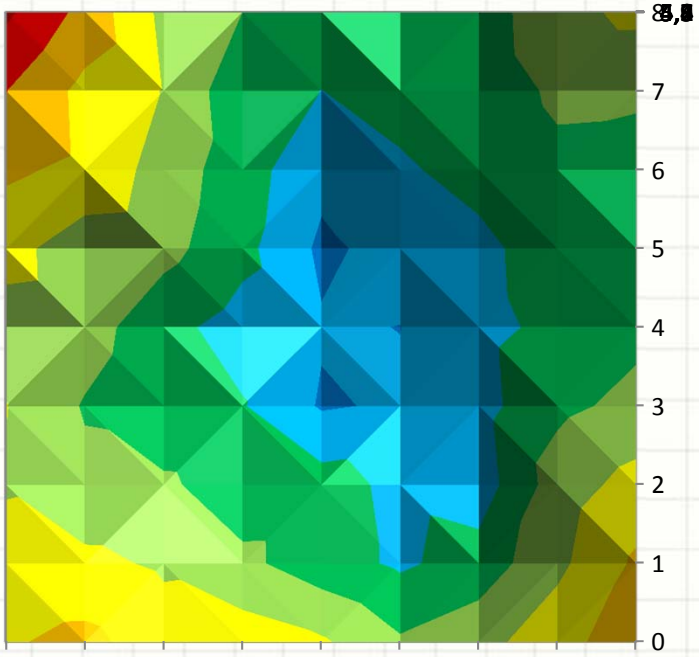

Variance

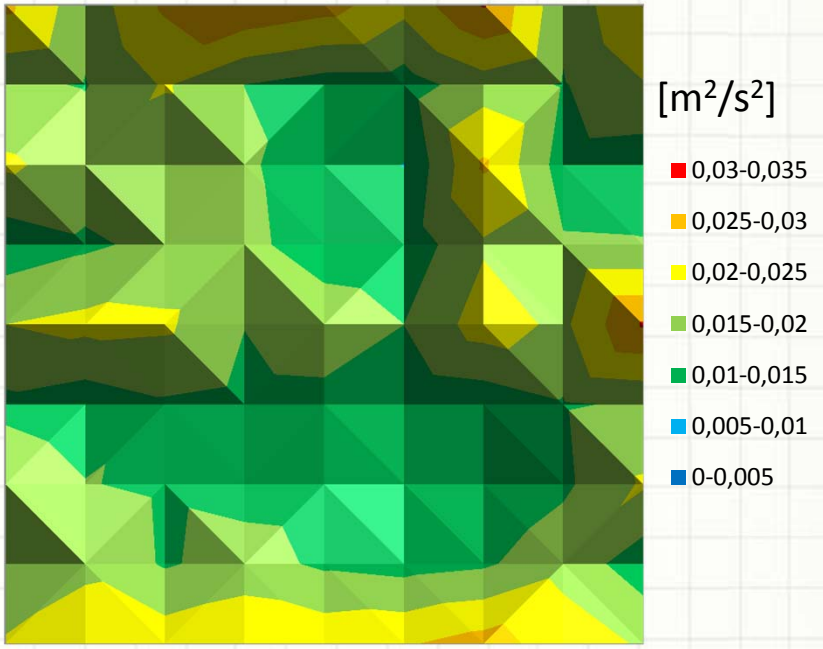

FLOW COMPARISON IN THE DIFFERENT MESHES

Probe	Single-Sensor
Flow 8x8	2.262314 m^3/s
Cell Cross-section	0.0072375 m^2
Flow 4x4	2.265724 m^3/s
Cell Cross-section	0.02895 m^2
Flow Difference	***1,51 %***

FLOW RATE OUT OF THE MESH

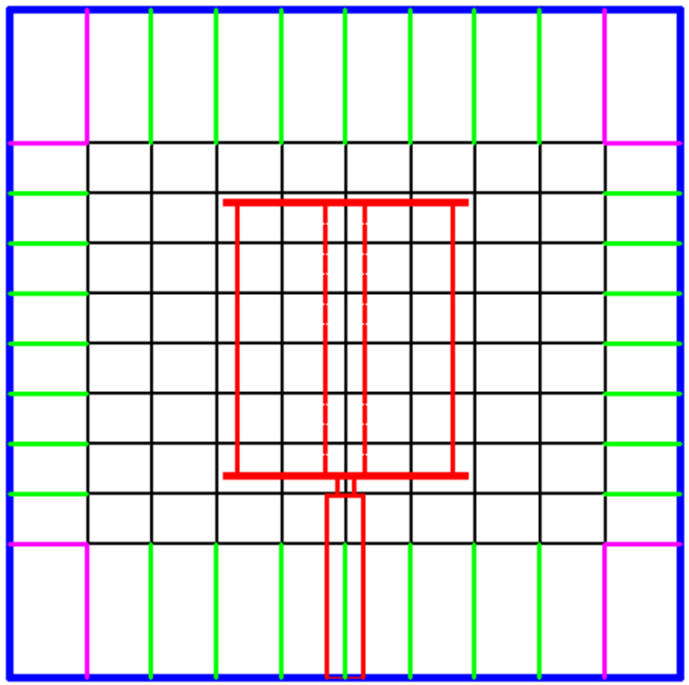

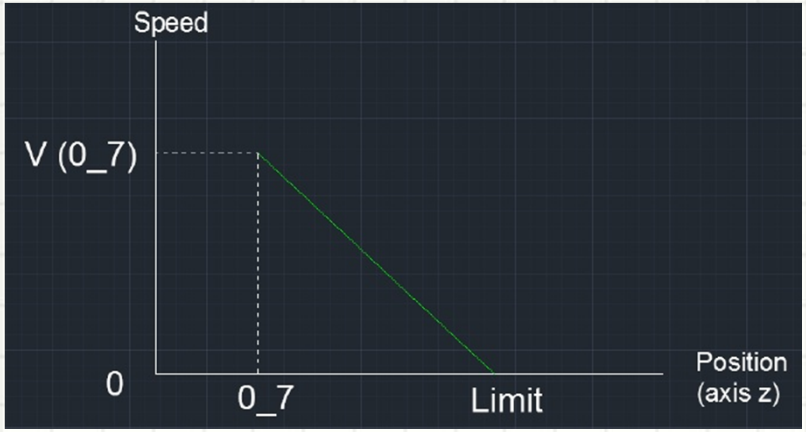

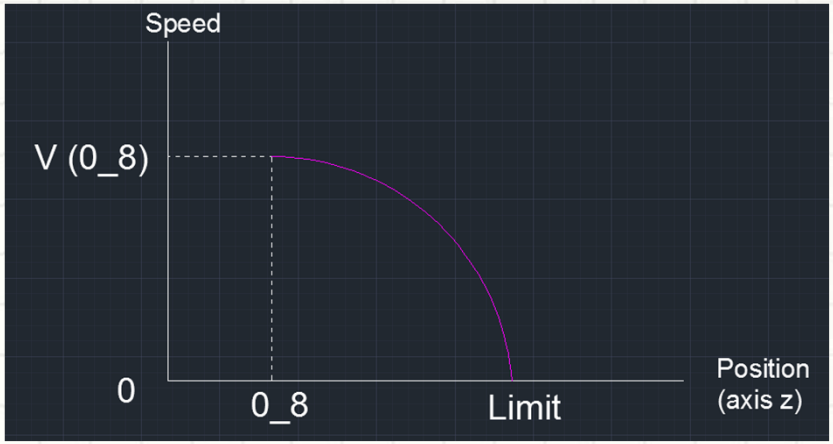

FLOW RATE OUT OF THE MESH

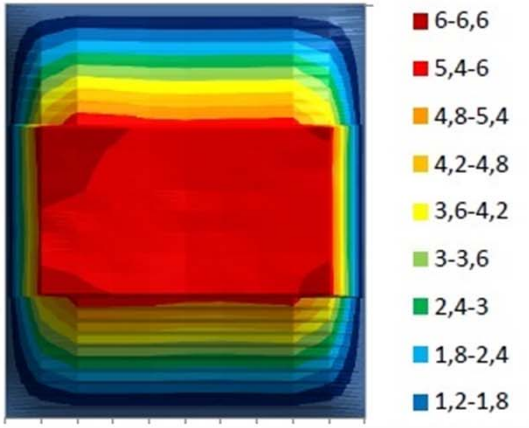

[m^3/s]

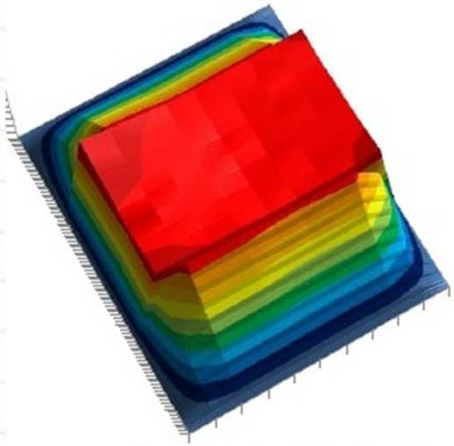

Configuration (rpm, Hz)	Flow through the mesh (m^3/s)	Total flow (m^3/s)	Flow out of the mesh (%)
200, 6	1.672	2.252	25.75
200, 8	2.254	3.022	25.41
200, 10	3.016	4.071	25.92
300, 6	1.702	2.273	25.12
300, 8	2.266	3.045	25.58
300, 10	2.863	3.837	25.38
400, 6	1.709	2.299	25.66
400, 8	2.324	3.105	25.15
400, 10	2.948	3.974	25.82

RELATION BETWEEN FLOW RATE AND WIND VELOCITY AT A REFERENCE POINT

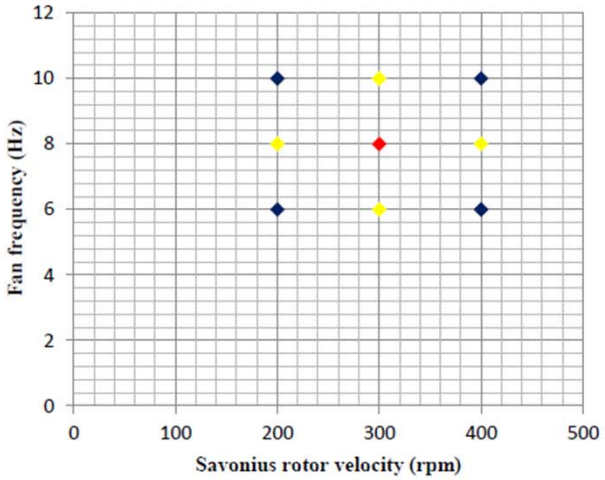

Analytical flow (m^3/s) = 0.6286 * Velocity at 4_8 (m/s)

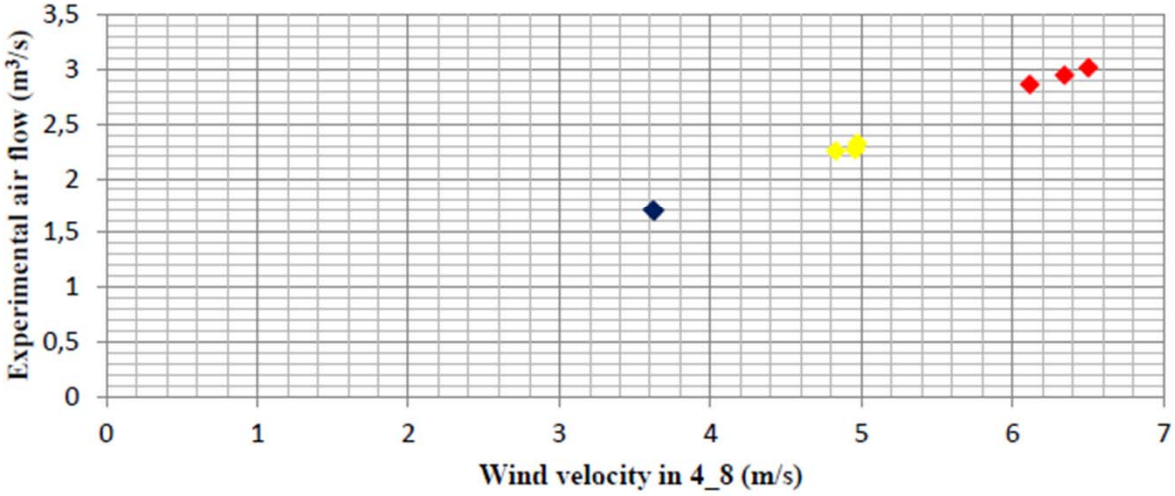

ANALYSIS OF THE FLOW BEHIND THE ROTOR

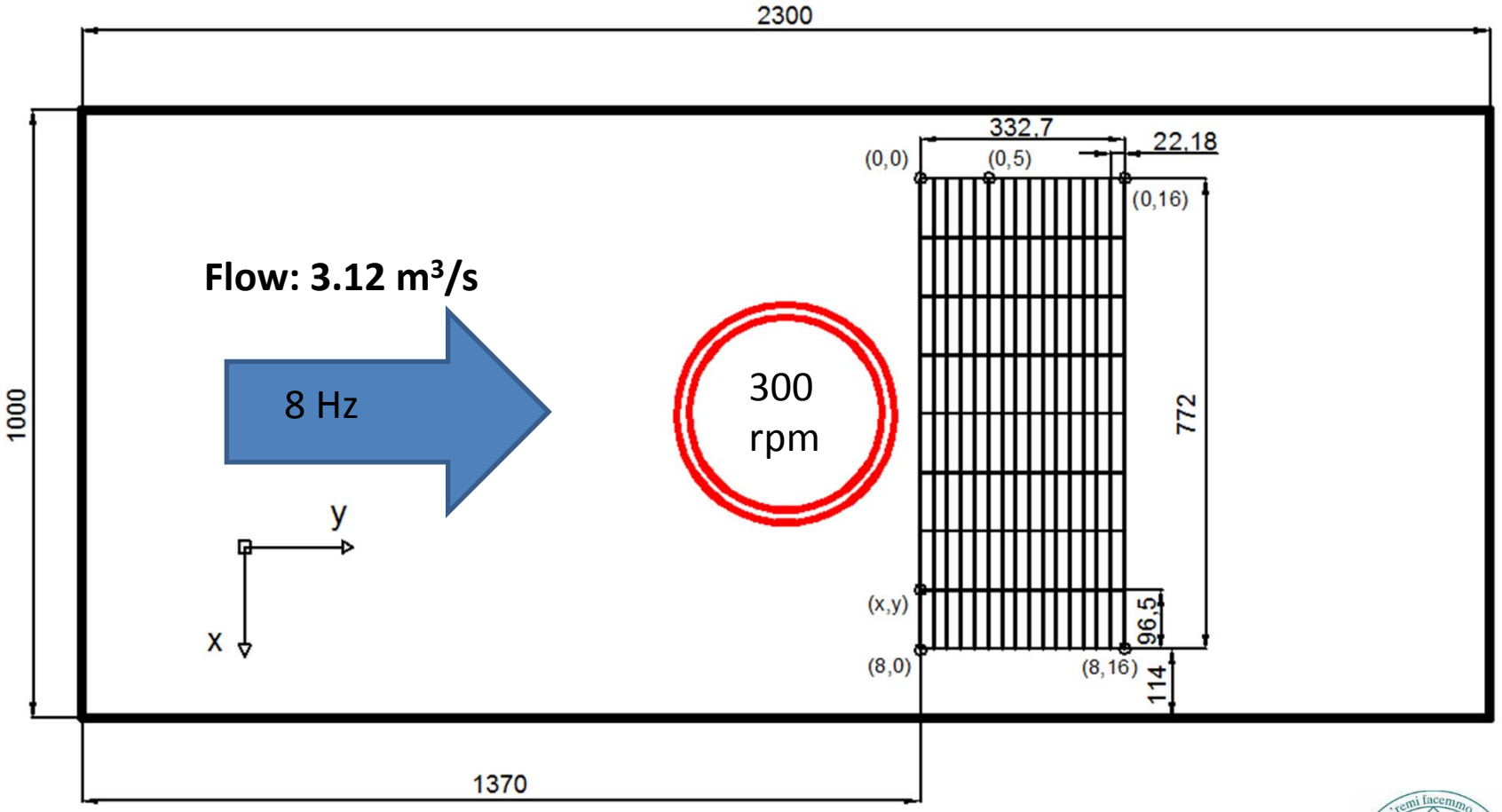

General Parameters

Average Velocity

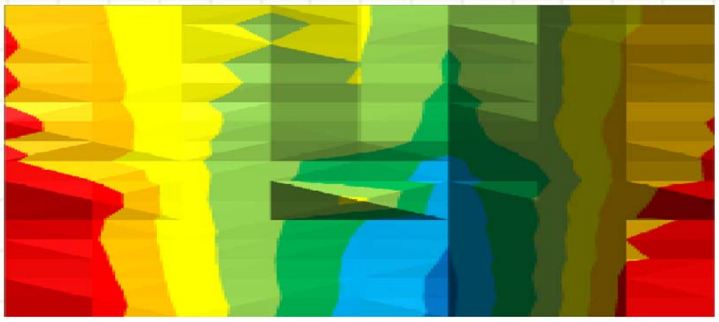

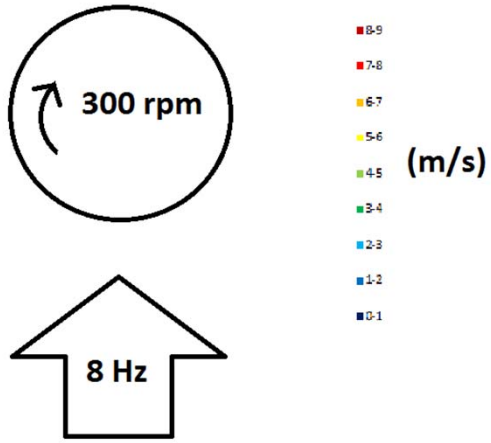

Variance

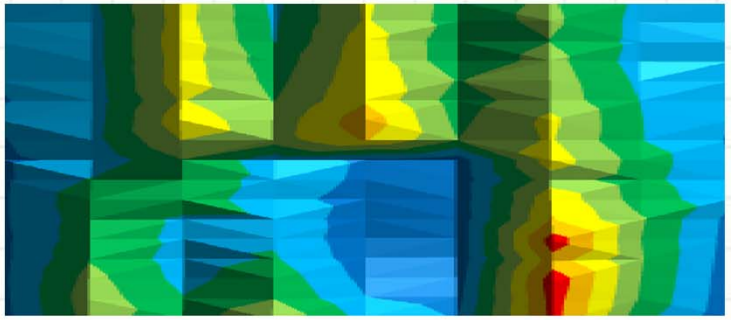

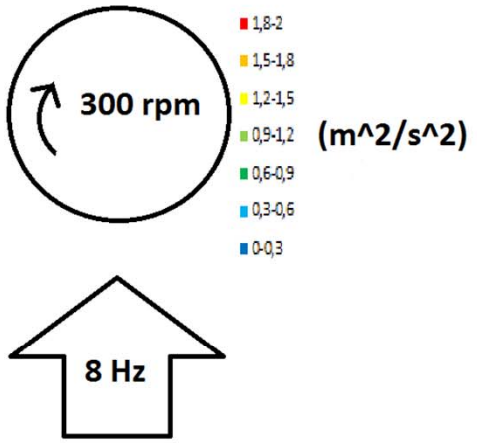

EVOLUTION OF EVERY COLUMN

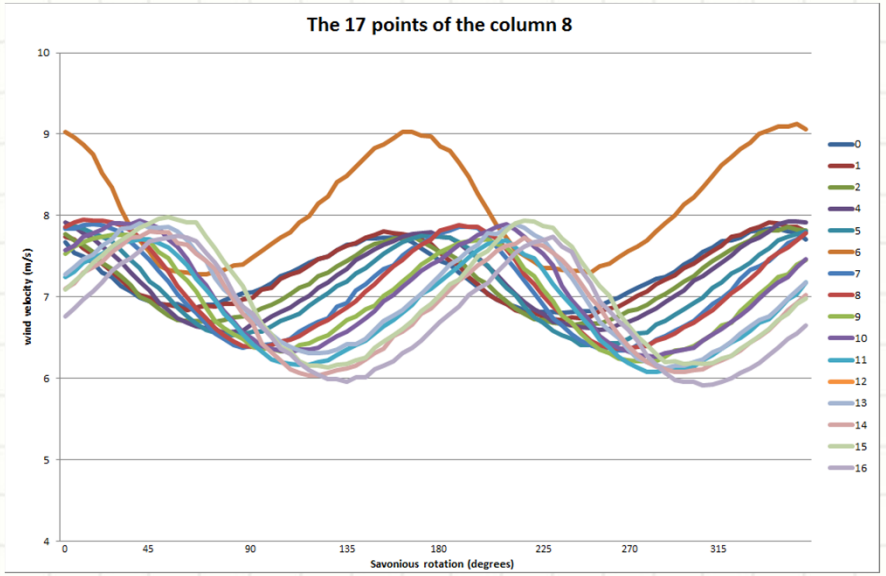

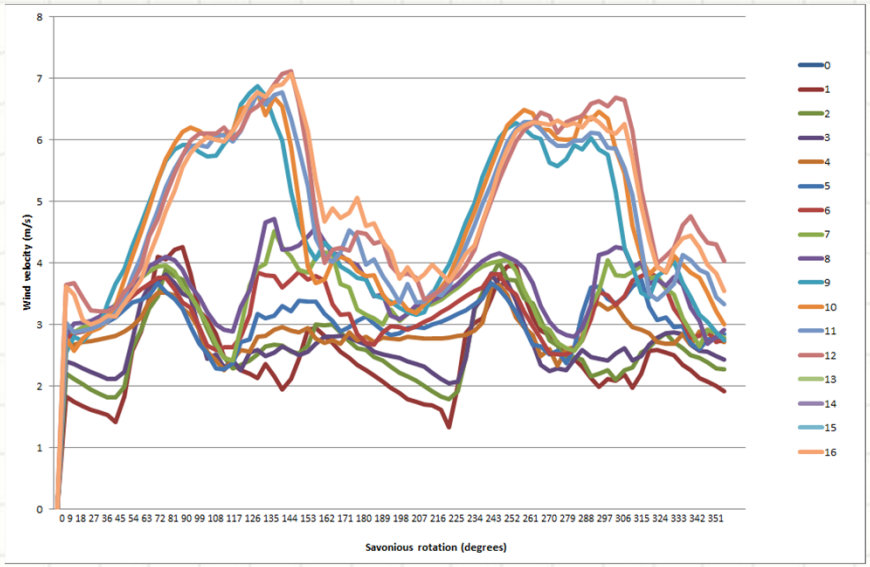

EVOLUTION OF THE WHOLE AREA

Wind

8 Hz
300 rpm

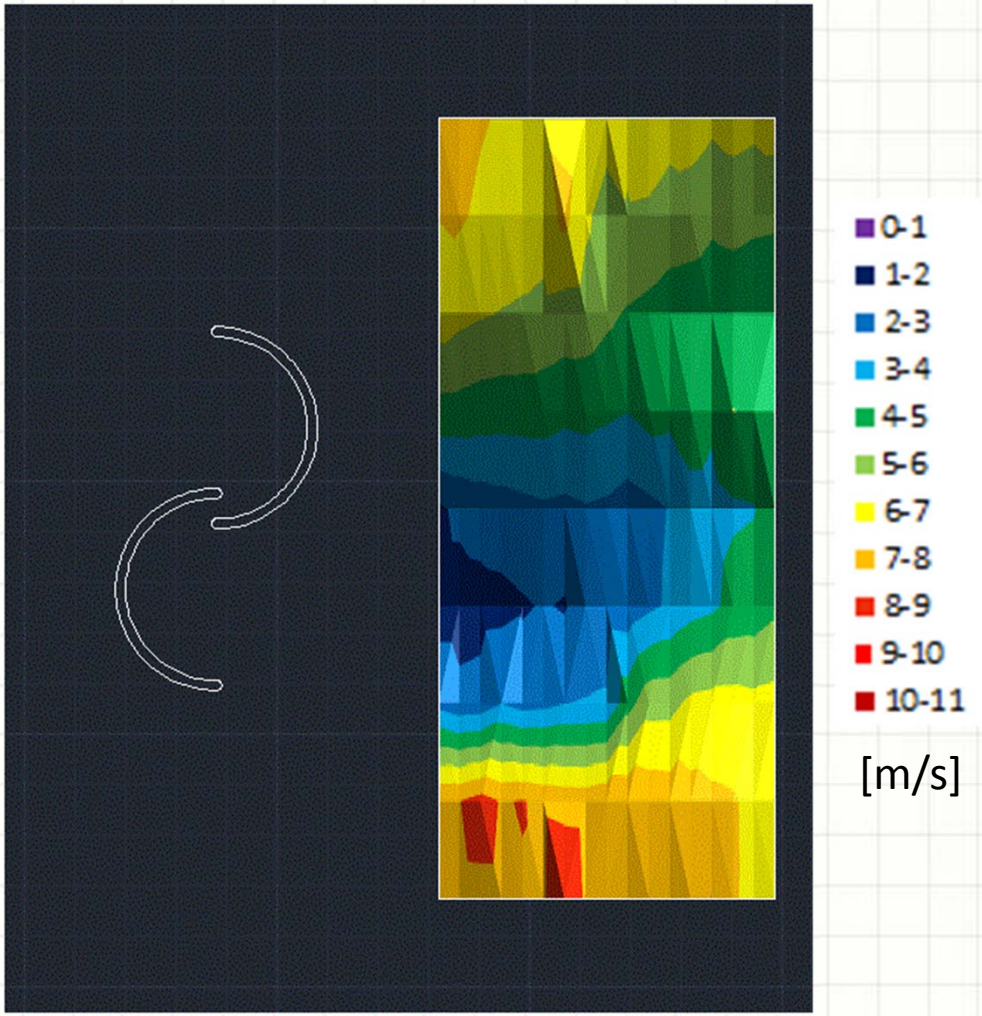

TORQUE

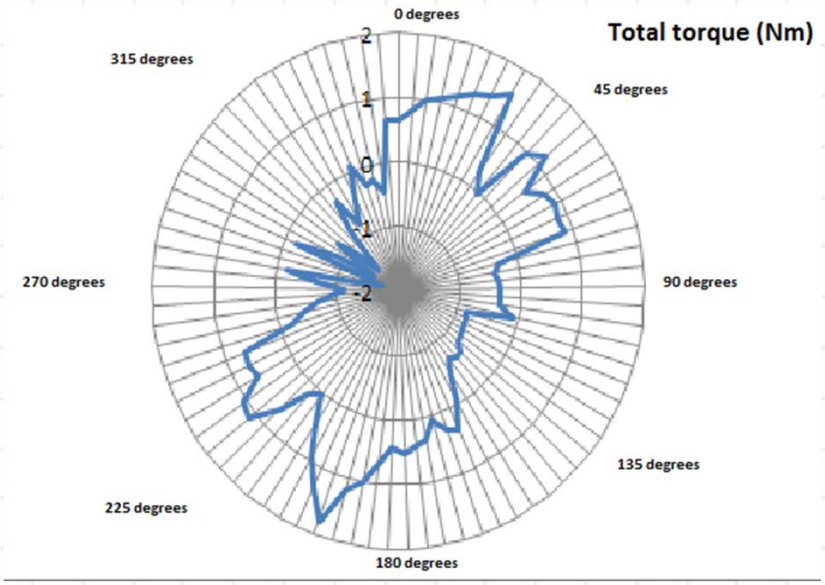

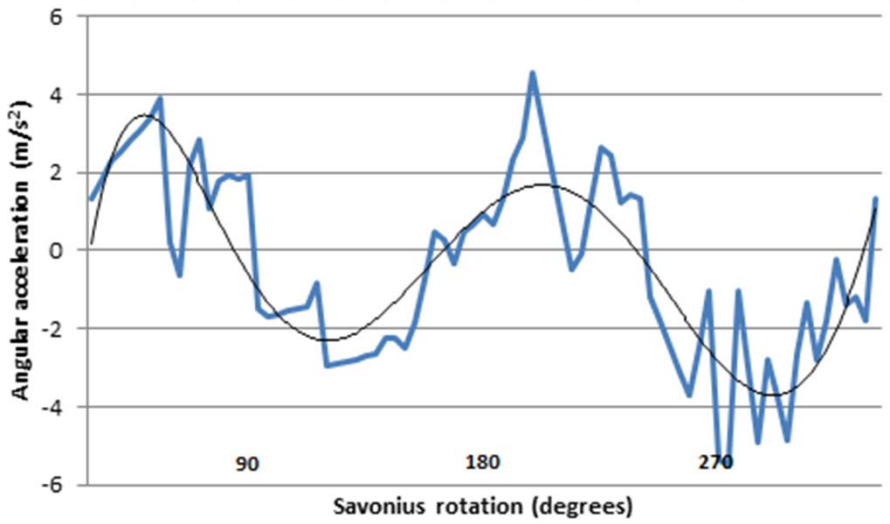

WITH MY MOST SINCERE THANKS

- Prof. Ing. Marco Torresi
- Giovanni Peroni
- Giuseppe Liberti
- Vito and Michele